NUMERICAL ANALYSIS OF THE RESPONSE OF SOFT FOUNDATION SOILS UNDER TALL EMBANKMENTS AND RETAINING WALLS

by

MERVE GIZEM BOZKURT

A thesis submitted in partial fulfillment of
the requirements for the degree of

MASTER OF SCIENCE
CIVIL AND ENVIRONMENTAL ENGINEERING

at the

UNIVERSITY OF WISCONSIN-MADISON

2013

NUMERICAL ANALYSIS OF THE RESPONSE OF SOFT FOUNDATION SOILS UNDER TALL EMBANKMENTSAND RETAINING WALLS

Merve Gizem Bozkurt

_____

Student's Name

Approved:

August 17, 2012

Signature, Date

Dante Fratta, Associate Professor

ABSTRACT

The construction of tall embankments on soft soils requires staged construction, which leads to the consolidation of foundation soils, an increase in their effective stress, reduction in void ratio, and gain in shear strength. However, retaining walls and tall embankments are not fully constrained, which contributes to the generation of lateral movements that magnify vertical settlements of the embankments, potentially leading to global failure of the foundation soil and embankment system. This study systematically presents how material properties and retaining wall geometries influence the safety of the retaining walls-foundation soil system and the relationship between lateral movements to the magnitude of vertical settlement on retaining walls using numerical analyses and analytical methods. PLAXIS, a finite element package, is used for modeling and analyzing deformation of retaining walls and foundations. The methods presented herein are validated using different case studies from cross-sections of a newly constructed STH 29 / USH 41 interchange in the State of Wisconsin in the United States. Parametric studies were conducted that involved combinations of retaining walls and soft soil conditions to assess failure mechanisms and the contribution of lateral deflection to vertical settlement. These results are validated using vertical settlement measurements at the edge of the retaining walls and pore pressure measurements under the foundation soil.

ACKNOWLEDGEMENTS

First and foremost, I would like to thank my advisor, Professor Dante Fratta, for his support and guidance throughout my graduate studies at the University of Wisconsin-Madison. I thank Professor Fratta for giving me the opportunity to join his research team and for his extensive help.

I thank Professors Tuncer B. Edil and James M. Tinjum for providing scholarly insight. I would like to thank to Professor Tuncer B. Edil for his guidance about life.

Most importantly, I would like to thank my entire family, with special thanks to my parents (Hatice and Yalcin Bozkurt) and my brother (Cagatay Bozkurt) for their love and support. I would like to thank my uncle (Muzaffer Sezer), my grandmother and grandfather (Elif and Hakki Sezer) for believing my success and supporting me throughout my education life.

I would like to thank all my friends back in Turkey, specially my best friends Buket Baylan and Yagmur Hazal Sadirvan. I would like to thank Onur Kutlu for his help and support during my graduate studies. I will be always grateful.

I would like to thank fellow colleagues Jeff Newgard and Maximiliano G. Villarreal for their assistance on several different occasions.

This thesis is dedicated to my family.

Funding for this study is provided by WisDOT's Wisconsin Highway Research Program (WHRP).

TABLE OF CONTENTS

ABSTRACT II

ACKNOWLEDGEMENTS III

TABLE OF CONTENTS IV

LIST OF FIGURES VII

LIST OF TABLES XIII

1 Introduction 1

2 General Description of the Study Site 4

2.1 Geological Description of the Site 5

2.2 Site Characterization 11

3 Mechanical Response of Embankments 13

3.1 Settlement of Structures 13

3.1.1 Immediate Settlement 15

3.1.2 Consolidation Settlement 16

3.1.3 Secondary Consolidation Settlement 19

3.2 Time Rate of Consolidation 20

3.3 Embankment Construction 24

3.3.1 Settlement Measurement during Construction 27

3.3.2 Stability Analysis of an Embankment 29

3.3.3 Embankment Foundations 30

3.3.4 Embankment Construction Methods 32

3.4 Geotechnical Instrumentation Methods 34

3.4.1 Geotechnical Instrumentation Devices 35

4 Numerical Model Methods 38

4.1 PLAXIS 2D 39

4.2 PLAXIS 3D 40

4.3 Material Models 41

4.4 Dimensional Analysis for Embankment Construction over Soft Soils 52

5 Numerical Model Development 54

5.1 Numerical Model of MSEW on Soft Foundation Soil 54

5.1.1 Simulating Construction Site Conditions 57

5.1.2 Numerical Model of MSEW at Howard, Wisconsin 74

5.1.3 Numerical Modeling Calculations for a Parametric Study on MSEW at Howard, Wisconsin 79

5.1.4 Numerical Modeling Results for a Parametric Study on the MSEW at Howard, Wisconsin 85

5.2 Parametric Studies with PLAXIS 3D 104

6 Conclusions 109

REFERENCES 112

APPENDICES 117

LIST OF FIGURES

Figure 1. A typical MSEW cross-sectional view (FHWA, 2001) 2

Figure 2. General overview of the project site – Before and after construction of the intersection 4

Figure 3. USGS Green Bay West Topographic Quadrangle Map (1995) 7

Figure 4. Glaciation of Wisconsin (Clayton et al., 2006) 8

Figure 5. Geologic history of Wisconsin, with emphasis on the Ice Age (Clayton et al., 2006).... 9

Figure 6. Geological units of the surficial material map by WisDOT (map compiled from data of previously published maps by Lineback et al. 1983, Farrand et al. 1984, Hallberg et al. 1991).. 10

Figure 7. Profile of boring and CPT tip resistance at STH 29/ USH 41 site 12

Figure 8. The Leaning Tower of Pisa (Retrived from http://en.wikipedia.org/wiki/File:Leaning_tower_of_pisa_2.jpg) 14

Figure 9. Simplified approximation of a laboratory compression curve in soils..... 17

Figure 10. Correlations of Cv with Liquid Limit..... 22

Figure 11. Sketch of staged construction of an embankment 25

Figure 12. Increase in undrained strength with staged construction..... 26

Figure 13. Difference between two displacements (Poulos et al., 1972)..... 27

Figure 14. Examples of circular & non-circular failure surfaces (Chin and Sew, 2000) 29

Figure 15. Embankment foundation problems (Sowers and Sowers, 1970)..... 30

Figure 16. Reduction in slope and using of berms in embankment improvement (Chin and Sew, 2000) 32

Figure 17. Illustration of an application of wick drains (Retrieved from http://www.johngrazelinc.com/foundationsst.htm) 33

Figure 18. Typical slope inclinometer parts and inclinometer casing 36

Figure 19. Simple rod settlement gauge 37

Figure 20. Expanded Burland Triangle 38

Figure 21. Simple definition of modeling (Barbour and Krahn, 2004) 39

Figure 22. Nodes and Stress points, a) 15-node triangular element b) 6-node triangular element (PLAXIS 2D Tutorial Manual, 2002) 40

Figure 23. An elastic perfectly plastic model (PLAXIS 3D Material Manual, 2007) 42

Figure 24. Representations of shear intercept and friction angle on Mohr's circle 43

Figure 25. Visualization of concept behind the Jointed Rock model (PLAXIS 2D Material Manual, 2002) 44

Figure 26. Hyperbolic stress-strain relation in primary loading for a standard drained triaxial test (PLAXIS 2D Material Manual, 2002) 46

Figure 27. Definition of $Eoedref$ in oedometer test results (PLAXIS 2D Material Manual, 2002) 47

Figure 28. Idealized stress-strain curve from oedometer test with division of strain increments into elastic and a creep components (Vermeer and Neher, 2000) 49

Figure 29. Photographs of the MSE wall constructed at 3600 south and I-15 in Salt Lake City-Utah (Budge et al., 2006) 54

Figure 30. Soil profile and selected instrumentation for MSE wall (Budge et al., 2006)..... 55

Figure 31. Comparison of vertical inclinometer data to PLAXIS model data (Budge et al., 2006) 55

Figure 32. Comparison of horizontal inclinometer data to PLAXIS model data (Budge et al., 2006) 56

Figure 33. Boring Profile and PLAXIS Model (Location R-05-67)..... 57

Figure 34. Pressure Transducer Field Data at Location 1102FSW 60

Figure 35. Pressure Transducer Field Data at Location 1104FSW 61

Figure 36. Location of Pressure Transducers A, B & C 62

Figure 37. Pressure isobars for uniformly loaded flexible square and strip foundations (Sivakugan and Das, 2010) 63

Figure 38. Construction Time (25 days) versus Excess Pore Water Pressure 64

Figure 39. Construction Time (50 days) versus Excess Pore Water Pressure 64

Figure 40.Construction Time (100 days) versus Excess Pore Water Pressure 65

Figure 41. Construction Time (200 days) versus Excess Pore Water Pressure 65

Figure 42. Staged construction embankment problem (Kelln et al. 2007) 66

Figure 43. Staged construction effect on both excess pore pressure and displacements (Staged construction interval time, 100 days) 67

Figure 44. Staged construction effect on both excess pore pressure and displacements (Staged construction interval time, 100 days) 68

Figure 45. Cumulative Horizontal Displacement Plot 69

Figure 46. Strip load imposing a uniform stress 70

Figure 47. Shear Stress Distribution under uniformly loaded steel plate 71

Figure 48. Shear Stress Distribution under MSEW 72

Figure 49. Shear stress distribution comparison 2.5 m away from the wall facing 73

Figure 50. Application in which geogrids are used (PLAXIS 2D Reference Manual, 2002) 76

Figure 51. MSEW Model with structural elements 78

Figure 52. Initial stresses and pore pressure distribution (the size of the crosses indicate the magnitude of the stresses) 79

Figure 53. Staged Construction of MSEW 81

Figure 54. Deformed Shape and Total Displacement representing the MSEW Failure Mechanism (Scale 1:20) 82

Figure 55. Deformed Shape and Total Displacement representing the Foundation Soil Failure Mechanism (Scale 1:20) 83

Figure 56. Calculation steps in PLAXIS..... 84

Figure 57. Effect of boundaries in MSEW System Response 85

Figure 58. Effect of Boundary Fixities on Vertical (U_y) and Horizontal (U_x) Displacements at the top of the wall 86

Figure 59. Cross section of MSEW 87

Figure 60. Effect of friction angle of the backfill and dimensionless ratio H/L on Factor of Safety 88

Figure 61. Effect of dimensionless ratio Su/Eu of Layer 2 on Factor of Safety..... 89

Figure 62. Effect of backfill friction angle to the factor of safety 90

Figure 63. Effect of dimensionless ratio Su/Eu of Layer 2 on Factor of Safety..... 91

Figure 64. Effect of dimensionless ratio $(\gamma H)/S_u$ on Factor of Safety 92

Figure 65. Effect of Poisson's ratio of Layer 2 on Factor of Safety 93

Figure 66. Effect of Poisson's ratio on displacements 94

Figure 67. The elastic perfectly plastic Mohr-Coulomb Model 95

Figure 68. Effect of dimensionless ratio S_u/E_u on vertical settlements..... 95

Figure 69. Effect of Dimensionless ratio S_u/E_u on dimensionless ratio $-U_y/U_x$..... 96

Figure 70. Effect of dimensionless ratio $(\gamma H)/Eu$ of layer 2 on vertical settlements 97

Figure 71. Horizontal Displacements for NCC (Extreme U_x = 92.54* 10^{-3} m)..... 99

Figure 72. Horizontal Displacements for OCR = 12 (Extreme U_x = 30.58* 10^{-3} m)..... 100

Figure 73. Vertical Displacements for NCC (Extreme U_y = -272.71* 10^{-3} m)..... 101

Figure 74. Vertical Displacements for OCR=12 (Extreme U_y = -133.17* 10^{-3} m) 101

Figure 75. Contribution of Lateral Displacements to Vertical Settlements..... 102

Figure 76. Ratio of Lateral Displacements to Vertical Settlements versus OCR 103

Figure 77. Soil Embankment Geometry and Deformed Shape after Consolidation (Scale 1:50) 104

Figure 78. Relation between the changes in Young's Modulus and vertical settlements in the embankment..... 106

Figure 79. Total horizontal displacement plot 107

Figure 80. Lateral displacement contribution to vertical settlement..... 108

LIST OF TABLES

Table 1. Shape and rigidity factors, *Is* (Winterkorn and Fang, 1975) 16

Table 2. Benefits of using geotechnical instrumentation by Dunnicliff (1993) 35

Table 3. Relationship to Cam-Clay parameters 51

Table 4. Relationship to internationally normalized parameters 51

Table 5. Soil Parameters (Location R-05-67) 58

Table 6. Wall facing data set parameters from PLAXIS 2D Manual 58

Table 7. Geogrid parameter from PLAXIS 2D Manual 58

Table 8. Soil Description at STH 29/ USH 41 site (Location R-5-231) 75

Table 9. Soil and interface parameters (Location R-5-231) 75

Table 10. Wall facing data set parameters from PLAXIS 2D Manual 76

Table 11. Geogrid material parameter 77

Table 12.Undrain shear strength and Young's Modulus values for OC Clays 98

Table 13. Soil and Embankment Properties 105

1 Introduction

Soft soils consist of fine grained particles having a diameter less than 0.075 mm with low strength and low stiffness. Soft soils also have very low hydraulic conductivity (ranging from 10^{-7} m/s to 10^{-13} m/s - Salgado, 2008). This low hydraulic conductivity leads to the slow dissipation of excess pore water pressure after loading. Moreover, soft soils are highly compressible due to their high initial void ratio, which may lead to severe settlement problems and also having low shear strength may cause a failure of structure or foundation soil bearing capacity problems. Because of these detrimental properties, soft saturated soils present difficult challenges for the design and construction of embankments.

The construction of tall embankments and retaining walls on top of saturated soft soils often requires staged construction that allows the dissipation of excess pore water pressure, a slow increase in effective stress and shear strength improvement while the void ratio decreases and the embankment settles. Staged construction helps improving the shear strength of soils by allowing for an increase of effective stress in the foundation and a reduction in post-construction settlements. Fill placement causes vertical compression and lateral expansion toward zones of lower confining pressure. Since the foundation soils under tall embankments and retaining walls are not fully constrained in lateral directions, the problem is magnified. The engineering challenge is that the contribution of lateral movements to vertical settlements is not well understood. This project studies the numerical analysis of the response of soft foundation soils under tall embankments and retaining walls.

In urban areas, the cost of land for transportation construction is high. In those situations, the footprint of embankments can be reduced by implementing mechanically stabilized earth (MSE) construction. MSE is a cost-effective soil retaining structure method which includes reinforced earthen material to support its own weight (FHWA, 2001- Figure 1). Geosynthetics or geogrids are commonly used as reinforcing elements while constructing the MSE.

MSE walls are typically constructed using three main structural components: geogrid reinforcement, wall facing, and backfill soil (Hossain et al., 2009). The reinforcement is placed horizontally at predetermined elevation as the backfill is placed in the reinforced zone of the wall. Wall facing is used to prevent sliding of backfill soil. Backfill soil could be divided into two components: retained backfill and the reinforced backfill. Retained backfill is the fill material located between mechanically stabilized soil mass and the natural soil and the reinforced backfill is the fill material in which the reinforcements are placed.

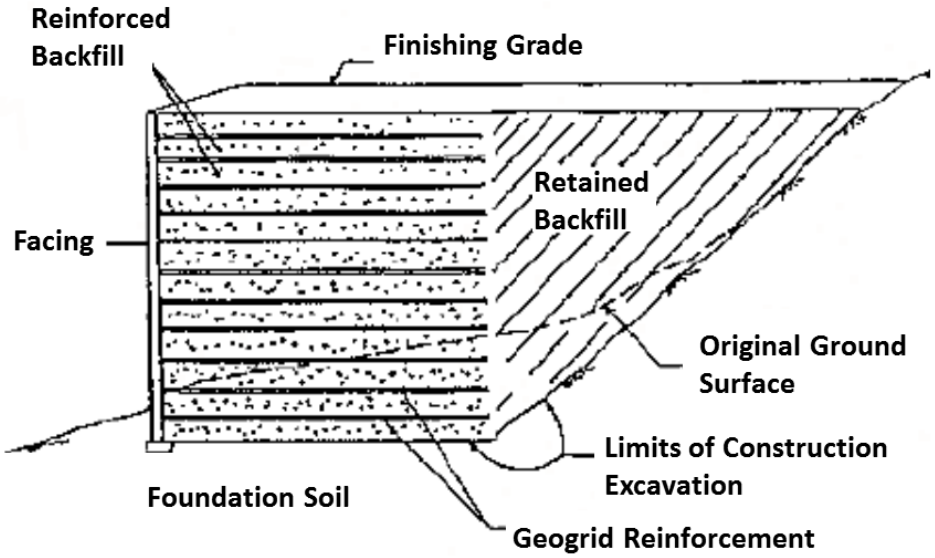

Figure 1. A typical MSEW cross-sectional view (FHWA, 2001)

This project investigates, using numerical modeling, the response of soft foundation soils under an MSE wall. The effect of the contribution of lateral deformations on vertical settlement and potential bearing capacity failure of the MSE wall were the main focus areas of the study that also included:

1. Review of engineering properties of an MSE wall in Howard, Wisconsin.
2. Development of a numerical model to investigate the mechanical respond of the MSE wall using a finite element model, PLAXIS.
3. Parametric studies of the various factors that govern the failure of MSE wall. The effects of the following parameters were studied in this study:
    - The effect of embankment height: 1 m, 2 m, 3 m, 4 m and 5 m
    - The effect of backfill friction angle: 30°, 35° and 40°
    - The effect of soft foundation soil properties - Undrained shear strength: 14 kPa, 17 kPa and 24 kPa; Young's modulus: 1,000 kPa, 5,000 kPa, 10,000 kPa, 20,000 kPa and 25,000 kPa; and Poisson's ratio: 0.1, 0.2, 0.3 and 0.35.
4. Analysis of contribution of lateral displacements to vertical settlements by conducting parametric studies.
5. Comparison of geotechnical instrumentation data from construction site with PLAXIS analysis results.

2 General Description of the Study Site

The project site is geographically located in the Village of Howard, Brown County in the State of Wisconsin in the United States. The project is located between at the intersection State Highway 29 and US Highway 41 (Figure 2).

Figure 2. General overview of the project site – Before and after construction of the intersection (Map renderings from http://maps.google.com)

2.1 Geological Description of the Site

Geologically, the site of study lies within the Fox River flatlands. These flatlands created a valley of relatively flat land gently sloping toward the Fox River and Green Bay. Figure 3 provides a topographic map of the area showing local topography. The surface slope mimics the eroded Pleistocene sedimentary bedrock surface produced when the Green Bay lobe of the Laurentide ice sheet moved across the area during the glaciation in Wisconsin more than 10,000 years ago (Clayton et al., 2006). During this glaciation, up to 60% of Wisconsin's land surface was covered by ice at some time (Figures 4-5). The Paleozoic sedimentary rocks dip gently to the East, toward Lake Michigan, as a result of the Wisconsin dome (Dott and Attig, 2004).

The Pleistocene deposits of Brown County include till units, silty and clayey offshore lacustrine sediment of several ages, and melt water and stream sediment of several ages (Need, 1985). Geological units of the surficial material map are presented in Figure 5. Underlying these Pleistocene units are crystalline Precambrian basement rocks that do not influence the behavior of the upper bedrock or unconsolidated sediments.

The Green Bay lobe of the Laurentide ice sheet extended through the present Green Bay area and reached as far south as Rock County, WI about 18,000 years ago (Dott and Attig, 2004). A series of seven tills record four glacial events across the region (Need, 1985) in late Wisconsian time. Only one of these tills was deposited after the Two Creeks forest dated to 11,750 years ago. Figure 6 shows deep water lake sediment locally surrounding the project area. As the ice front fluctuated north and south about the City of Green Bay, the proglacial Lake Oshkosh was formed in the Fox River lowland where glacial meltwaters were trapped from draining into Green Bay. At its maximum, glacial Lake Oshkosh was at approximately elevation

250 m above mean sea level (Need, 1985). At this point, the lake was able to drain through an outlet in Portage, WI. As the ice sheet wasted northward, lower outlets were opened, thus allowing the lake level to drop. As the ice continued to recede towards the North, the continental crust rebounded due to removal of the ice overburden pressure. As the region raised, lake outlets varied in elevation and caused the water levels in the Great Lakes to fluctuate. This processes continued to the present time where crustal rebound and climatic conditions determine the level of Lake Michigan.

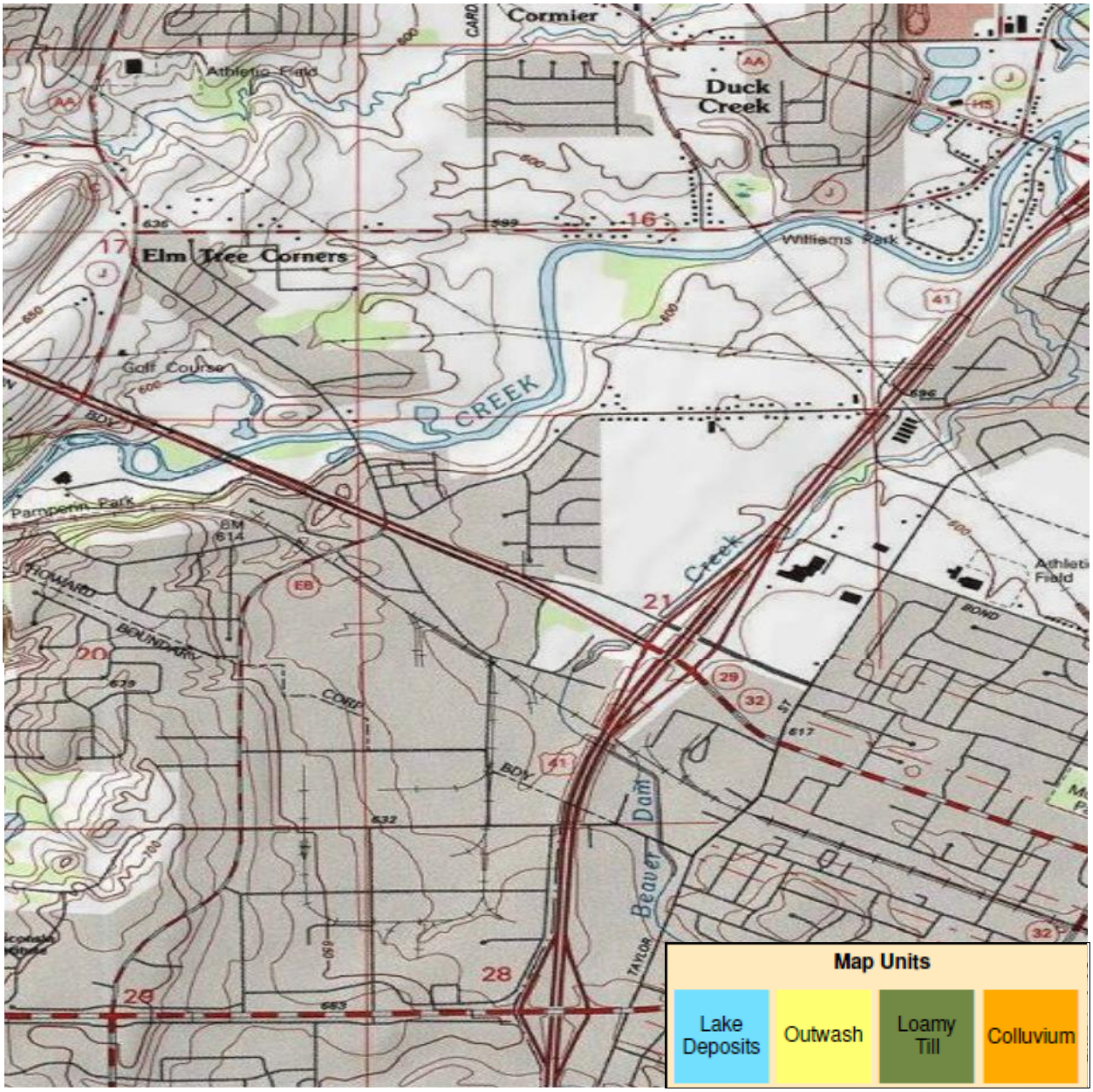

Figure 3. USGS Green Bay West Topographic Quadrangle Map (1995)

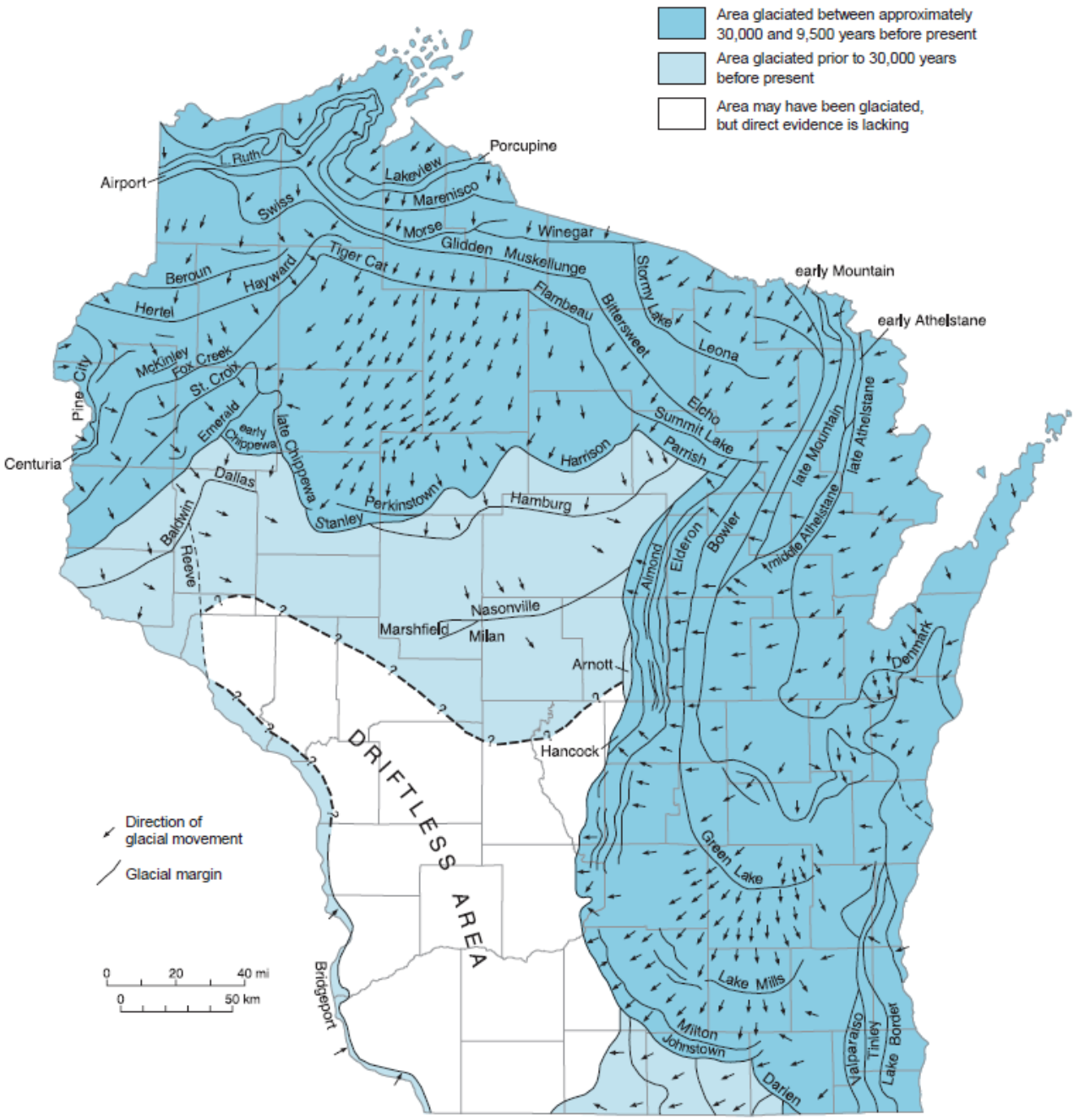

Figure 4. Glaciation of Wisconsin (Clayton et al., 2006)

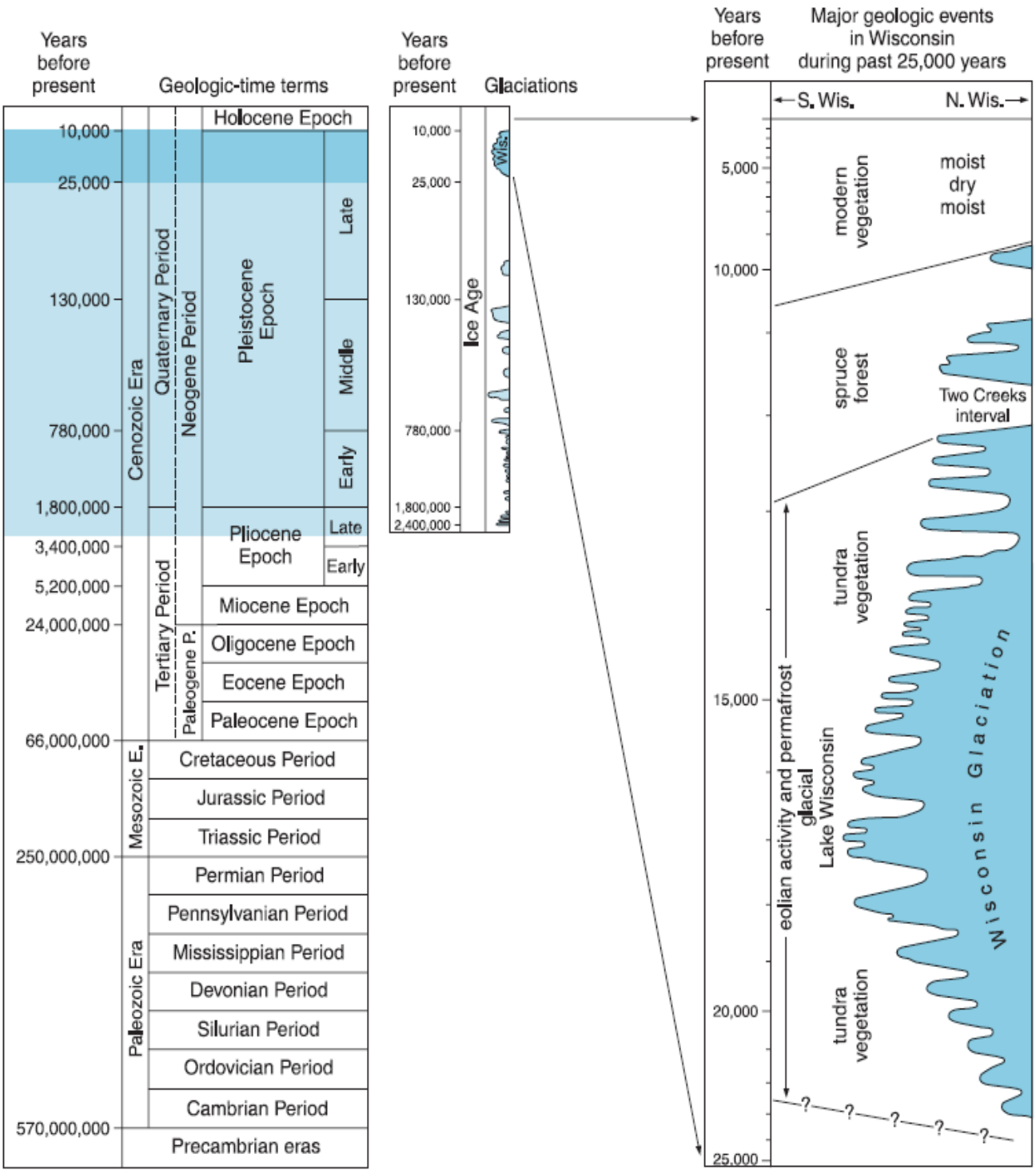

Figure 5. Geologic history of Wisconsin, with emphasis on the Ice Age (Clayton et al., 2006)

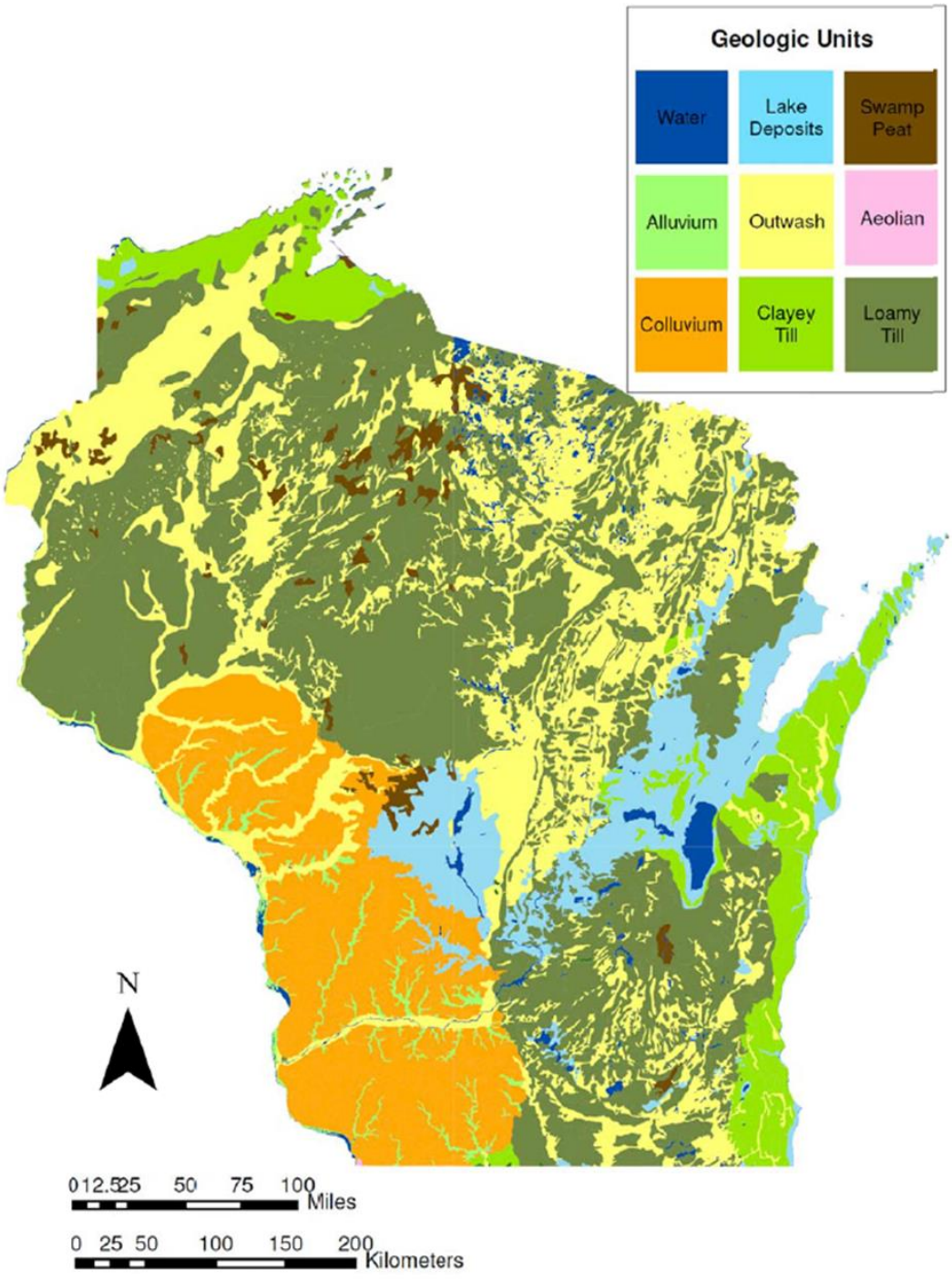

Figure 6. Geological units of the surficial material map by WisDOT (map compiled from data of previously published maps by Lineback et al. 1983, Farrand et al. 1984, Hallberg et al. 1991)

2.2 Site Characterization

Site characterization of the interchange area was obtained using borings and cone penetration testing (CPT). These tests were run by prof. J. Schneider as part of a WHRP project (if you know the project, please add a reference). The results obtained are presented in Figure 7. Profiles show the interval from 0 m to 21 m below ground surface logs in detail. There are three main layers with different soil properties; i.e., grain size distribution, Atterberg limits, unit weight, and shear strength. The soil column consists of a brown, overlain a red wet clay. The clay lies on top of a silt with a deep water lake deposit layer between 4 m and 16 m. These shallow strata sit on top of a very stiff clay that is found at 16 m logs.

Cone penetration testing (CPT) was used to identify subsurface conditions generally in the upper 30 m of the subsurface and the tip resistance is determined by the force required to push the tip of the cone. The tip resistance is related to the undrained shear strength of saturated fine-grained soils, while the sleeve friction is related to the friction of the horizon being penetrated (Robinson and Campanella, 1986). Undrained shear strength of clay, S_u, was estimated from the cone resistance data, q_c, collected from the construction site using an equation of the form:

$$S_u = (q_c - \sigma'_v)/N_k \qquad [2.1]$$

where N_k is the cone factor (roughly in the 9-10 range) and σ'_v is the vertical effective stress (Salgado, 2008). Tip resistance is generally high in sands and low in normally consolidated clays due to the generation of positive excess pore water pressure. The data collected at site show that tip resistance is very low within the loose clay layer, which is an indication of weak soil within this layer (Figure 7).

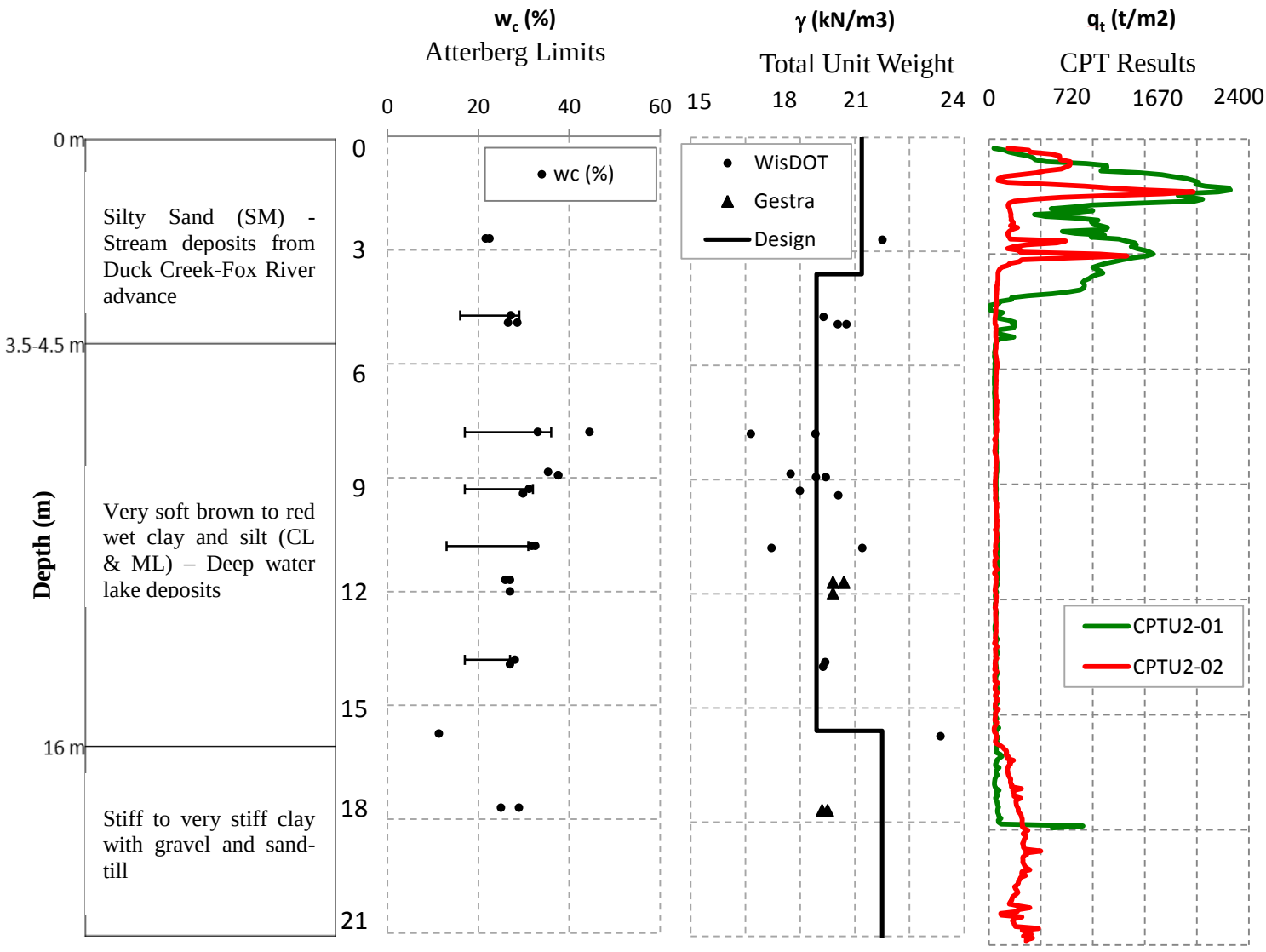

Figure 7. Profile of boring and CPT tip resistance at STH 29/ USH 41 site

3 Mechanical Response of Embankments

3.1 Settlement of Structures

Settlement is the vertical displacement of ground under loading and occurs due to an increase in effective stress (Birand et al., 2002). A decrease in volume due to an increase in effective stress leads to stronger, stiffer soils. One mechanism for increase in effective stress is dewatering. During dewatering, the lowering of the water table and the negative pore water pressure induced increases the effective stresses in the soil consolidating it and creating settlements on the surface. The surface settlement is also known as subsidence. Another mechanism for increase in effective stress is application of a surcharge load. Settlement is an important criterion in the design of foundations systems due to serviceability constraints or in assessing allowable bearing pressure.

Structures can settle uniformly or nonuniformly, so settlements of structures are presented as total and differential settlements. This distinction is the crucial design consideration (Grant et al., 1974). Differential settlement is the difference in settlement under different parts of a single structure. Generally most structures can tolerate large total settlement but can only tolerate certain levels of differential settlements. The maximum amount of acceptable differential settlement depends on type of construction, type of equipment housed inside, and the time period over which the settlement occur. If the settlement is not kept to tolerable limits, the desired use of the structure may be impaired and the design life of the structure may be reduced. There are some dramatic examples of differential settlement in the world, such as the Leaning Tower of Pisa which has leaned at an angle of 3.99° and settled about 3 m due to very soft lacustrine clay with a void ratio 6.90 (Burland et al., 2009 - Figure 8).

Allowable settlement is the tolerated maximum amount of total settlement assigned to different foundation types in different soils. Birand et al. (2002) states that for isolated footings on sand allowable maximum settlement could be taken as 40 mm, for rafts up to 65 mm and for isolated footings and rafts on clay corresponding values are 65 mm and 100 mm, respectively. Moreover, the design limit for maximum differential settlements between isolated foundations on sand and clay could be taken as 25 mm and 40 mm, respectively (Birand et al., 2002).

Figure 8. The Leaning Tower of Pisa (Retrived from http://en.wikipedia.org/wiki/File:Leaning_tower_of_pisa_2.jpg)

The overall settlement of a foundation has three components: (1) immediate, (2) consolidation and (3) secondary settlement. Total settlement is the summation of these three components.

3.1.1 Immediate Settlement

Immediate settlement occurs during load application and is completed shortly after the load is completely applied. Although immediate settlement may not be completely linear and elastic, it is typically calculated with linear and elastic theory. Immediate settlement is a very large percent of total settlement in coarse-grained soils even under saturated conditions. This is because the excess pore water pressure in coarse-grained soils rapidly dissipates due to high hydraulic conductivity (Holtz et al., 2011). Immediate settlements must be considered in the design of shallow foundations that are sensitive to rapid settlements. The vertical settlement (S_i) under a loading area carrying a uniform pressure (q) on the surface of a semi-infinite, homogeneous, isotropic mass (with a linear stress-strain relationship) expressed as,

$$S_i = \frac{q.b}{E}.(1-\vartheta^2).I_s \qquad [3.1]$$

where I_s is the influence factor (a function of the shape of the loaded area), ϑ is the Poisson's ratio, E is the Young's modulus and b is the width of the loaded area. Values of I_s are given in Table 1.

There is an alternative calculation for immediate settlement (Janbu et al., 1956 and modified by Christian and Carrier, 1978) which presents average vertical displacements under a flexible area carrying a uniform pressure, q,

$$S_i = \frac{q.b}{E}.\mu_0.\mu_1 \quad [3.2]$$

where μ_0 and μ_1 are empirical influence factors for shape and the depth for a compressible soil. Values of μ_0 and μ_1 are given in Figure A.1.

Table 1**.** Shape and rigidity factors, I_s (Winterkorn and Fang, 1975)

Shape and Rigidity	**Center**	**Corner**	**Edge/Middle of Long Side**	**Average**
Circle (flexible)	1.0		0.64	0.85
Circle (rigid)	0.79		0.79	0.79
Square (flexible)	1.12	0.56	0.76	0.95
Square (rigid)	0.82	0.82	0.82	0.82
Rectangle (flexible) length/width				
2	1.53	0.76	1.12	1.30
5	2.10	1.05	1.68	1.82
10	2.56	1.28	2.10	2.24
Rectangle (rigid) length/width				
2	1.12	1.12	1.12	1.12
5	1.6	1.6	1.6	1.6
10	2.0	2.0	2.0	2.0

3.1.2 Consolidation Settlement

Consolidation settlement is a time-dependent process and is mainly observed in soils with low hydraulic conductivity such as saturated fine-grained soils. The rate of consolidation settlement is related to the rate of excess pore water dissipation because consolidation settlement

takes place as a result of volume reduction of soils and the increase of effective stresses caused by squeezing out pore water from soil (Birand et al., 2002).

An oedometer cell is used to measure compression (i.e., deformation) and consolidation (i.e., rate of excess pore water dissipation) properties in the laboratory. The applied load and specimen deformation are carefully measured to assess the relationship between load and rate of deformation of soils. A simplified approximation of a laboratory compressibility curve is shown in Figure 9.

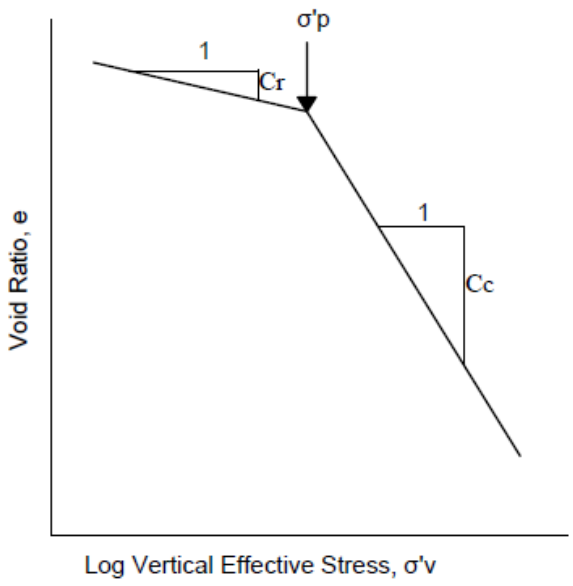

Figure 9. Simplified approximation of a laboratory compression curve in soils

Figure 9 defines several important parameters. The preconsolidation pressure (σ'_p) is the stress at which the soil begins to yield in volumetric compression, and so it separates the region of elastic deformation and small strains ($\sigma'_v < \sigma'_p$) from the region of plastic deformation and large strains ($\sigma'_v > \sigma'_p$) (Fox, 2003). Total consolidation settlement of a compressible layer is highly dependent on the value of the preconsolidation pressure. If applied final stress (σ'_v) is less

than σ'_p, the consolidation settlement will be relatively small. However, if the final stress is larger than σ'_p, higher settlements will occur. Therefore, the most important step in a settlement analysis is to determine the preconsolidation pressure (Holtz et al., 2011).

Overconsolidation ratio, OCR, is the ratio of the preconsolidation stress to the existing vertical effective overburden stress. Soils that are normally consolidated have an OCR=1 and soils with an OCR>1 are overconsolidated. The slope of the overconsolidated range (i.e., $\sigma'_v < \sigma'_p$) is the *recompression index, C_r*. The slope of the normally consolidated portion (i.e., $\sigma'_v > \sigma'_p$) of the compressibility curve is the *compression index, C_c*.

- *Settlement of Normally Consolidated Soils* (i.e., σ'_{v0} and $\sigma'_{v0}+\Delta\sigma_v > \sigma'_p$),

$$S_c = C_c.\frac{H_0}{1+e_0}.log\left(\frac{\sigma'_{vo}+\Delta\sigma_v}{\sigma'_{vo}}\right) \quad [3.3]$$

where σ'_{v0} is the existing vertical overburden stress and $\Delta\sigma_v$ is the additional stress applied by structure, e_0 is the initial void ratio and H_0 is the initial soil layer thickness.

- *Settlement of Overconsolidated Soils,* (i.e., $\sigma'_{v0} < \sigma'_p < \sigma'_{v0}+\Delta\sigma_v$),

$$S_c = C_r.\frac{H_0}{1+e_0}.log\left(\frac{\sigma'_p}{\sigma'_{vo}}\right) + C_c.\frac{H_0}{1+e_0}.log\left(\frac{\sigma'_{vo}+\Delta\sigma_v}{\sigma'_p}\right) \quad [3.4]$$

- *Settlement of Overconsolidated Soils,* (i.e., $\sigma'_{v0} < \sigma'_{v0}+\Delta\sigma_v < \sigma'_p$),

$$S_c = C_r.\frac{H_0}{1+e_0}.log\left(\frac{\sigma'_{vo}+\Delta\sigma_v}{\sigma'_{vo}}\right) \quad [3.5]$$

3.1.3 Secondary Consolidation Settlement

Secondary consolidation settlement, also referred to as creep settlement, results from the time-dependent rearrangement of soil particles under constant effective stress over long periods of time. According to simple consolidation theory, consolidation ends when excess hydrostatic pressures within a fine-grained layer are fully dissipated (Mitchell and Soga, 2005). However, soil continues to deform overtime under constant effective stress. Sliding at interparticle contacts and rearrangement of adsorbed water molecules and cations into different positions create the mechanism of secondary compression (Mitchell and Soga, 2005).

For highly organic and sensitive soils, such as soft clays and peats, secondary compression is important. The secondary compression index, C_α, is the change of void ratio per log cycle of time,

$$C_\alpha = -\frac{\Delta e}{\Delta log t} \quad [3.6]$$

The secondary compression indeed C_α could be estimated from the compression index ratio C_α/C_c (Mesri and Castro, 1987):

C_α/C_c = 0.04 ± 0.01 for soft inorganic clays

C_α/C_c = 0.05 ± 0.01 for highly organic plastic clays

The secondary consolidation settlement is calculated as:

$$S_s = C_\alpha \cdot \frac{H_0}{1 + e_0} . log\left(\frac{t_f}{t_p}\right) \quad [3.7]$$

where t_p is the time at the end of primary consolidation, and t_f is the time horizon for which secondary compression settlement is determined, in general the design life of the structure.

3.2 Time Rate of Consolidation

A soil consists of solid particles with voids that are filled with gas, liquid or a combination of both. Volume changes in soils are caused by changes in effective stresses. There are three common causes that may lead to a decrease in volume: compression of the solid skeleton, compression of water and air within the voids, and the drainage of water from voids. Soils with low hydraulic conductivity need a considerable time for the drainage process to occur. That is, the process of consolidation is a time-dependent response to the expulsion of water from the soil pores. Changes in void ratio of low hydraulic conductivity soils is proportional to the amount of excess pore water pressure that is dissipated, thus the rate of settlement is directly related to the rate of excess pore water pressure dissipation (Holtz et al., 2011).

K. Terzaghi in 1925 presented the one-dimensional consolidation theory. This theory quantitatively describes soil compression and its relation to the changes of effective stress and the rate at which it occurs (Holtz et al., 2011). According to Terzaghi's one-dimensional theory, some assumptions and limitations are needed for the analysis of the problem. The consolidating soil layer is assumed to be homogeneous and completely saturated, the mineral grains in the soil and the water in the pores are assumed to be incompressible, the relationship between void ratio

and effective stress is linear, and properties of the soil do not change during the consolidation process. Darcy's law (i.e., laminar flow) is assumed to govern and drainage and compression is assumed to be one dimensional. Stress increments are assumed to produce only small strains in the soil, which makes the coefficient of compressibility, a_v, and the hydraulic conductivity, k, constant during the consolidation process.

The coefficient of compressibility is obtained by relating the change in void ratio to the change in effective stress,

$$a_v = \frac{e_1 - e_2}{\sigma'_2 - \sigma'_1} \quad [3.8]$$

The coefficient of consolidation, c_v, is a key parameter that governs the consolidation process by containing material properties,

$$c_v = \frac{k}{\rho_w g} \cdot \frac{1 + e_0}{a_v} \quad [3.9]$$

where ρ_w is the density of water and e_0 is the initial void ratio.

Since a_v and k are assumed as constant during the consolidation process, c_v is also a constant during a loading cycle for one-dimensional consolidation theory. Approximate correlations of c_v with liquid limit are presented in Figure 10.

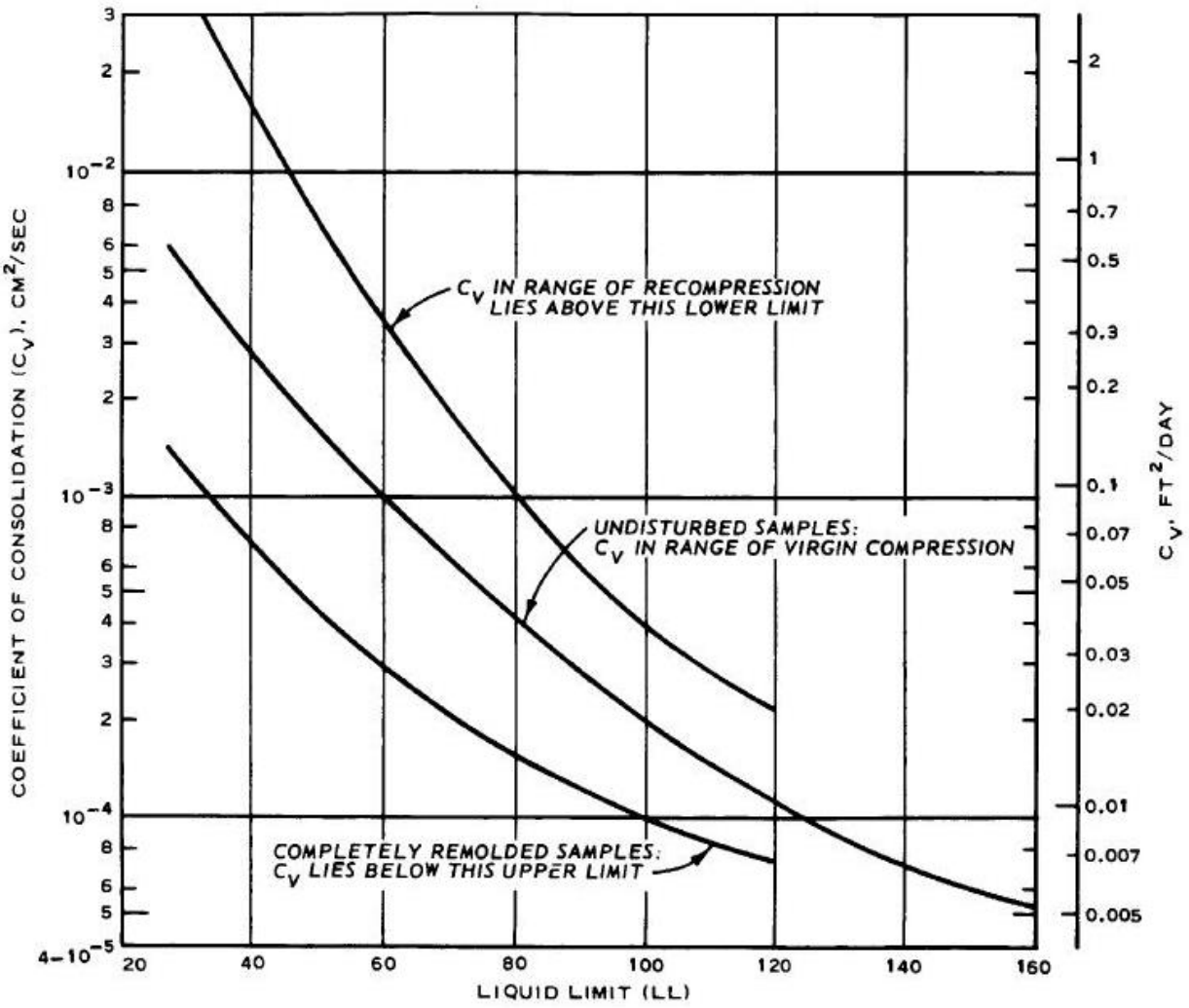

Figure 10. Correlations of C_v with Liquid Limit

Terzaghi (1943) also described two and three dimensional processes of consolidation. Excess water drains out of the fine-grained soil in parallel planes in two dimensional consolidation and the flow occurs in radial planes or the water particles travel along flow lines in three dimensional consolidation.

The differential equation for three-dimensional flow and deformation is written as,

$$\frac{\partial u}{\partial t} = c_v \left(\frac{\partial^2 u}{\partial x^2} + \frac{\partial^2 u}{\partial y^2} + \frac{\partial^2 u}{\partial z^2}\right) \quad [3.10]$$

where u is the excess pore water pressure, t is the time, and x, y, z are directions.

If the flow occurs only in one direction, assuming in the direction of the z axis, the other two terms in the brackets become zero and the differential equation becomes identical with the one-dimensional consolidation equation [3.11].

$$\frac{\partial u}{\partial t} = c_v \frac{\partial^2 u}{\partial z^2} \quad [3.11]$$

3.3 Embankment Construction

The process of changing the configuration of the ground surface is called earthwork. Soil or rock can be removed or added to make the construction site more suitable for the proposed development. An embankment is any artificial mound of soils used to build railroads and highways structures across low areas or to raise the profile of the structure, or to contain water (Sowers and Sowers, 1970). An embankment consists of multiple compacted layers or lifts of suitable soils, which are placed on top of each other until the level of the subgrade surface is reached. The subgrade surface is the top of the embankment. Engineering properties of the soils used in embankments and fills are controlled by method of construction, degree of compaction, and grain size distribution (Abramson et al., 2002). Any suitable material such as natural soils and aggregates may be used to construct embankments. Sands, gravels, silts, clays and the mixture of these soils are generally used for embankment fills.

Compacted properties of soil are very important because they control the final engineering properties of the embankment system. Compacted properties include optimum water content, maximum dry density, compressibility, shear strength, and hydraulic conductivity. The key geotechnical engineering design and construction parameters of embankments include stability and settlement of the underlying soils, the impact of the stability and settlement on the construction staging and time requirements, and the impact to adjacent and nearby structures (WSDOT Geotechnical Design Manual, 2010).

Most embankments are constructed by incremental processes. For example, Clough and Woodward (1967) presented a methodology to simulate the construction of an embankment by building it up as a series of discrete layers and assuming that the material is linearly elastic.

Construction of tall embankments on soft soils with low shear strength and high compressibility cannot be built rapidly because of the low shear strength of the subgrade. Staged construction is needed to overcome this problem. Staged construction of tall embankments on soils is shown in Figure 11. Applying loads in several steps leads to consolidation and strength gain in each step for the next loading shown in Figure 11.

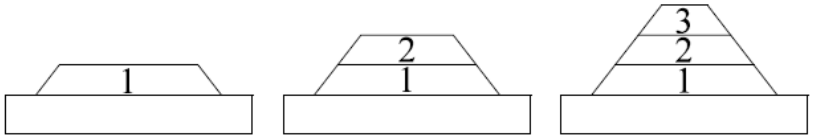

Figure 11. Sketch of staged construction of an embankment

The increase in undrained shear strength ΔS_u has been modeled by Edil (2013, personal communication) as

$$\Delta S_u = U\left(\frac{\Delta\sigma_v + 2\Delta\sigma_h}{3}\right) tan\varphi_{su} \qquad [3.12]$$

where U is the average degree of consolidation, $\Delta\sigma_v$ is vertical stress increase due to the stage, $\Delta\sigma_h$ is horizontal stress increase and φ_{su} is consolidated undrained friction angle. A representation of this gain in undrained shear strength during staged construction is represented in Figure 12.

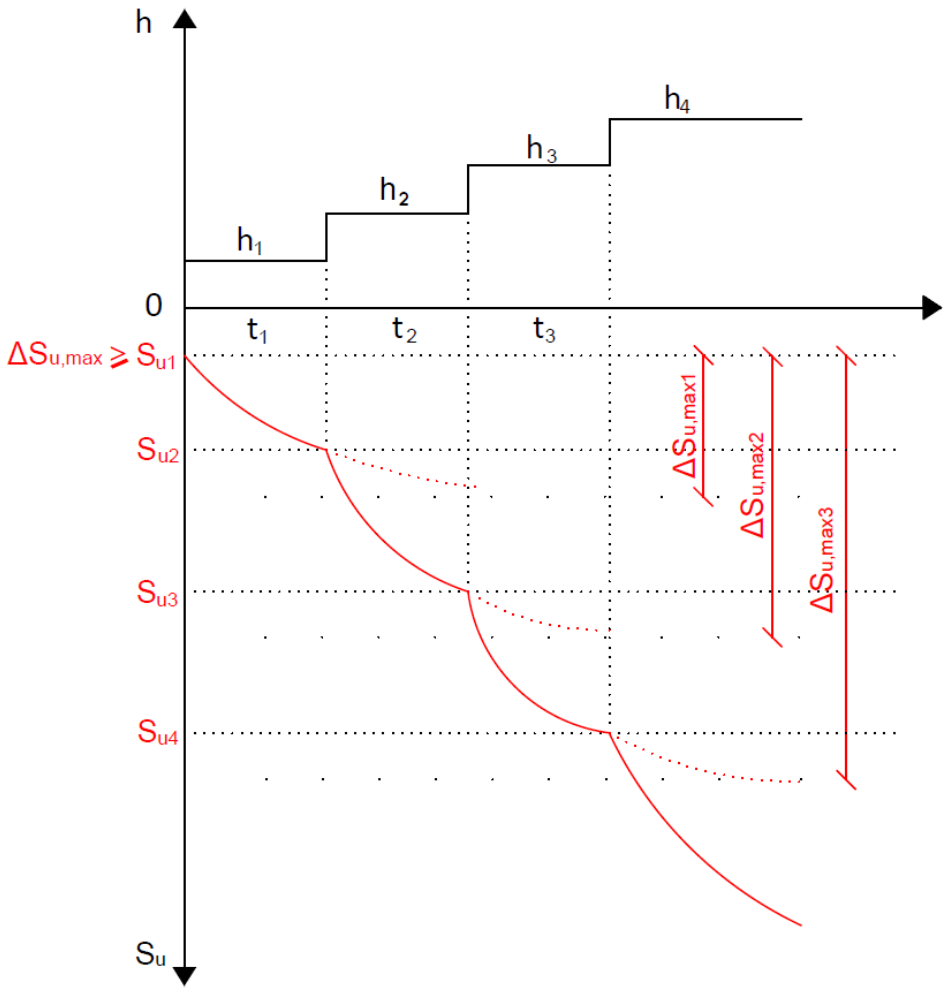

Figure 12. Increase in undrained strength with staged construction

3.3.1 Settlement Measurement during Construction

A high initial void ratio within foundation soils creates a condition in which large settlement may occur when effective stresses are increased. For this reason settlement measurements are very important for the monitoring of the response of soft soils during construction. Settlement measurement devices could be installed at various levels to measure settlements. These measurement devices are fixed to a point on the embankment to observe settlement relative to a moving datum. Therefore, this settlement is different from the vertical displacement usually considered in classical elastic theory, which is measured with reference to a fixed datum (Poulos et al., 1972).

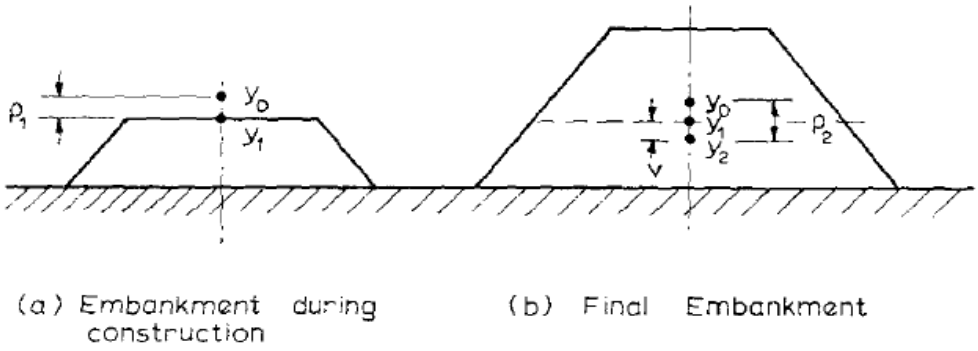

Figure 13. Difference between two displacements (Poulos et al., 1972)

In the study by Poulos et al. (1972), y_o represents the initial position of a point when no settlement occurs, y_1 is the position of that point after settlement due to construction to that level occurs and y_2 is the position of the point after completion of construction of the whole embankment shown in Figure 13. Poulos et al. (1972) indicated that the observed settlement will be the difference between the settlement of the final embankment (ρ_2) and the settlement of the partially constructed embankment (ρ_1).

Staged preload construction with surcharging is preferred to reduce post-construction settlements while allowing an increase in the shear strength of the foundation soil. Fill placement is monitored using a combination of surface and deep settlement gauge, standpipe, and pneumatic piezometers and slope inclinometers (Weech et al., 2009). Staged consolidation leads to an increase in effective stress, gain in shear strength and a reduction in void ratio of the embankment soil. With staged construction, embankments could be built on weak foundation materials. The most critical soil types for the embankment design are soft saturated soils because of their low hydraulic conductivity and their inability to rapidly dissipate excess pore water pressure (Weech et al., 2009). Fill material leads to an increase in total stress within the soil beneath the embankment and an initial increase in pore water pressure. Materials with high clay content have a low hydraulic conductivity; therefore, dissipation of excess pore water pressure is slow. These soils also show undrained behavior during embankment construction. Fill placement causes vertical compression and lateral expansion toward zones of lower confining pressure. These deformations cause increases in the shear strains and shear stresses within the foundation soils under the embankment and beyond the toe of the embankment (Weech et al., 2009).

Embankment fills over soft clay foundations tend to be stiffer than the foundation soils, which leads to problems such as embankment cracking when the foundation soil deforms and settles. Embankment fill over a soft clay foundation might also trigger failures due to stress-strain incompatibility between the embankment and the foundation (Abramson et al., 2002). Failure conditions occur when the applied shear stresses reach shear strength of the soil which means no additional stresses can be resisted. The ratio of the load to the available strength of subsoil must be within the acceptable factor of safety; therefore, the rate of increase in loading during construction must be limited (Chin and Sew, 2000).

3.3.2 Stability Analysis of an Embankment

Factor of safety is defined as the ratio of the structural capacity of the structure to the applied loads (Abramson et al., 2002). However, for soil bodies such as road and rail embankments or earthen dams the situation is different, as the dominating load comes from soil embankment weight itself and not from an external service force (Brinkgreve and Bakker, 1991). Factors of safety used in stability analysis depend on the method of analysis, reliability of the design method, reliability of the design soil parameters and consequences of failure in terms of human life and economic loss (Chin and Sew, 2000). There is not a specific value or method for factor of safety determination in embankment design but, in practice, generally the factor of safety ranges between 1.2 and 1.5 (O'Riordan and Seaman, 1993). A low factor of safety leads to an increase in possibility of large vertical settlements and lateral deformations and risk of failure.

Different potential failure surfaces must be considered during the stability analysis of the embankment. Examples of circular and non-circular failure surfaces are showed in Figure 14. Circular failure surfaces may not yield the lowest factor of safety, especially for embankments where thin clay layers exist. In this case, translational failure generally dominates (Chin and Sew, 2000).

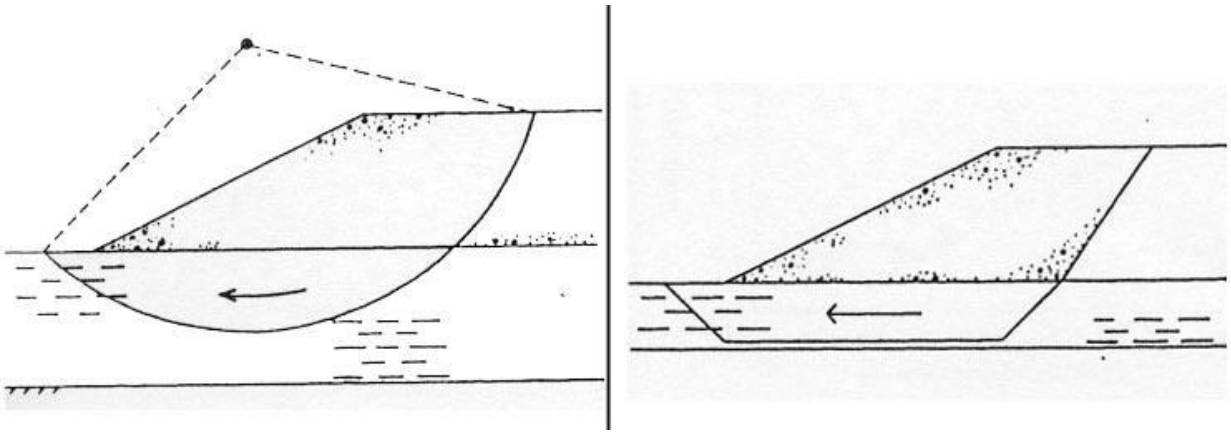

Figure 14. Examples of circular & non-circular failure surfaces (Chin and Sew, 2000)

3.3.3 Embankment Foundations

As indicated before, the most critical soil types for the embankment design and construction are soft saturated soils. However, there are three more embankment foundation types which are termed faulty foundations and are critical for embankment construction (Sowers and Sowers, 1970 - Figure 15). Staged construction is needed for the strength improvement of soft soils beneath embankments, and also light weight fill materials or flat slopes could be used to reduce the stresses beneath the fill to a safe amount (Figure 15a). A gravel berm near the toes of the slope acts as a counterweight to prevent bulging from taking place and also to help prevent failures.

In Figure 15b, soil is considered strong enough to support the fill without failure but it is so compressible which leads to severe settlements. Organic silts, organic clays and peat could be listed for highly compressible soils (Sowers and Sowers, 1970). Slow construction, use of sand piles or excavation of the compressible soil could be done to prevent excessive settlements.

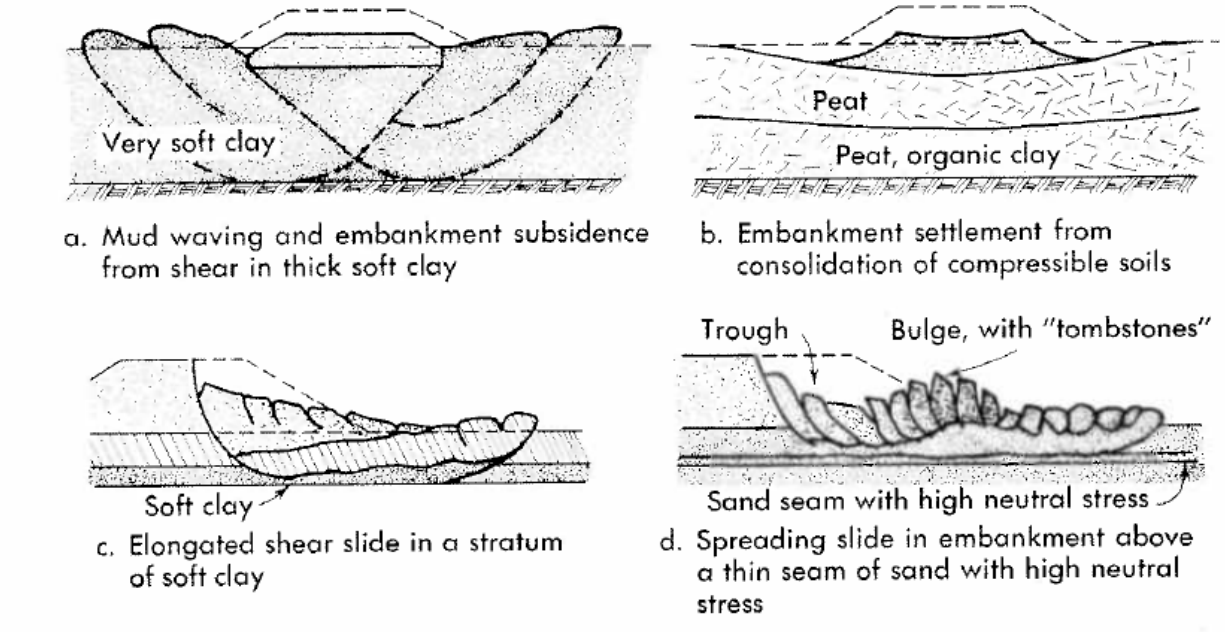

Figure 15. Embankment foundation problems (Sowers and Sowers, 1970)

The third type of faulty foundation of embankment includes the presence of thin strata of soft clay as seen in Figure 15c. Fills on thin soft soil fail by sliding horizontally along failure surface. Lightweight fills, flat slopes, and slow construction are the main methods to increase the safety of embankment (Sowers and Sowers, 1970).

When pressure builds up in thin strata beneath the embankment, failure may take place suddenly without any warning because near the toe the confining effective stress is small and $(\sigma - u)\, tan\varphi$ may approach zero (Sowers and Sowers, 1970 - Figure 15d). Safety of the embankment can be increased by drains that intercept the pervious strata.

3.3.4 Embankment Construction Methods

To increase the embankment stability, modifications can be done to the embankment geometry. Stability of the embankment can be increased by reducing the slope angle or adding geotextiles to increase the shear strength of the embankment. Construction of counterweight berms also help in improving the stability of an embankment by increasing the length of potential failure surfaces (Figure 16 - Chin and Sew, 2000). The disadvantage of using counterweight berms is the need of larger land take and for the increase of fill materials.

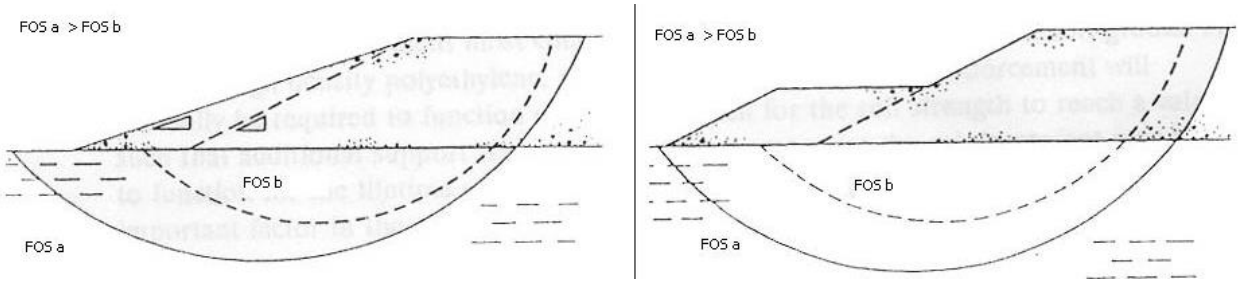

Figure 16. Reduction in slope and using of berms in embankment improvement (Chin and Sew, 2000)

During embankment construction loading, induced normal and shear stresses on the saturated soft soil are initially, and in part, taken by the pore water in the soil pores (Holtz et al. 2011). After time passes, excess pore water pressure from the soil is dissipated. This process could take years to occur depending on the thickness and the hydraulic conductivity of the formation. The engineering concern is that the initial shear strength demand may overcome the available shear strength in the foundation soil. The soil gains shear strength during the consolidation processes. To speed up the phenomenon of excess pore water pressure dissipation,

vertical drains or wick drains are installed vertically into soft soils during construction. Then, the pore water drainage paths are shortening by the drains, therefore permitting the saturated clay to consolidate in much shorter periods of time. Vertical drains may be used with staged construction to improve effectiveness of the method. Vertical drains should have sufficient capacity to discharge the water above or below the consolidating layer.

Figure 17 shows an illustration of an application of vertical drains. The installation process is generally performed by vibratory hammers and/or static methods.

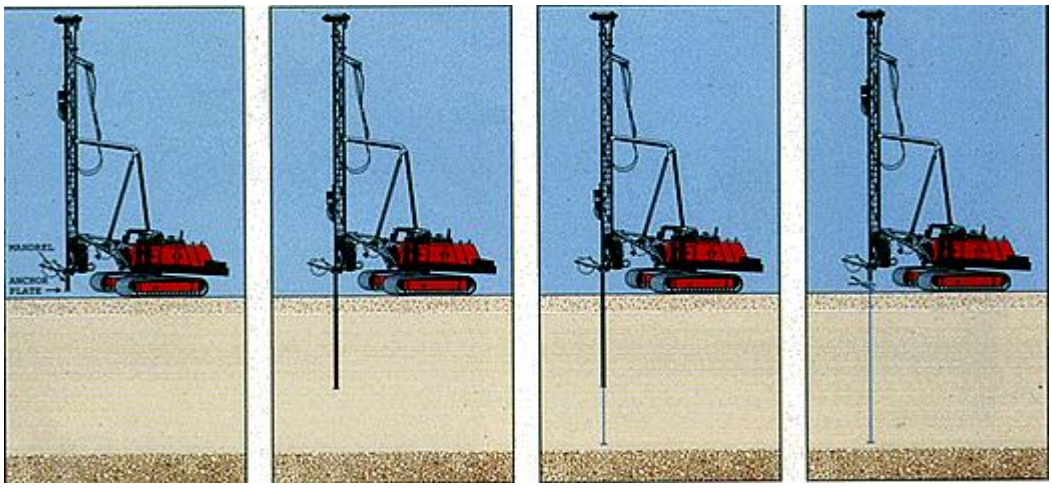

Figure 17. Illustration of an application of wick drains (Retrieved from http://www.johngrazelinc.com/foundationsst.htm)

Replacement of natural soft soils with a soil with better engineering properties could be used as an alternative to increase the stability of an embankment. However, if the soft foundation soil layer is thick, this procedure may not the most practical or economical way of construction. Ground water level also plays an important role on this technique. If the ground water level is higher than the soft soil layer, this method is more difficult to apply.

3.4 Geotechnical Instrumentation Methods

The main reasons for monitoring the geotechnical performance of structures are to reduce costs associated to uncertainties; damages and delays, decrease costs, and lessen risks (Marr 2001). Benefits of geotechnical instrumentation are listed in Table 2.

In general, there are two main types of measuring instruments. The first type is used to identify *in situ* properties of soils and rocks and the second type is used to monitor construction phases or operation of a long-term project (Dunnicliff 1993). Determination of strength, compressibility and hydraulic conductivity are the examples of the identification of in situ soil properties. Measurements of groundwater pressure, total stress, deformation and strain could be listed as the second type of measurement methods.

Since time-dependent behavior is important in the overall behavior of structures, geotechnical instrumentation is used to better understand soil behavior, ensure safety, control construction procedure, and provide data for measurement of quantities during the construction of an embankment. The behavior of embankments on soft soils is dominated by the properties of the soft ground, and the loading of the embankment leads to vertical settlement and lateral bulging of the soft ground. Dunnicliff (1993) indicates that the most frequent use of instrumentation for embankments on soft ground is to monitor the progress of consolidation and determine whether the embankment is stable.

Table 2. Benefits of using geotechnical instrumentation by Dunnicliff (1993)

Benefits During Design	Benefits During Construction	Benefits After Construction
1. Definition of initial site conditions 2. Proof testing 3. Fact finding in crisis situations	1.Safety 2.Observational Method 3.Construction control 4. Providing legal protection 5.Measurement of fill quantities 6.Enhancing Public Relations	Performance monitoring over the life of a structure, using observations and instrumentation is the only way to ensure long term safety.

3.4.1 Geotechnical Instrumentation Devices

3.4.1.1 Slope Inclinometers

Inclinometers, also referred as slope inclinometers, probe inclinometers and slope indicators, are used to determine the magnitude, rate, direction, depth and type of landslide movement (Stark and Choi, 2007). Inclinometers measure deformations normal to the axis of a pipe that guides the location of the sensor. There is a gravity-sensing transducer inside the probe to measure inclination with respect to the vertical (Dunnicliff, 1993). They are often used to monitor the performance of slopes and embankments. A typical inclinometer probe, cable, readout device and inclinometer casing are showed in Figure 18. Inclinometers could be installed in a borehole, embedded in a fill, cast in concrete or attached to a structure.

Figure 18. Typical slope inclinometer parts and inclinometer casing

(Retrived from http://onlinepubs.trb.org/onlinepubs/circulars/ec129.pdf)

3.4.1.2 Pore Pressure Transducers

Pore pressure transducers or piezometers are used to measure and monitor soil pore pressure or water table in boreholes. The sensors are sealed within the ground so that they respond only to groundwater pressure around themselves and not to ground water pressure at other elevations (Dunnicliff 1993). Piezometric pressures determine the pore water pressure and therefore the effective stresses influencing the shear strength of soil or rock. The dissipation of pore water pressure is directly related to the rate of consolidation. Therefore, piezometers can be used to control the rate of fill placement during embankment construction over soft soils (NDOT Geotechnical Policies and Procedures Manual, 2005). It is important to place piezometers before the construction in the strata that contribute to the settlement or shear strength. If the strata thickness is more than 3 m, additional piezometers should be placed to provide adequate coverage with depth (NDOT, 2005).

3.4.1.3 Settlement Gauges

Settlement gauges are used to monitor time dependent settlements that are related to average degree of consolidation as shown in Figure 19. The surveyed readings of the settlement gauge and the fill levels are used to determine the change in elevations. Soil settlement gauges help to determine the effectiveness of soil improvement techniques such as wick drains, dynamic compaction and preloading.

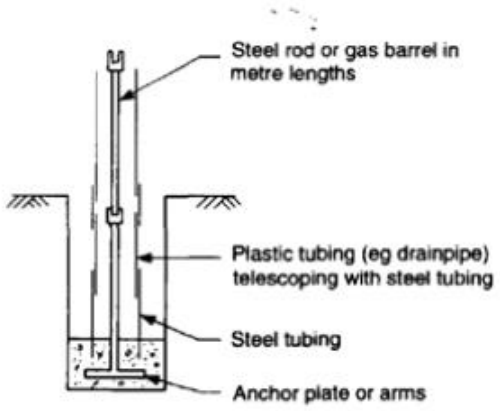

Figure 19. Simple rod settlement gauge

(Retrived from http://www.geotechnique.info/SI/SI%20Book%20Chapter%2010.pdf)

4 Numerical Model Methods

Burland (1987) presented a chart known as the Burland Triangle that explains geotechnical engineering practice to be comprised of three parts: (1) establishing the ground profile, (2) defining ground behavior and (3) modeling (Figure 20). The Burland Triangle aims at highlighting the process of modeling as an integral and integrated part of the engineering design process. All of these three major parts are dependent on each other. Ground profile investigation, sampling is necessary to identify soil behavior by conducting laboratory and field tests. Soil properties and profiles are necessary to model and analyze the critical results.

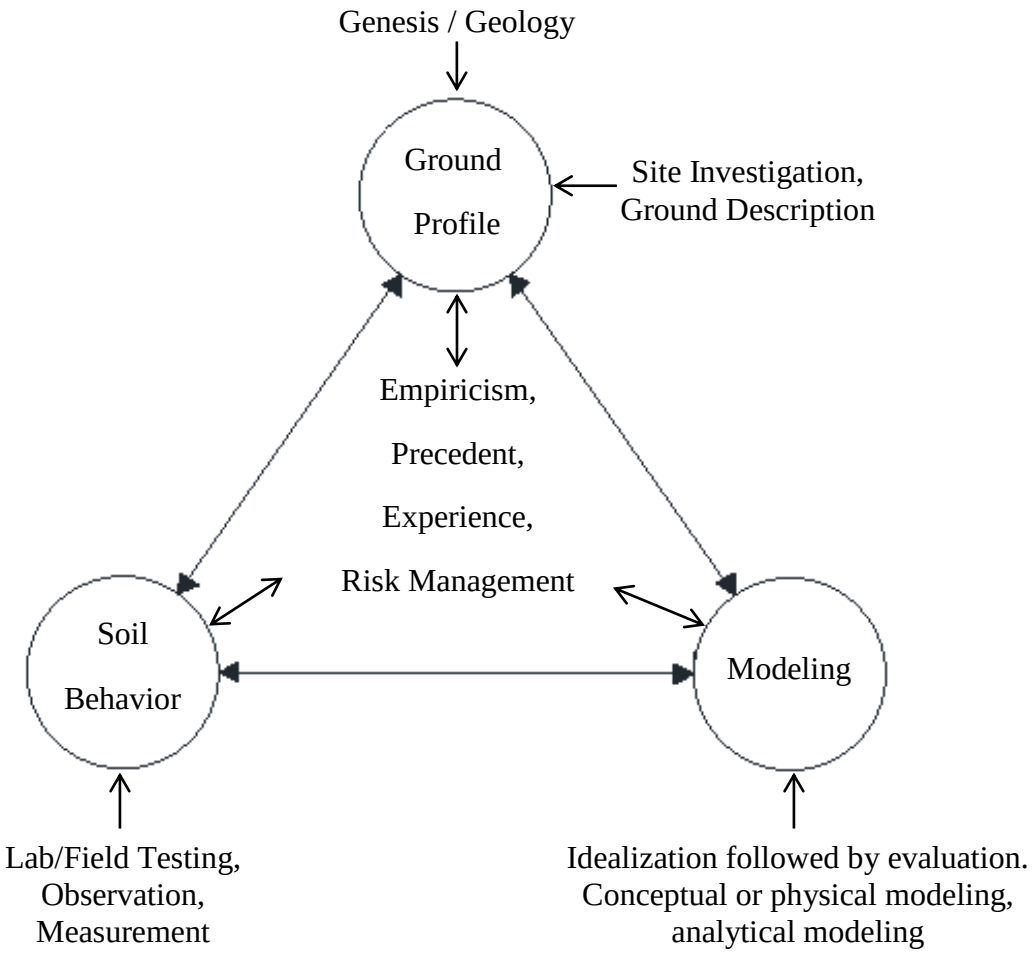

Figure 20. Expanded Burland Triangle

Modeling is the process used to construct a simplified mathematical reality from a more complex physical reality (Barbour and Krahn, 2004 - Figure 21).

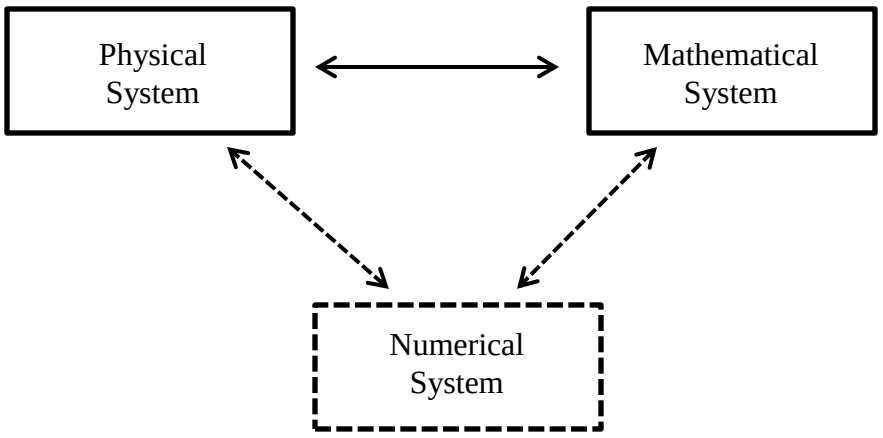

Figure 21. Simple definition of modeling (Barbour and Krahn, 2004)

4.1 PLAXIS 2D

PLAXIS 2D is a finite element package used to analyze deformation and stability of geotechnical applications intended for two-dimensional analysis. Advanced constitutive models are used for the simulation of the nonlinear, time dependent and anisotropic behavior of soils and rocks. Automatic unstructured 2D finite element meshes with options for global and local mesh refinement can be generated. There are five different options of mesh coarseness: very coarse, coarse, medium fine and very fine with an increase of number of elements approximately from 50 to 1000. Quadratic 6-node and 4^{th} order 15-node triangular elements are available to model the deformation and stresses in the soil (PLAXIS 2D Manual, 2002). The 6-node triangles provide for quick calculation but the 15-node elements provide a more accurate calculation of stresses and failure loads. During finite element calculations, displacements are calculated at the

nodes: however, stress and strains are calculated at individual Gaussian integration points (or stress points) rather than at nodes. The 15-node triangular element has 12 stress points and the 6-node triangular element has 3 stress points. Distribution of the nodes and stress points over an element is shown in Figure 22.

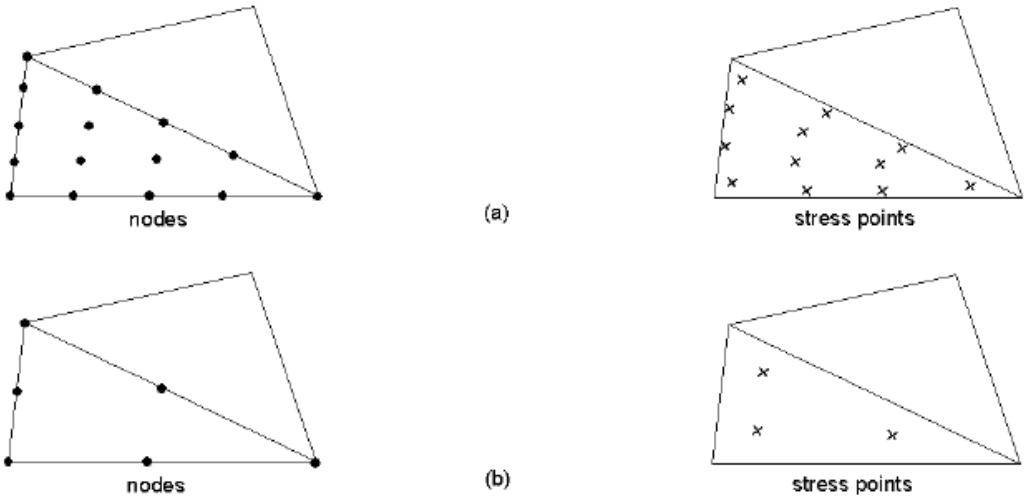

Figure 22. Nodes and Stress points, a) 15-node triangular element b) 6-node triangular element (PLAXIS 2D Tutorial Manual, 2002)

4.2 PLAXIS 3D

PLAXIS 3D FOUNDATION is a finite element package intended for three-dimensional deformation and stability analysis of foundation structures including piled foundations and offshore structures. Static elasto-plastic deformation, advanced soil models, consolidation and safety analysis can be done with the 3D version. Three-dimensional calculations are needed to simulate soil behavior, soil-structure interaction and structural behavior (PLAXIS 3D Foundation Tutorial Manual, 2007). Quadratic 15-node wedge elements are available to model deformations

and stresses in the soil. Soil stratigraphy and structure levels as defined in boreholes and work planes are taken into account to generate 3D meshes.

Both of the PLAXIS models are used during parametric studies for different embankment and soil geometry, soil properties, boundaries and time intervals.

4.3 Material Models

There are five different material models for PLAXIS 2D: (1) Mohr-Coulomb model, (2) jointed rock model, (3) hardening soil model, (4) soft soil creep model and (5) soft soil model. The Mohr-Coulomb, hardening soil and soft soil creep models are the three main material models that are used in PLAXIS 3D. Each model has different advantages and disadvantages depending on the soil conditions, loading type, creep and time effects.

Mohr-Coulomb Model (MC Model): This is the most simple and limited non-linear perfect plasticity, model which is frequently used to model soil behavior in finite element applications (Brinkgreve, 2004). Plasticity is related to irreversible strains and to understand whether or not plasticity occurs the yield function, f, is introduced as a function of stress and strain. A perfectly plastic model is defined by model parameters and is not affected by plastic straining (PLAXIS 2D and 3D Material Manual, 2002-2007).

The basic principle of elasto-plasticity is that strains are decomposed into elastic and plastic components. The material is linearly elastic up to the yield point and then becomes perfectly plastic, which means the material continues to strain even when no additional stresses are applied (Holtz et al., 2011). The basic idea of an elastic perfectly plastic model is provided in Figure 23.

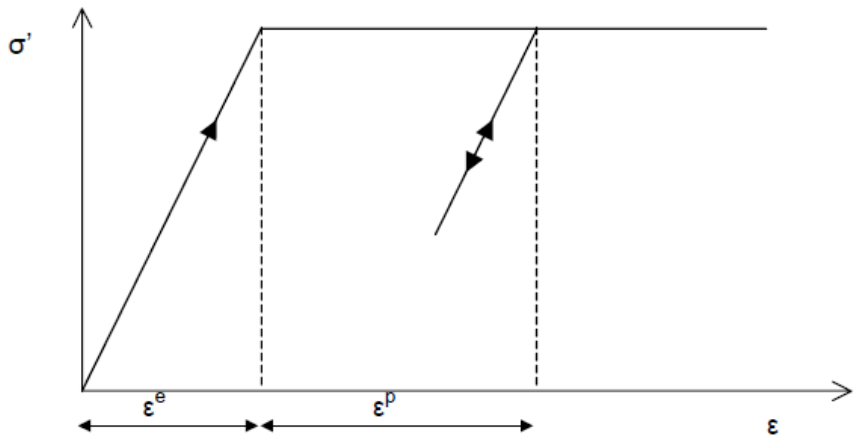

Figure 23. An elastic perfectly plastic model (PLAXIS 3D Material Manual, 2007)

Young's modulus (E), Poisson's ratio (ν), friction angle (ϕ), shear intercept (c) and dilatancy angle (ψ) are the five basic parameters of the Mohr-coulomb model:

- *Young's modulus* is defined as the ratio of the uniaxial stress (σ) to the strain (ϵ) in the direction of the applied stress.
- *Poisson's ratio* is defined as the negative ratio of the strain in the direction perpendicular to loading to the strain parallel to the loading direction.
- *Shear intercept* is defined as the intercept of the straight line which is drawn to fit through measured shear stress and normal stress values. PLAXIS cannot handle truly frictional materials such as soils; therefore, at least a small value (c > 0.2 kPa) must be entered into the code. This is a limitation of the code as soils are always frictional materials with no shear intercept unless the soil particles are cemented.

- *Friction angle* is the angle on the Mohr's circle of the shear stress and normal effective stresses at which shear failure occurs and entered in degrees. Shear intercept and friction angle are provided in Figure 24.
- *Dilatancy angle* is entered in degrees and depends on both the density and effective state of stress. Normally consolidated clays and loose sands tend to show little dilatancy (ψ~0). For dense sands and the overconsolidated clays the dilation angle is calculated by,

$$\Psi = atan\left(\frac{\delta y}{\delta x}\right) \quad [4.1]$$

where δy is the change in vertical displacement and δx is the change in horizontal displacement. When the volume of soil remains constant due to sliding and rotating of soil particles such so that the soil has reached a critical state, then $\delta y/\delta x = 0$ and the dilation angle becomes zero.

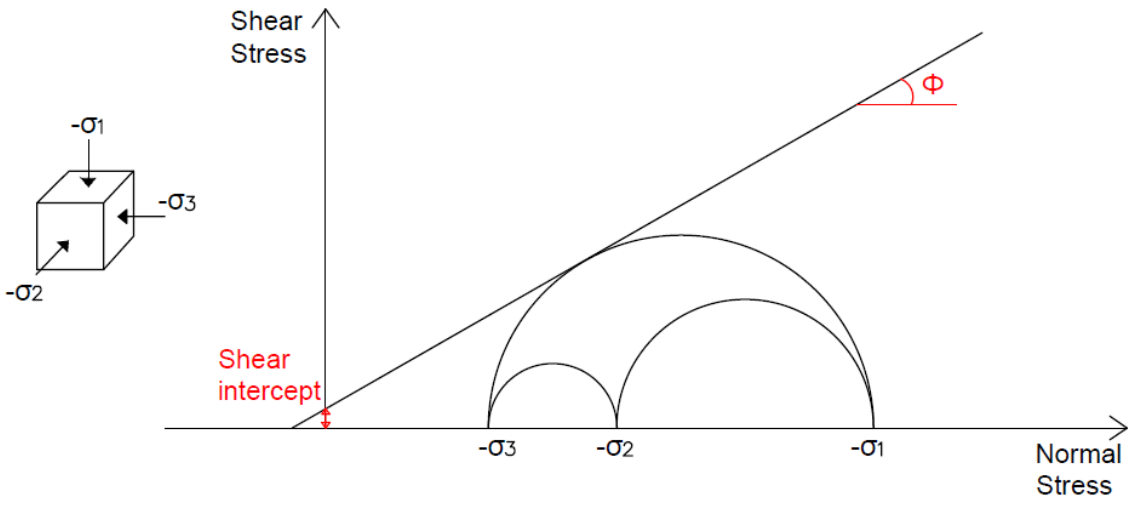

Figure 24. Representations of shear intercept and friction angle on Mohr's circle

The Jointed Rock Model (Anisotropy): An isotropic material has different mechanical properties in different directions. In general clay deposits are assumed to be isotropic but the actual mechanical behavior of most clays is directionally dependent, which means shear strength and compressibility depend on the direction of deposition and the in-situ stresses (Holtz et al., 2011). Elastic anisotropy refers to the use of different elastic stiffness properties in different directions and plastic anisotropy refers to the use of different strength properties in different directions which is considered as Jointed Rock Model. The Jointed Rock model is an anisotropic, elastic, perfectly plastic model which is used to simulate the behavior of stratified and jointed rock layers (PLAXIS 2D Material Manual, 2002). The mechanical behavior of jointed rock masses is strongly affected by the properties and geometry of the joints (Cai and Horii, 1992). Assumption of intact rock with an eventual stratification direction and major joint directions is provided in Figure 25. The Jointed Rock Model is suitable for rocks therefore not related with this study.

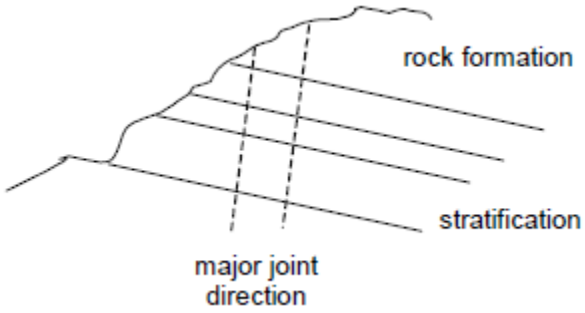

Figure 25. Visualization of concept behind the Jointed Rock model

(PLAXIS 2D Material Manual, 2002)

The Hardening Soil Model (Isotropic Hardening): Hardening soil model (HS-Model) is an advanced hyperbolic soil model formulated in the framework of hardening plasticity. In the

model, the total strains are calculated using a stress-dependent stiffness, which is different for virgin loading and unloading, which is the main difference with the Mohr-Coulomb model (Schanz et al., 2000). Triaxial loading stiffness (E_{50}), triaxial unloading stiffness (E_{ur}) and the oedometer loading stiffness (E_{oed}) are identified in this model. The hardening soil model took the place of well-known hyperbolic model by Duncan and Chang (1970) by using the theory of plasticity rather than the theory of elasticity, secondly including soil dilatancy and thirdly introducing a yield cap. The plastic strains are calculated by introducing a multi-surface yield criterion by Schanz et al. (2000). That yield surface is not fixed but can expand during plastic straining (PLAXIS 2D Material Manual, 2002).

Friction angle, shear intercept and dilatancy angle are the failure parameters as in Mohr-Coulomb model. Besides these parameters, secant stiffness in standard drained triaxial test (E_{50}^{ref}), tangent stiffness for primary oedometer loading (E_{oed}^{ref}), and power for stress-level dependency of stiffness (m) are the basic parameters for soil stiffness. There are seven advanced parameters which are advised for use as default settings in PLAXIS which are listed below (PLAXIS 2D Material Manual, 2002): E_{ur}^{ref}: Unloading / reloading stiffness (default $E_{ur}^{ref} = 3 * E_{50}^{ref}$)

ν_{ur}: Poisson's ratio for unloading-reloading (default ν_{ur}=0.20)

p^{ref}: Reference stress for stiffness (default p^{ref}=100stress units)

R_f: Failure ratio qf / qa (default R_f=0.9, where qa is the asymptotic value of the shear strength, Figure 26)

K_0^{nc}: K_0-value for normal consolidation (default K_0^{nc}=1-sinϕ)

$\sigma_{tension}$: Tensile strength (default $\sigma_{tension}$=0 stress units)

$c_{increment}$: As in Mohr-Coulomb model (default $c_{increment}$=0)

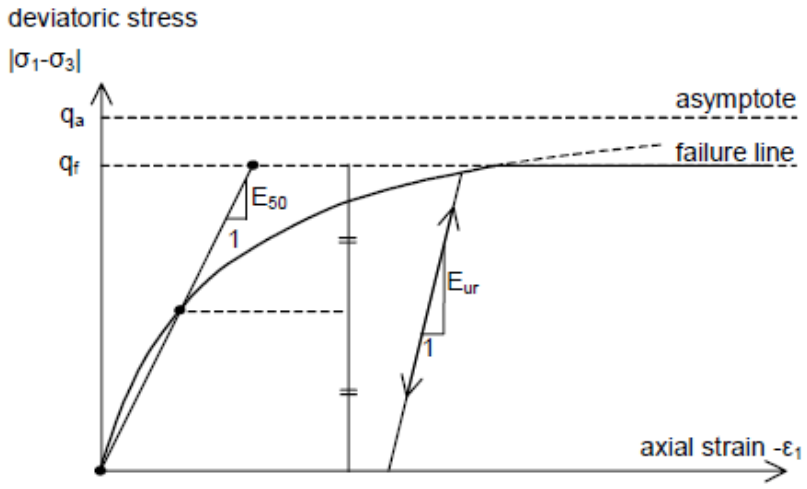

Figure 26. Hyperbolic stress-strain relation in primary loading for a standard drained triaxial test

(PLAXIS 2D Material Manual, 2002)

$$E_{50}=E_{50}^{ref}\cdot\left(\frac{c\cdot cos\varphi-\sigma'_3\cdot sin\varphi}{c\cdot cos\varphi+p^{ref}\cdot sin\varphi}\right)^{m} \quad [4.2]$$

$$E_{ur}=E_{ur}^{ref}\cdot\left(\frac{c\cdot cos\varphi-\sigma'_3\cdot sin\varphi}{c\cdot cos\varphi+p^{ref}\cdot sin\varphi}\right)^{m} \quad [4.3]$$

where σ'_3 is the confining pressure in the triaxial test, m is taken as 1 for soft clays, 0.5 for Norwegian sands and silts (Janbu, 1963) and 0.5< m<1 (Von Soos, 1980).

$$\mathrm{E}_{oed}=\mathrm{E}_{oed}^{ref}\cdot\left(\frac{c\cdot cos\varphi-\sigma'_3\cdot sin\varphi}{c\cdot cos\varphi+p^{ref}\cdot sin\varphi}\right)^{m} \quad [4.4]$$

where E_{oed}^{ref} is a tangent stiffness at a vertical stress is equal to p^{ref} which is provided in Figure 27.

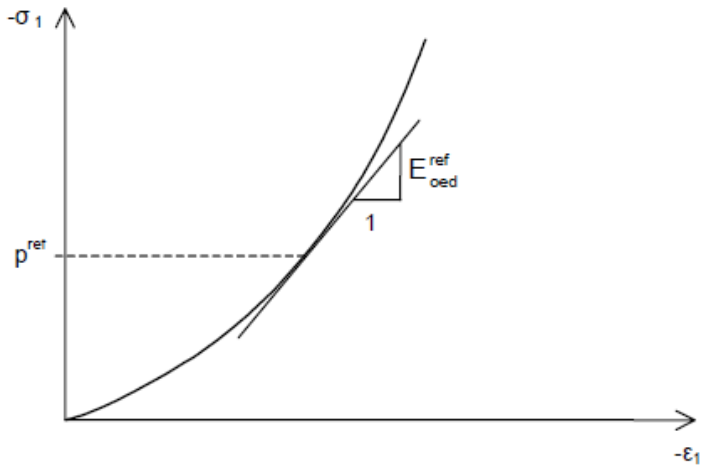

Figure 27. Definition of E_{oed}^{ref} in oedometer test results (PLAXIS 2D Material Manual, 2002)

Soft Soil Model: The Soft Soil Model (SS model) is known as the Modified Cam Clay model. A logarithmic relationship between the volumetric strain and mean effective stress is assumed in SS-model (Neher et al., 2001). There is an improved version of the SS-model, which includes time and strain-rate effects, termed the Soft Soil Creep Model (SSC model). Brinkgreve's study (2004) proved that when all parameters in the SSC model are similar to the corresponding parameters in the SS model, similar settlements under the embankment after construction with 100 days; however, the SSC model shows larger settlements than the SS model at 1000 days after construction due to the creep effect.

Soft Soil Creep Model (Time-dependent Behavior): Vermeer and Neher (2000) presented Buisman's observation (1936) on total soft soil settlements that cannot be solely explained by

classical consolidation theory. A constitutive law for creep was thus proposed creep behavior under constant effective stress is formulated as,

$$\varepsilon = \varepsilon_c - C_B \log\left(\frac{t}{t_c}\right) \; for \; t > t_c \qquad [4.5]$$

where ε_c is the strain up to the end of consolidation, t the time measured from the beginning of loading, t_c the time to the end of primary consolidation and C_B is a material constant.

Vermeer and Neher (2000) also presented Butterfield's equation (1989) to describe secondary compression,

$$\varepsilon = \varepsilon_c + C \ln\left(\frac{\tau_c + t'}{\tau_c}\right) \qquad [4.6]$$

where ε is the logarithmic strain defined as,

$$\varepsilon = -\ln\left(\frac{1+e}{1+e_0}\right) \qquad [4.7]$$

and the parameter C is calculated by,

$$C = \frac{C_\alpha}{(1+e_0)\, ln10} = \frac{C_B}{ln10} \qquad [4.8]$$

Vermeer and Neher (2000) describe the end of consolidation strain ε_c by an equation of the form,

$$\varepsilon_c = \varepsilon_c^e + \varepsilon_c^c = A\ ln\ \frac{\sigma'}{\sigma_0'} + B\ ln\ \frac{\sigma_{pc}}{\sigma_{p0}} \quad [4.9]$$

where σ_0' represents the initial effective pressure loading and σ' is the final effective loading pressure, σ_{p0} and σ_{pc} represent the preconsolidation pressure before loading and end of consolidation state, respectively. Parameters A and B are calculated by

$$A = \frac{C_r}{(1+e_0)\ ln10}\ B = \frac{(C_c\ C_r)}{(1+e_0)\ ln10} \quad [4.10]$$

where C_r is the swelling index and C_c is the compression index. Combining equations (4.6) and (4.9), the total logarithmic strain due to an increase in effective stress is calculated by

$$\varepsilon_c = \varepsilon_c^e + \varepsilon_c^c = A\ ln\ \frac{\sigma'}{\sigma_0'} + B\ ln\ \frac{\sigma_{pc}}{\sigma_{p0}} + C \ln\left(\frac{\tau_c + t'}{\tau_c}\right) \quad [4.11]$$

The parameters used in equation (4.11) presented in Figure 28.

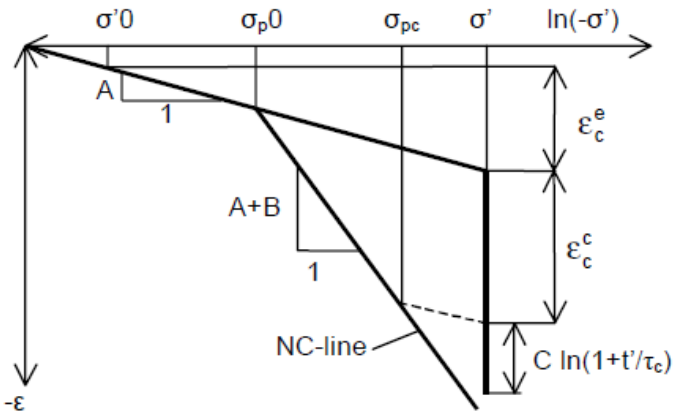

Figure 28. Idealized stress-strain curve from oedometer test with division of strain increments into elastic and a creep components (Vermeer and Neher, 2000)

The Soft Soil Creep model is an elastic viscoplastic model, formulated as a relationship between stress rates and total strain rates, which are decomposed into elastic strain rates and creep strain rates (Brinkgreve, 2004). Normally consolidated clays, clayey silts and peat are considered as soft soils and their high degree of compressibility is the main property of these materials. Vermeer and Neher (2000) indicated that HS-Model is perfectly suitable for soft soils but is not suitable when considering creep as all real soils exhibit some level of creep, therefore, primary compression is always followed by a certain amount of secondary compression. Even if it is assumed that secondary compression is a small percentage of the primary compression, creep effects are important in problems involving large primary compression.

Large primary compression generally occurs on road, river or dam embankments on soft soils. Friction angle, shear intercept and dilatancy angle are the failure parameters as in Mohr-coulomb model. Besides these parameters, there are additional five failure parameters which are listed below (Vermeer and Neher, 2000):

K^*: Modified swelling index

λ^*: Modified compression index

μ^*: Modified creep index

ν_{ur}: Poisson's ratio for unloading-reloading

M: Slope of the critical state line

Isotropic compression test and oedometer test are used to obtain these parameters and also there are mathematical relations to determine the parameters,

Table 3**.** Relationship to Cam-Clay parameters

$\lambda^* = \frac{\lambda}{1+e}$	$K^* = \frac{K}{1+e}$

Table 4**.** Relationship to internationally normalized parameters

$\lambda^* = \frac{C_c}{2.3 \cdot (1+e)}$	$K^* \sim \frac{2}{2.3} \cdot \frac{C_r}{1+e}$	$\mu^* \sim \frac{C_\alpha}{2.3 \cdot (1+e)}$

where e is void ratio, C_c is compression index, C_α is creep index, C_r is swelling index and λ and K are Cam-Clay parameters. There are additional correlations exist to make a rough estimate of model parameters, λ^*/μ^* is in the range 15 to 25 and the λ^*/K^* is in the range 5 to 10 (Vermeer and Neher, 2000). Brinkgreve (2004) used the ratio λ^*/K^*=5 in soft plastic clay. Poisson's ratio is an elastic constant with a range between 0.1 and 0.2 in the Soft Soil Creep model (Vermeer and Neher, 2000). Brinkgreve (2004) and Ozcoban (2007) used value of 0.15 in their Soft Soil Creep models.

The slope of the critical state line, M determines the steepness of the yield contour in p-q plane. In PLAXIS, the user may choose a value for K_0^{NC} that corresponds to the default setting M which means user do not enter directly a particular value of M (PLAXIS 2D Material Manual, 2002). Corresponding value of M is calculated from the relation (Brinkgreve, 1994):

$$M = \sqrt[3]{\frac{(1-K_0^{NC})^2}{(1+2K_0^{NC})^2} + \frac{(1-K_0^{NC})*(1-2\nu_{ur})*(\frac{\lambda^*}{K^*}-1)}{(1+2K_0^{NC})*(1-2\nu_{ur})*\frac{\lambda^*}{K^*}-(1-K_0^{NC})*(1+\nu_{ur})}} \quad [4.12]$$

4.4 Dimensional Analysis for Embankment Construction over Soft Soils

Dimensional analysis is used to reduce the large group of variables which arise in practical problems to a minimum set and also to design dimensionally valid models of many kinds (Butterfield, 1999). Buckingham's "Pi" theorem (Buckingham 1914) is used to identify the dimensionless parameters controlling the behavior of the physical problem. "A dimensionless quantity is one of which the numerical value does not change when the sizes of fundamental units alter, so long as the relations between the derived and the fundamental units are kept unchanged" (Buckingham 1914).

Friction angle (φ), embankment height (H), reinforcement length (L), Young's Modulus (E), Poisson's ratio (ν), unit weight (γ), undrained shear intercept (S_u), hydraulic conductivity (k), bending stiffness (EI) and axial stiffness (EA) are the main input parameters for MSEW problem at the Green Bay embankment site. These parameters are used in the dimensional analyses modeling of the problem in PLAXIS 2D.

These eleven quantities must be connected by some sort of relation symbolized by writing;

$$F = (\varphi, H, L, E_u, \nu, \gamma, S_u, k, EI, EA) = 0$$

$\varphi = dimensionless$

$H = l$

$L = l$

$E_u = m\, l^{-1} t^{-2}$

$\nu = \ dimensionless$

$\gamma = m\, l^{-2}\, t^{-2}$

$S_u = m\, l^{-1}\, t^{-2}$

$k = m\, t^{-1}$

$EA = m\, l\, t^{-2}$

$EI = m\, l^{\,3} t^{-2}$

There are 10 separate kinds of quantities involved in the relation so that n=10, but the units needed for measuring them can all be derived from k=3 fundamental units which are mass m, length l, and time t. The independent parameters become n-k=7. Hence, whatever the nature of the relation may be, it must be reducible by applying a "PI" theorem,

$$f(\pi_1, \pi_2, \pi_3, \pi_4, \pi_5, \pi_6, \pi_7) = 0$$

containing not 10 but only 7 independent variables. These dimensional parameters for the case of the embankment problem could be listed as H/L, S_u/E_u, $(\gamma H)/S_u$, $(\gamma H)/E_u$, $k/(\Delta H/t)$, φ, ν.

As the Buckingham's "Pi" theorem does not provide information on which one of these parameters control the behavior of the physical system, most of the dimensional parameters are evaluated using a numerical model developed in PLAXIS.

5 Numerical Model Development

5.1 Numerical Model of MSEW on Soft Foundation Soil

Budge et al. (2006) presents a process used to calibrate PLAXIS software model using the vertical deformations measured during the construction of a MSE wall located at Salt Lake City, Utah. The wall was constructed on soft, compressible lacustrine deposits, and instrumentation was placed in this material to monitor foundation response. MSE wall photographs from the construction site are presented in Figure 29. Vertical and horizontal deformations within the wall and in the foundation material, stresses in the wall reinforcement, and increases in the vertical stresses within the wall were monitored during the construction (Budge et al., 2006).

Figure 29. Photographs of the MSE wall constructed at 3600 south and I-15 in Salt Lake City-Utah (Budge et al., 2006)

The soil profile and selected instrumentation for the MSE wall are shown in Figure 30. Constant rate of strain (CRS) consolidation tests and triaxial compression tests were used for

different soil layers to determine the strength and stiffness properties. A PLAXIS model was developed using the appropriate wall geometry and estimated soil properties.

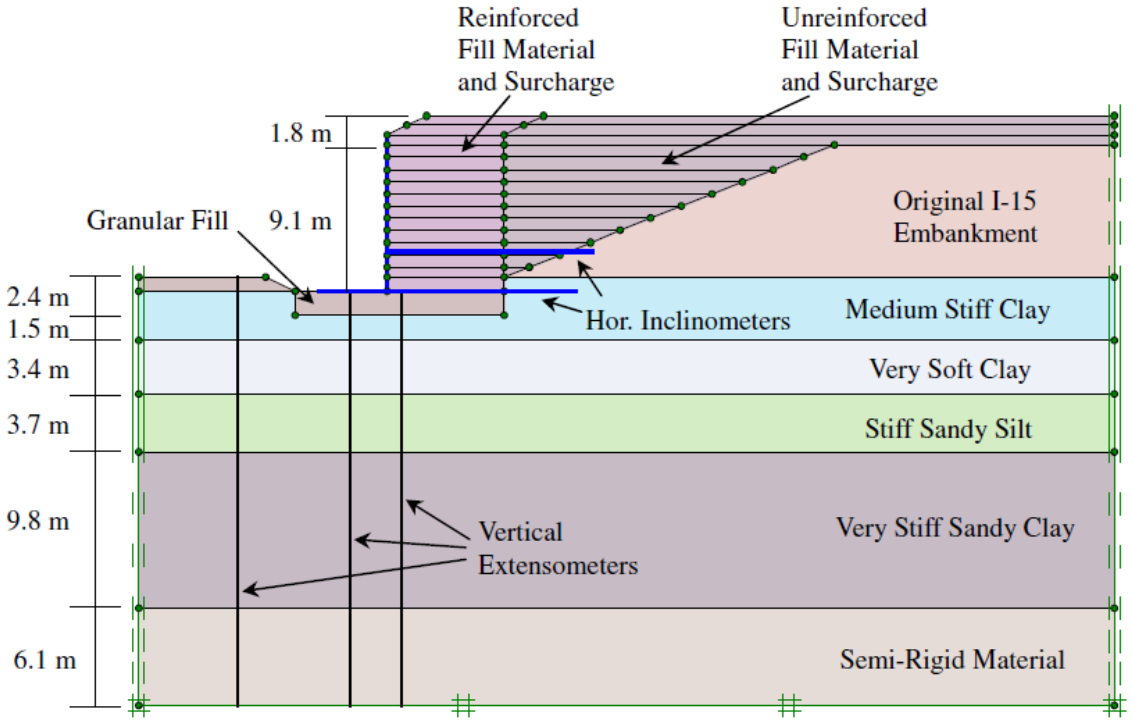

Figure 30. Soil profile and selected instrumentation for MSE wall (Budge et al., 2006)

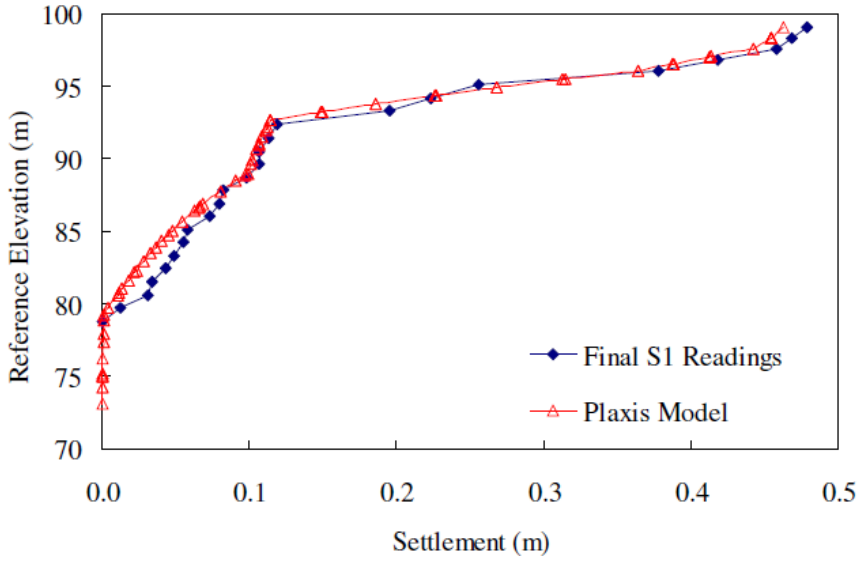

Figure 31. Comparison of vertical inclinometer data to PLAXIS model data

(Budge et al., 2006)

The Hardening Soil constitutive model, which allows soil moduli to vary as a function of stress, was used as a material model in PLAXIS. Budge et al. (2006)'s study compared the deformations measured in the vertical extensometer within the wall footprint with the vertical deformations at the same positions in the PLAXIS model. Figure 31 shows how vertical settlement in the model matches quite well with the measured data for the wall. Budge et al. (2006) adjusted the moduli if necessary and also they repeated the model for several iterations until deformations matched well. Significant deformation between reference elevations 96 m and 92 m is caused by the very soft clay layer. There is also a nice calibration for the vertical movement along the lower horizontal inclinometer shown in Figure 32. Budge et al. (2006) showed that the horizontal inclinometer comparison confirm that the model is able to replicate the measured foundation response.

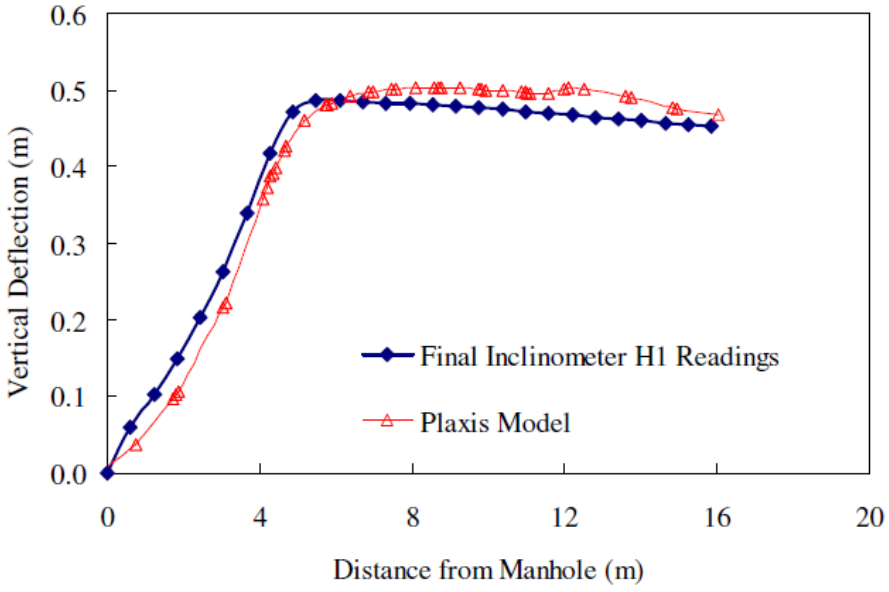

Figure 32. Comparison of horizontal inclinometer data to PLAXIS model data (Budge et al., 2006)

5.1.1 Simulating Construction Site Conditions

Pore pressure transducers and settlement gauges were used to observe the relationship between excess pore water pressure, time dependent settlements and staged construction of tall embankments at different locations of the construction site. Instrumentation data from settlement gauges and piezometers were used to validate with finite element model. The soil profile and PLAXIS model are shown on Figure 33. Due to symmetry about the vertical line through the center of the embankment, only half of the embankment was analyzed. Soil, wall facing and geogrid parameters presented in Tables 5-6-7.

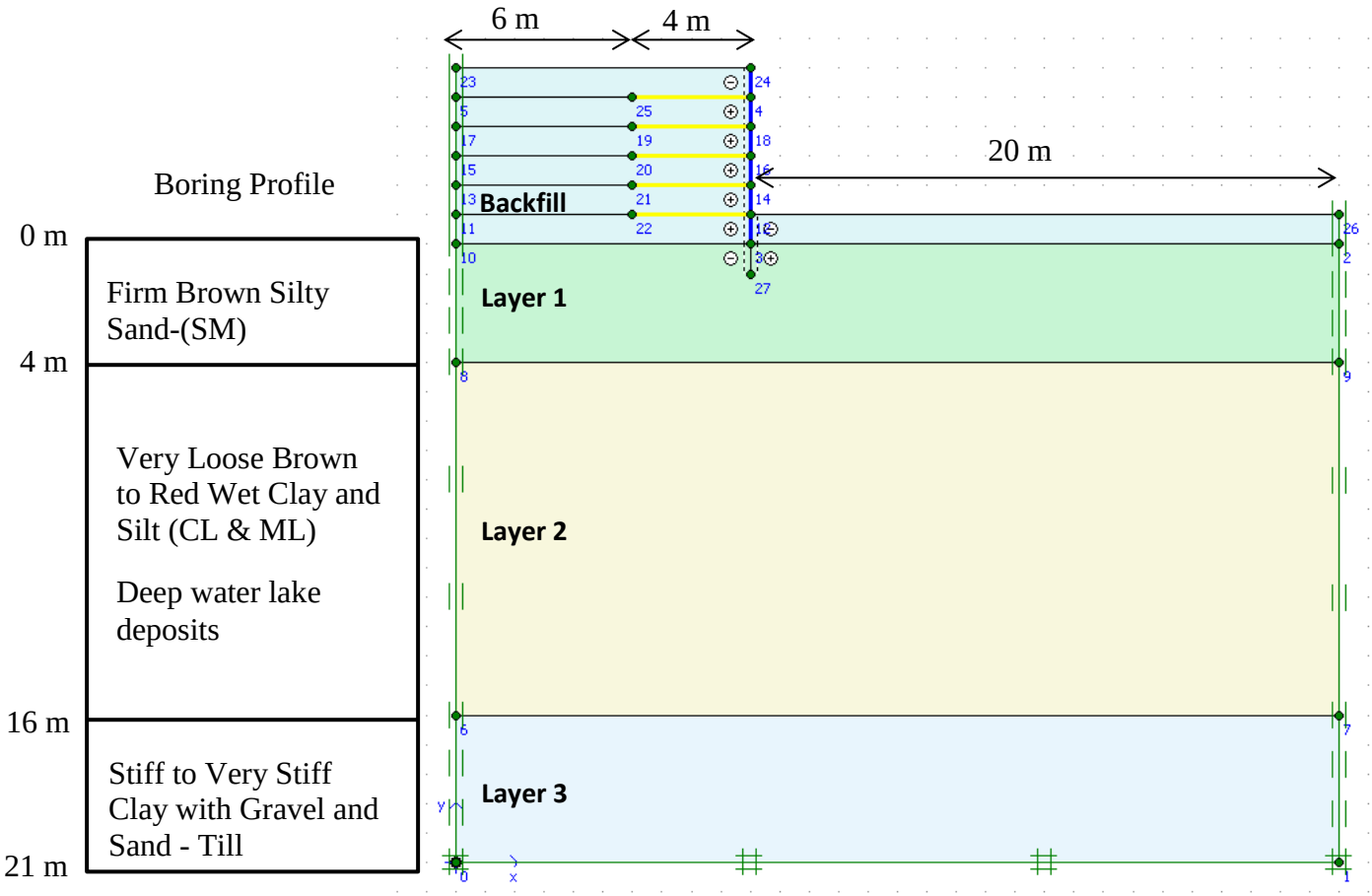

Figure 33. Boring Profile and PLAXIS Model (Location R-05-67)

Table 5. Soil Parameters (Location R-05-67)

Parameter	Name	Backfill	Layer 1	Layer 2	Layer 3	Unit
Material model	Model	MC	MC	MC	MC	-
Soil unit weight	γ	18.85	20.62	19.32	21.21	kN/m^3
Horizontal hydraulic conductivity	k_x	8	0.00023	0.00096	0.00048	m/day
Vertical hydraulic conductivity	k_y	8	0.00023	0.00096	0.00048	m/day
Young's modulus	E	1.00E+05	1.00E+04	5.00E+03	1.00E+04	kN/m^2
Poisson's ratio	ν	0.25	0.35	0.35	0.35	-
Shear intercept	S_u	0	465.13	75.173	287.83	kN/m^2
Friction angle	ϕ	30	0	0	0	°
Reduction Factor	R_{inter}	0.7	Rigid	Rigid	Rigid	-

Table 6. Wall facing data set parameters from PLAXIS 2D Manual

Parameter	Name	Value	Unit
Type of behavior	Material type	Elastic	-
Normal stiffness	EA	1.20E+07	kN/m
Flexural rigidity	EI	1.20E+05	kNm^2/m
Weight	W	8.3	kN/m/m
Poisson's ratio	N	0.15	-

Table 7. Geogrid parameter from PLAXIS 2D Manual

Parameter	Name	Value	Unit
Normal stiffness	EA	1.50E+05	kN/m

The undrained shear strength of clay is estimated from the cone resistance data q_c, collected by prof. J. Schneider at the construction site using:

$$q_c = N_k S_u + \sigma'_v \quad [5.1]$$

where N_k is the cone factor, which is roughly in the 9-10 range (Salgado, 2008).

The average cone resistance (Figure A.2) and vertical effective stress are calculated for each soil layer to calculate S_u. Calculated values are listed in Table 5. Hydraulic conductivity of each soil layer is calculated using an equation of the form:

$$k = \gamma_w M_v C_v \quad [5.2]$$

where coefficient of volume change, M_v, is calculated using equation 5.3 and consolidation test reports (Figures A.3- A.4- A.5) and coefficient of consolidation, C_v, is calculated by taking an average for each soil layer (Figure A.6).

$$M_v = a_v/(1 + e_0) \quad [5.3]$$

where a_v, modulus of soil (Eq. 3.8) and e_0, initial void ratio.

5.1.1.1 Pressure Transducer Data

The dissipation of the pore water pressure is directly related to consolidation rate. Therefore, piezometers were installed at different depths to control the rate of fill placement during embankment construction over soft soils. Figure 34 and Figure 35 show the pressure transducer data at locations 1102FSW and 1104FSW. Piezometers were installed 3 m apart from each other.

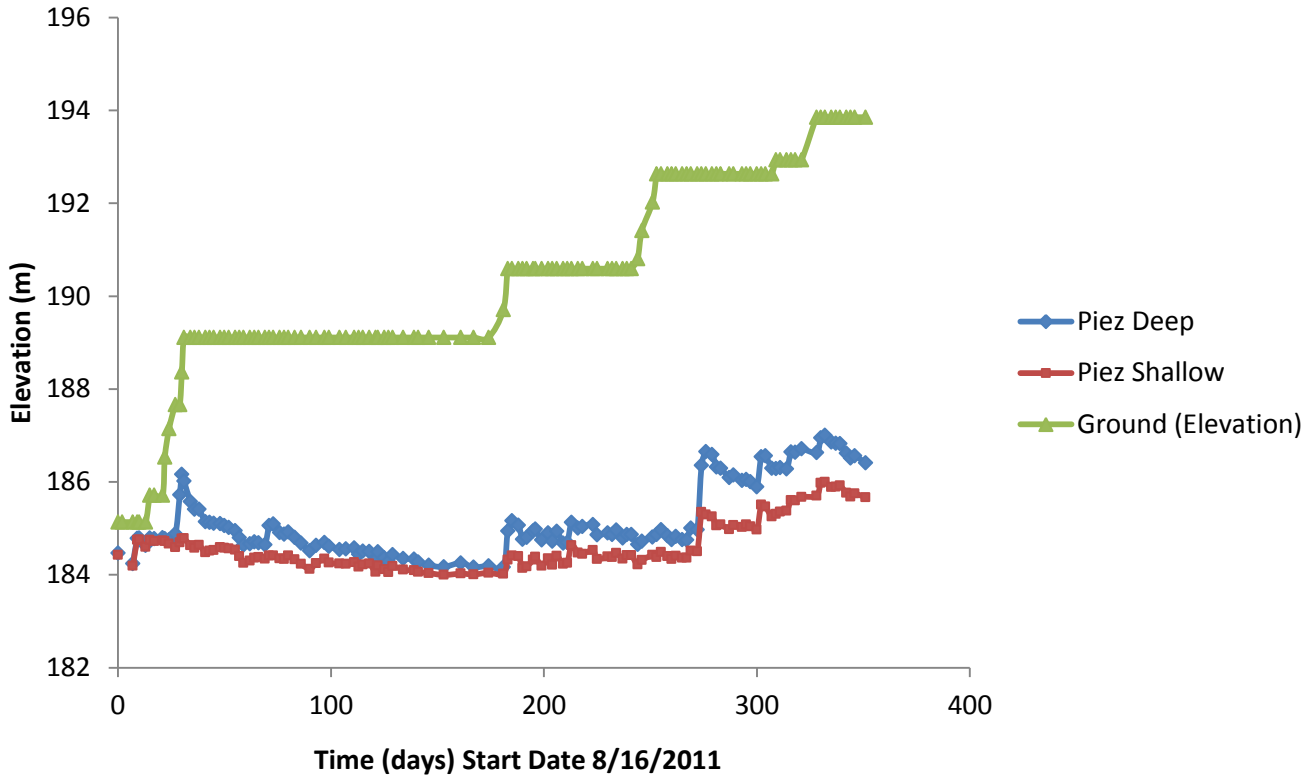

Figure 34. Pressure Transducer Field Data at Location 1102FSW

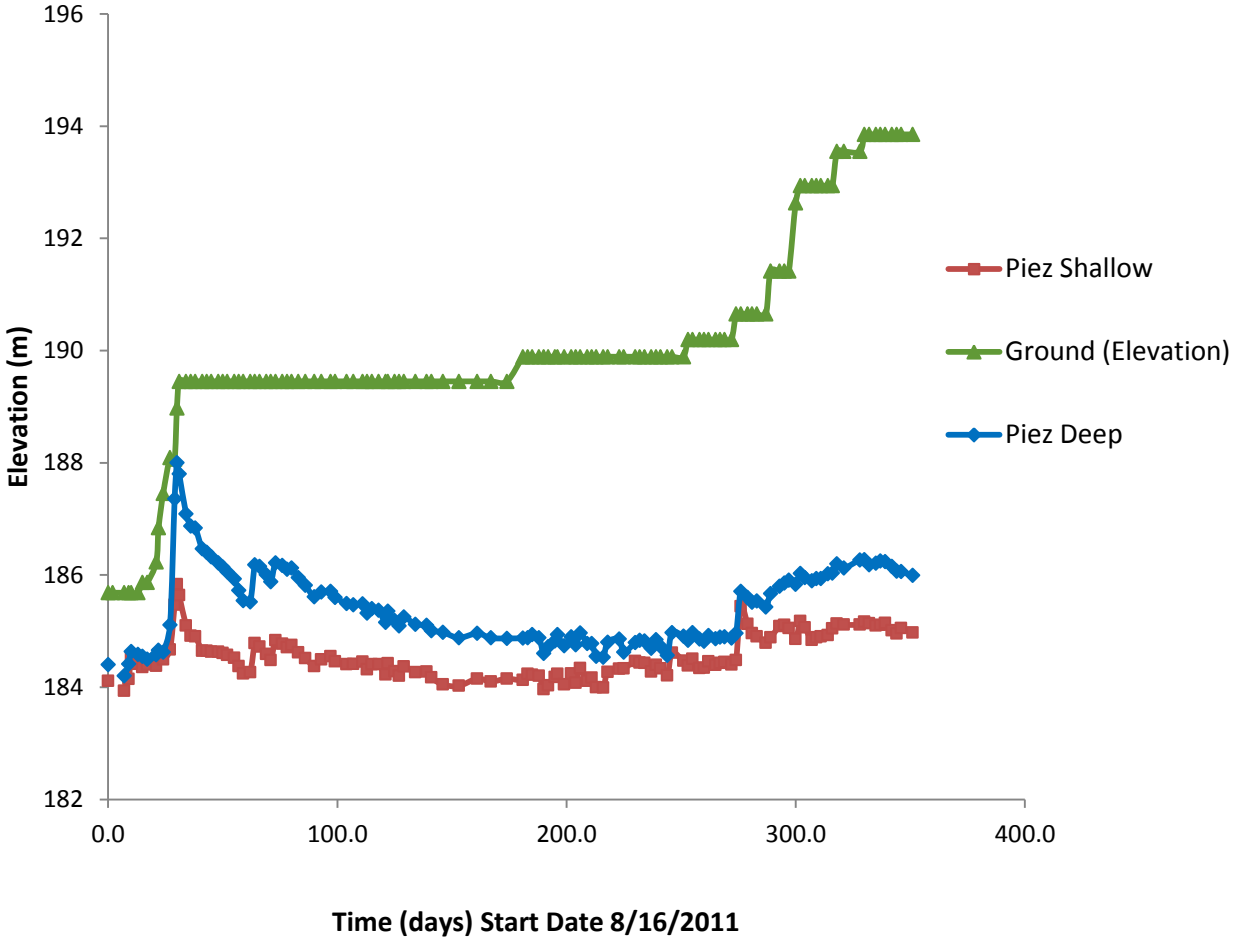

Figure 35. Pressure Transducer Field Data at Location 1104FSW

A sudden increase in excess pore water pressure due to staged construction is clearly seen in Figures 34 and 35; however, due to other construction activities in the site, some excess pore pressure variations are also observed in the collected data.

The PLAXIS model presented in Figure 33 was created to represent field conditions and conduct parametric studies to see the effect of time increments on excess pore water pressure dissipation on soft soils. The embankment was constructed in five 1-m lifts. The analyses were performed using equally sized time increments for each lift. Construction of each lift took 10 days and additional time intervals of 25, 50, 100 and 200 days were given to allow the excess pore pressures to dissipate. Pressure transducers were placed at 3 different locations to observe

the effect of transducer location on excess pore water pressure. All transducers are placed 2.5 m away from the wall facing which is equal to the half of the embankment height. Transducer A is placed at a depth 2.5 m below the ground surface, Transducer B is placed at 5 m depth and Transducer C is placed at 10 m depth as shown in Figure 36.

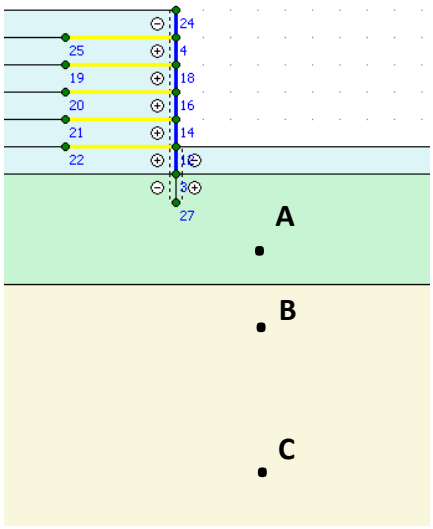

Figure 36. Location of Pressure Transducers A, B & C

Sivakugan and Das (2010) present Boussinesq's (1885) solution for the distribution of stresses for a load applied on the soil surface assuming the soil mass is elastic, isotropic, homogeneous, semi-infinite and also weightless. The distribution of vertical stress below a uniformly loaded foundation is shown in Figure 37.

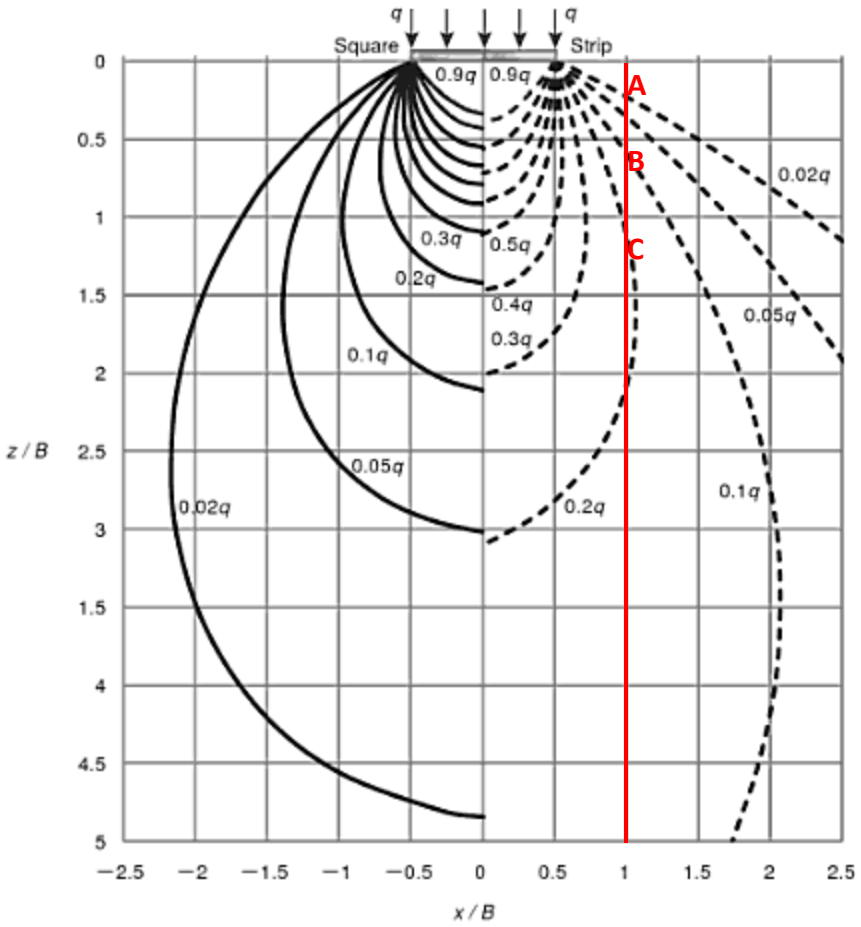

Figure 37. Pressure isobars for uniformly loaded flexible square and strip foundations (Sivakugan and Das, 2010)

Staged construction on soft soils leads to an increase in effective stress and increase in effective stress causes a sudden increase in excess pore water pressure. Pressure isobars in Figure 63 shows the change in stress at Points A, B and C, since the highest vertical stress increase is seen at Point C, the highest excess pore water pressure increase is expected on Point C. Results are shown in Figures 38, 39, 40 and 41.

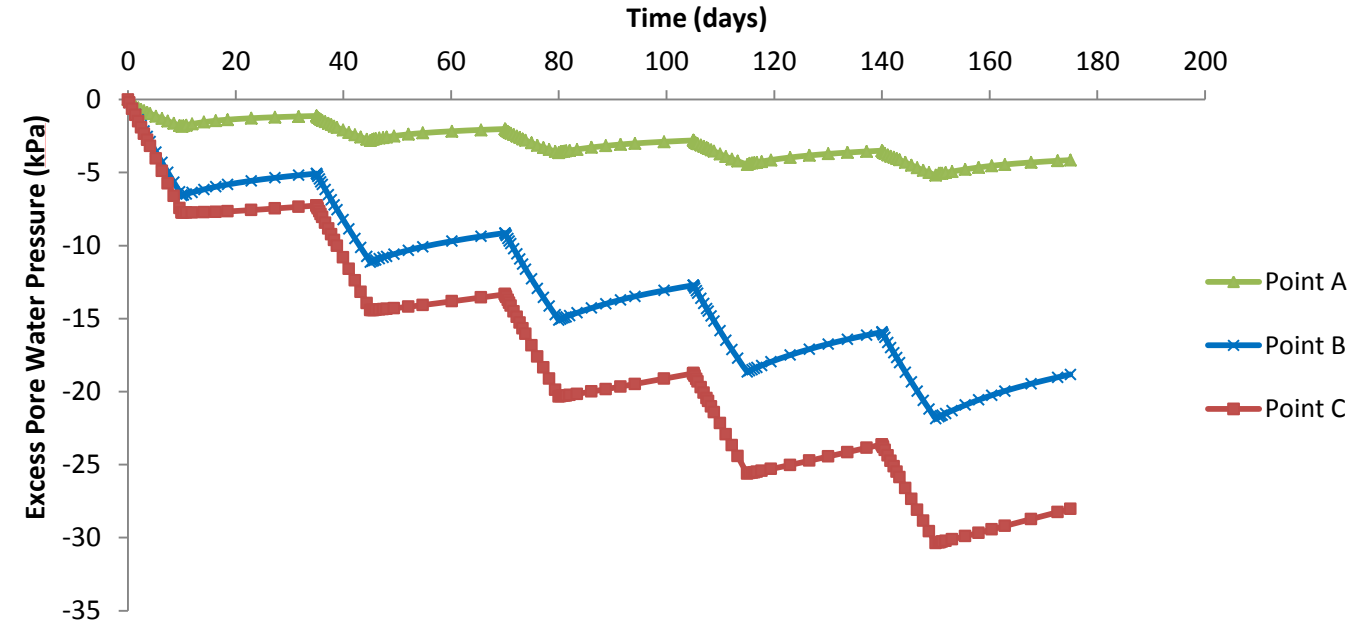

Figure 38. Construction Time (25 days) versus Excess Pore Water Pressure

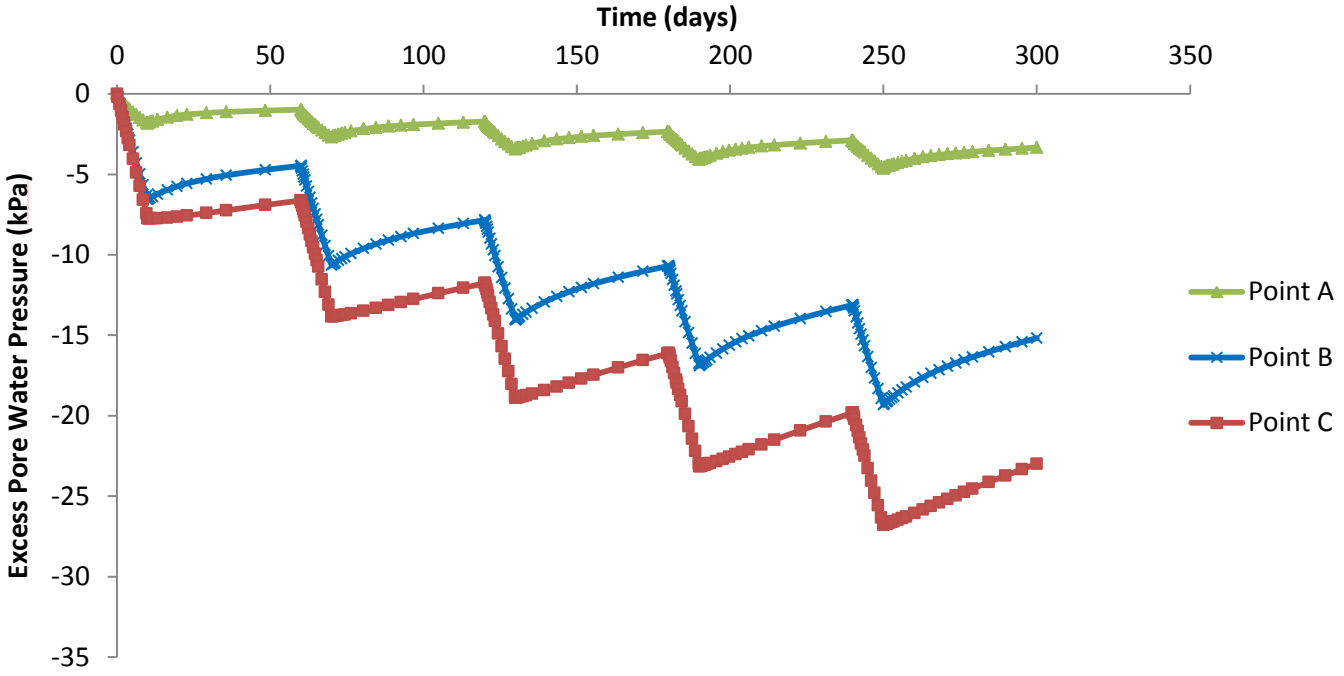

Figure 39. Construction Time (50 days) versus Excess Pore Water Pressure

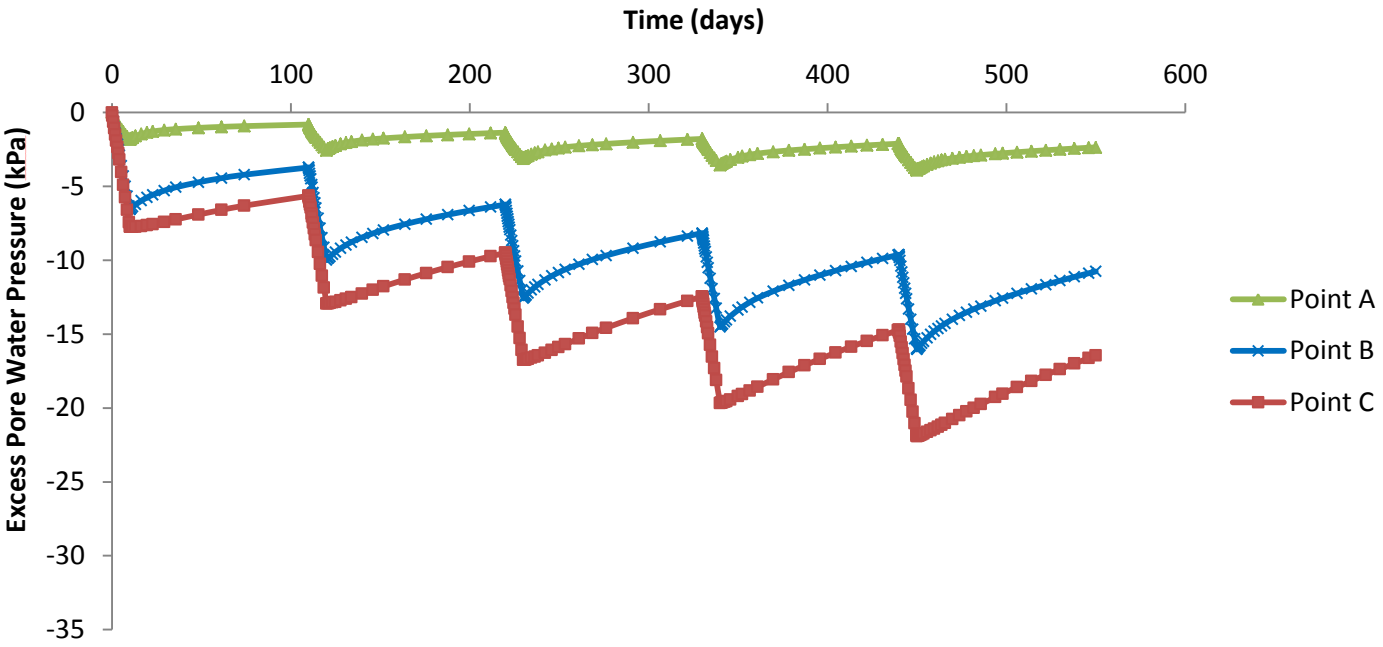

Figure 40.Construction Time (100 days) versus Excess Pore Water Pressure

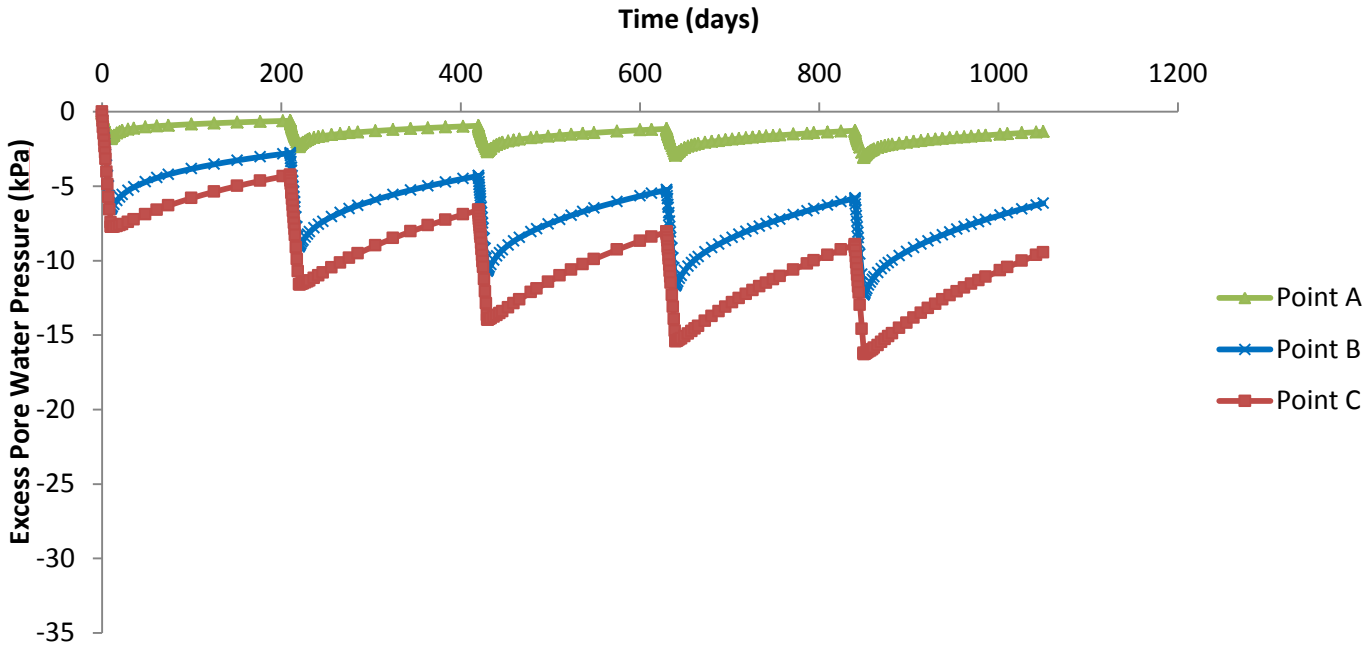

Figure 41. Construction Time (200 days) versus Excess Pore Water Pressure

Figures 38 to 41 show that the increase in effective stress due to staged construction leads to a sudden increase in excess pore water pressure (up to around 30 kPa for 25 days consolidation time intervals). However, the excess pore water pressure decreases to 16 kPa for 200 days consolidation time interval for each stage which shows that dissipation of excess pore water pressure is slow due to the low hydraulic conductivity of soft soils. Moreover, the deepest transducer, Point C, has the highest excess pore water pressure as expected.

Kelln et al. (2007) used both elastic-viscoplastic and modified cam clay numerical solutions for a staged construction embankment loading problem to show temporal variations in excess pore water pressure u, surface settlement δy and maximum horizontal displacement δx as shown in Figure 42.

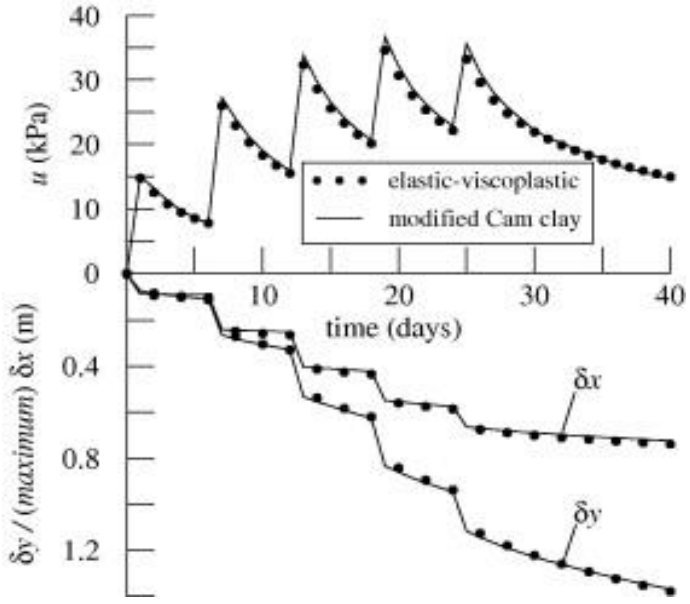

Figure 42. Staged construction embankment problem (Kelln et al. 2007)

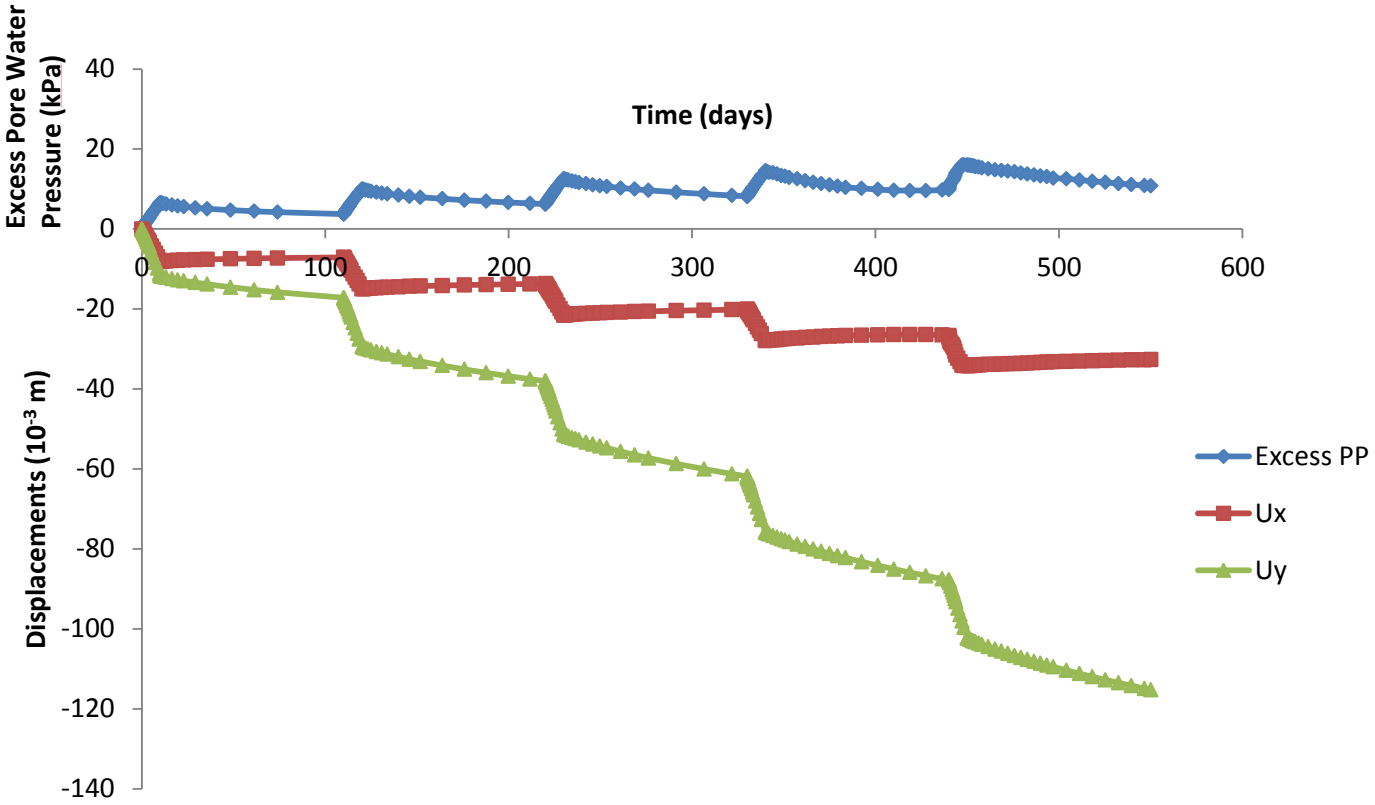

Figure 43. Staged construction effect on both excess pore pressure and displacements (Staged construction interval time, 100 days)

Saturated soils undergo volume deformations, compressing vertically and expanding laterally as shown in Figure 43. Figure 43 trends similarly to the Kelln et al. (2007)'s study. As excess pore water pressure decreases and goes to zero, settlements reach a constant value which shows end of consolidation in Figure 44. Excess pore water pressures are taken from Point A, horizontal settlements are taken 10 m away from the wall facing on the soil surface and vertical settlements are taken under the wall facing.

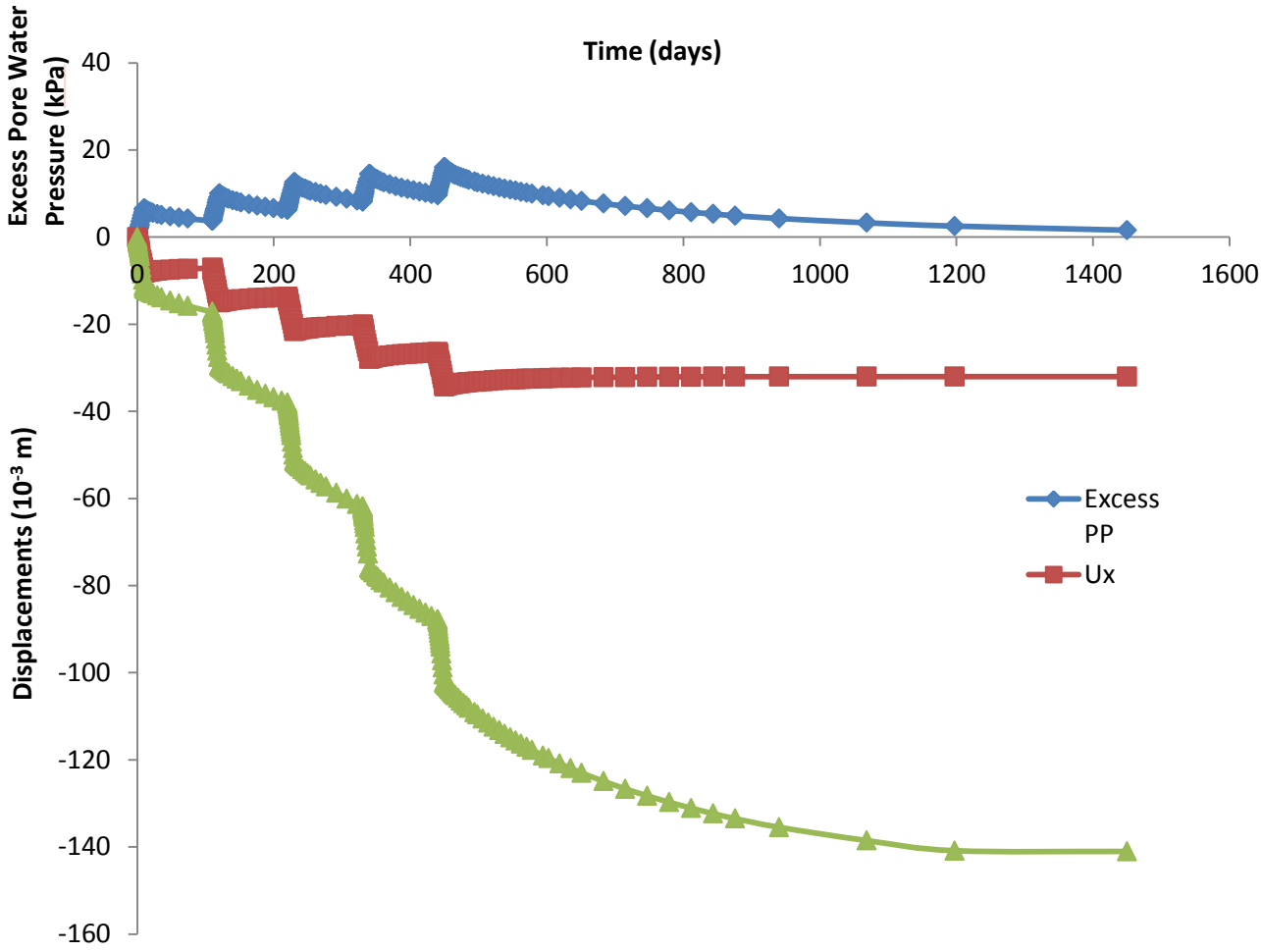

Figure 44. Staged construction effect on both excess pore pressure and displacements

(Staged construction interval time, 100 days)

5.1.1.2 Slope Inclinometer Data

All horizontal displacement data were taken 2.5 m away from the wall facing which is equal to the half of the embankment height till 22 m depth. It is clearly seen from Figure 45 that data points fairly well matched with the construction site.

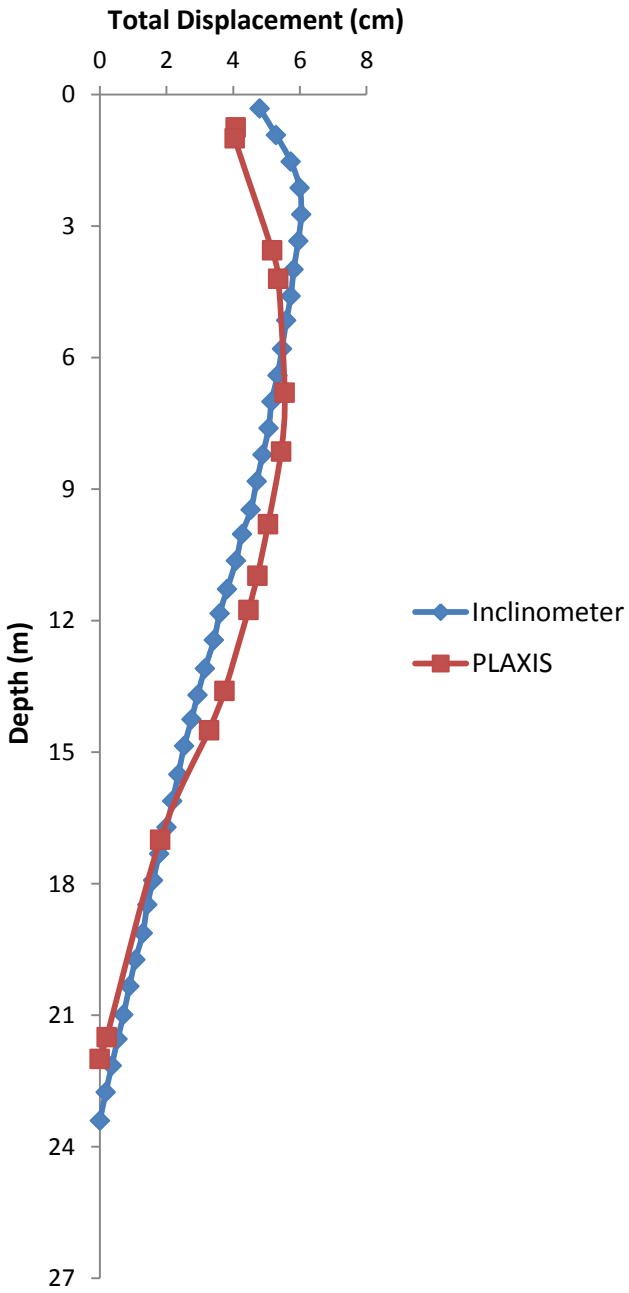

Figure 45. Cumulative Horizontal Displacement Plot

(D3 S29814, A-Axis Field Data and PLAXIS data comparison)

5.1.1.3 Shear Stress Distribution

A strip load is the load transmitted by a structure of finite width and infinite length on a soil surface. The PLAXIS 2D MSEW model represents a strip loading over soft soil. Embankment weight is distributed over an area of width 10 m. The increase in shear stress, $\Delta\tau_{xz}$ due to a surface stress, q_s is as follows (Budhu, 2007):

$$\Delta\tau_{xz} = \frac{q_s}{\pi}\,(sin\alpha * sin(\alpha + 2\beta)) \qquad [5.4]$$

where α and β are shown in Figure 46.

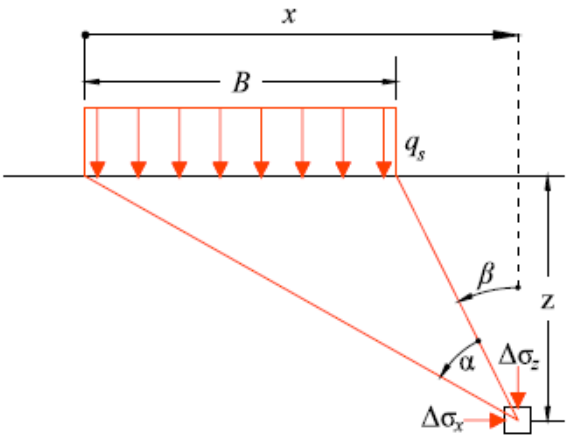

Figure 46. Strip load imposing a uniform stress

When the load is applied on a rigid plate, maximum shear stress occurs at the edge of the rigid plate. This assumption is proved with a simple model in PLAXIS. A rigid steel pate is placed on the soil and a uniform load is applied, with the results shown in Figure 47.

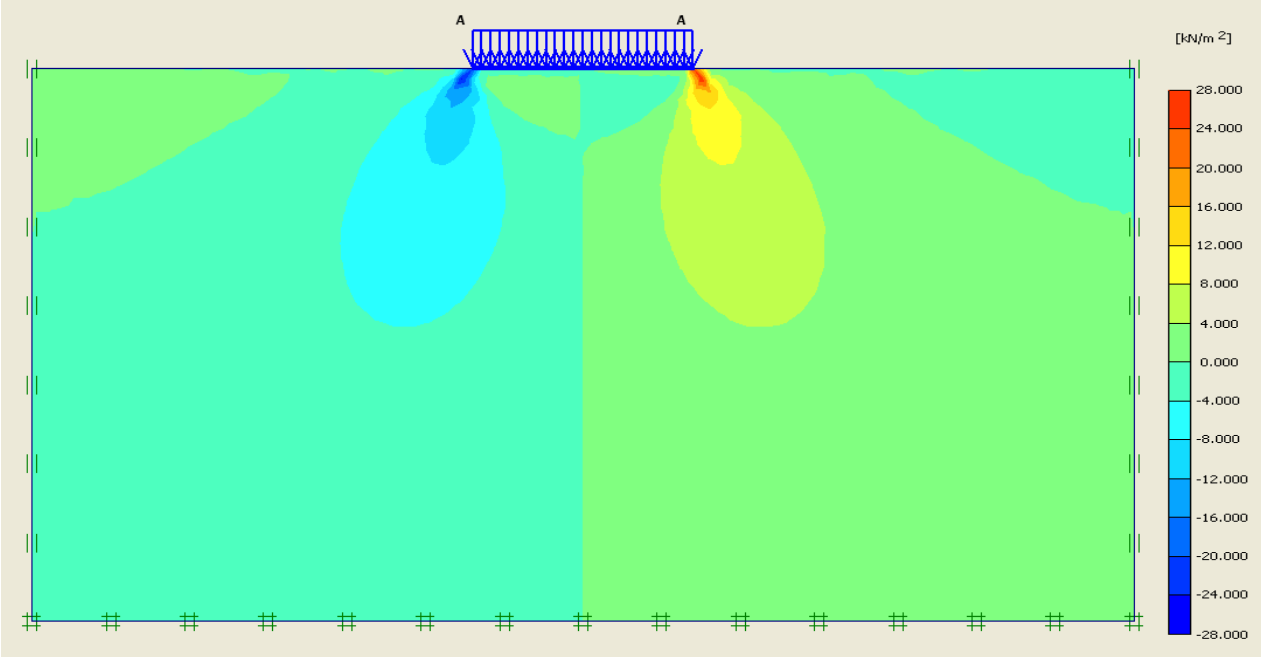

Figure 47. Shear Stress Distribution under uniformly loaded steel plate

The formulation presented in Equation 5.4 is compared with the finite element model created in the PLAXIS model. Surface stresses are calculated by multiplying height of the embankment with the unit weight of the backfill soil, which is equal to 94 kPa. Shear stresses are calculated 2.4 m away from the wall facing with different depths. Shear stress distribution under the MSEW is shown in Figure 48. Maximum shear stresses occurred at the corner of the MSEW having an extreme value 118.31 kPa. The plot including both PLAXIS and theoretical formula

values is shown in Figure 49. It is clearly seen from Figure 49, PLAXIS results fairly well matched with the theoretical formula.

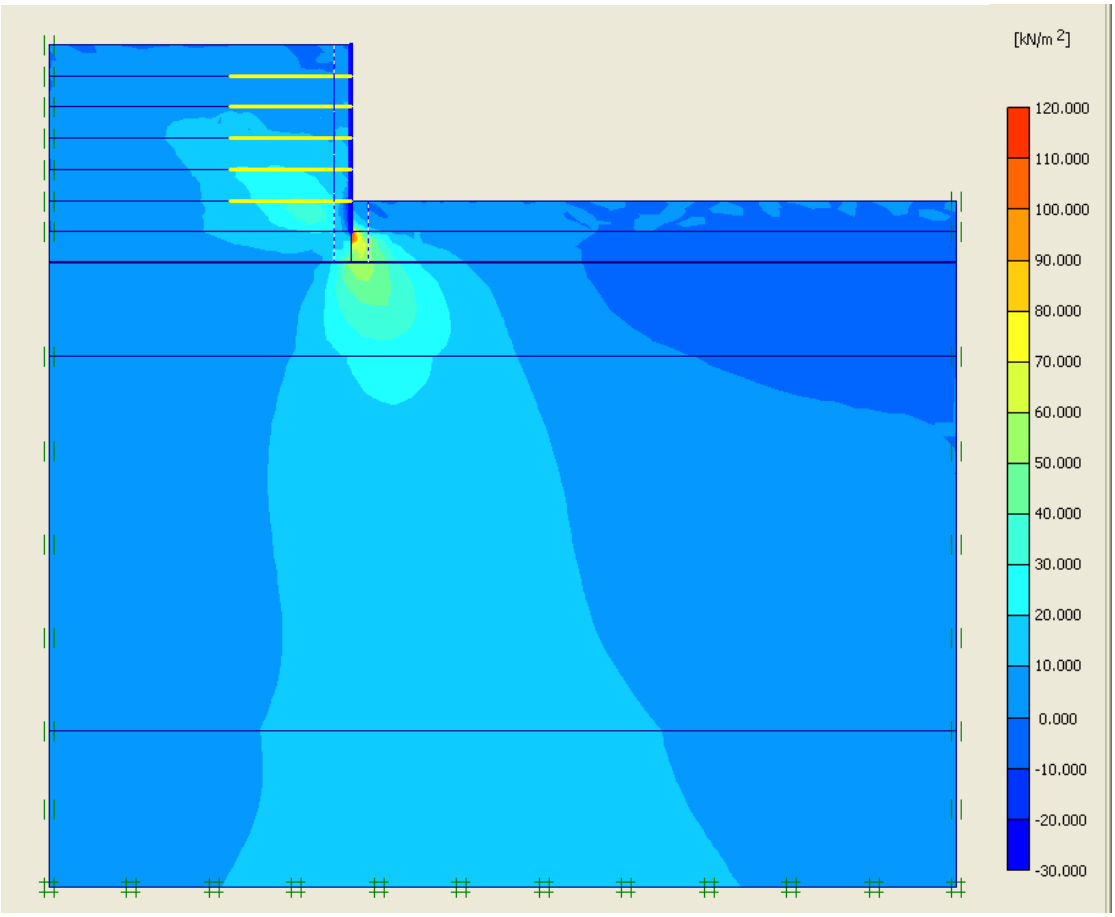

Figure 48. Shear Stress Distribution under MSEW

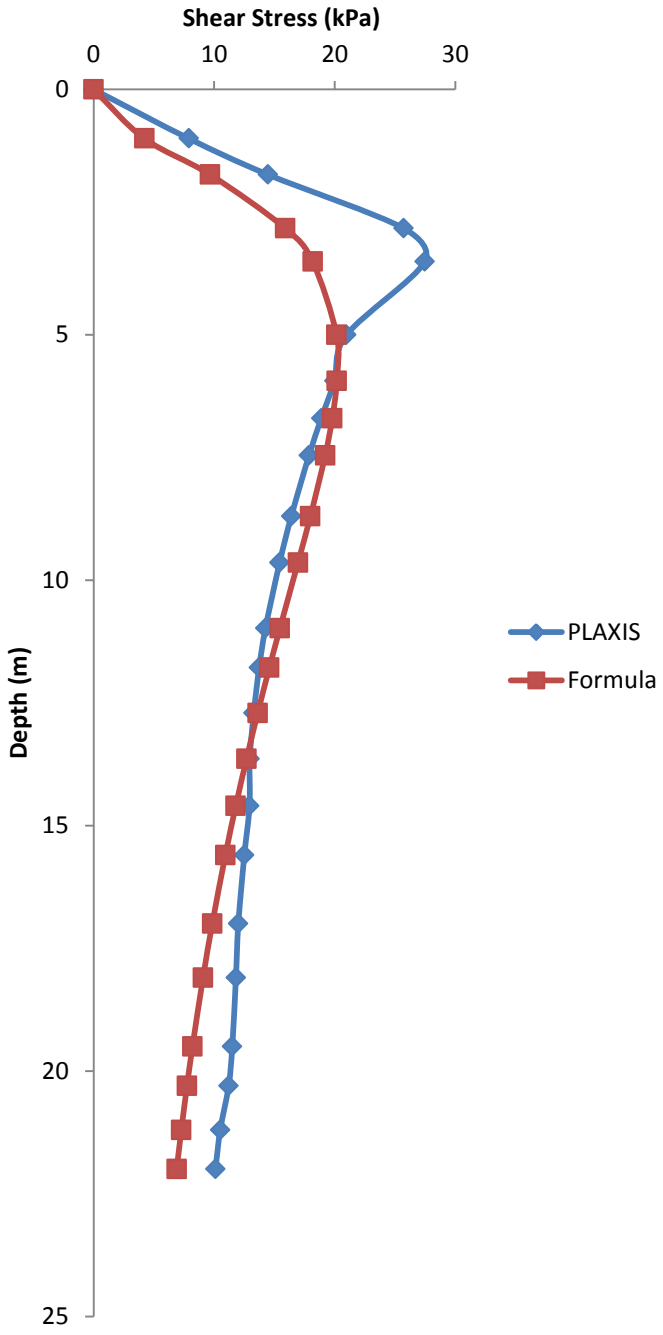

Figure 49. Shear stress distribution comparison 2.5 m away from the wall facing

5.1.2 Numerical Model of MSEW at Howard, Wisconsin

The two-dimensional finite element program PLAXIS is used to perform the numerical analysis of a MSEW at Howard, Wisconsin. Two-dimensional geometry model has been created in XY-plane, and then material properties and boundary conditions are specified to carry out a finite analysis using PLAXIS. The generation of an appropriate finite element mesh is very important to get accurate results and, for this model, global coarseness of the mesh arranged to "medium" with a refinement of wall facing. Generation of static water pressure and initial effective stresses has been generated before calculation process.

Plain strain model was used for finite element model in this analysis. Force is expressed in the units of force per unit of width in the out of plane direction in plain strain models. Displacements and strains in z-direction are assumed to be zero. 15-node elements are used for this study to provide an accurate calculation of stresses and failure loads.

Behavior of soils under MSEW has been modeled by Mohr Coulomb (MC) model which is considered as a first-order approximation of real soil behavior. Related soil parameters including unit weight, undrained shear strength and the friction angle are taken from the boring log information and cone penetration tests performed at the sites. Other soil parameters including hydraulic conductivity, Young's modulus, Poisson's ratio and the reduction factor are taken from the literature research since real site values are not available. There are two different embankment construction locations on the project area. Soil description at STH 29/ USH 41 interchange at location R-5-231 is presented in Table 8 and soil and interface parameters are presented in Table 9.

Table 8. Soil Description at STH 29/ USH 41 site (Location R-5-231)

Soil Description	Layer #
Granular Backfill	-
Clay, brown, some silt (Elevation 0 - 2 m)	1
Clay, gray, some silt (Elevation 2 - 5 m)	2
Silt, gray, some sand, trace clay (Elevation 5 - 13 m)	3
Silt, gray, little sand, some clay (Elevation 13 - 17 m)	4
Silt, gray, some clay (Elevation 17 - 25 m)	5
Limestone (Elevation 25 - 27 m)	6

Table 9. Soil and interface parameters (Location R-5-231)

Parameter	Name	Backfill	Layer 1	Layer 2	Layer 3	Layer 4	Layer 5	Layer 6	Unit
Material model	Model	MC	MC	MC	MC	MC	MC	MC	-
Soil unit weight	γ	18.85	17.28	17.28	17.28	18.85	18.00	22.00	kN/m^3
Horizontal hydraulic conductivity	k_x	8	0.0001	0.0001	0.0001	0.0009	0.0001	0.086	m/day
Vertical hydraulic conductivity	k_y	8	0.0001	0.0001	0.0001	0.0009	0.0001	0.086	m/day
Young's modulus	E	1.00E+05	8.00E+03	1.00E+03	8.00E+03	2.00E+04	1.40E+04	2.00E+07	kN/m^2
Poisson's ratio	ν	0.25	0.35	0.35	0.35	0.3	0.35	0.25	-
Undrain shear strength	S_u	0	36	17	24	72	48	4600	kN/m^2
Friction angle	ϕ	30	0	0	0	0	0	0	°
Reduction Factor	R_{inter}	0.7	Rigid	Rigid	Rigid	Rigid	Rigid	Rigid	-

"Plates" are used to generate wall facing of MSEW. Plates are structural elements which are used to model slender structures in the ground with a significant flexural rigidity and a normal stiffness. Wall facing data set parameters are taken from PLAXIS manual since real site values are not available.

Table 10. Wall facing data set parameters from PLAXIS 2D Manual

Parameter	Name	Value	Unit
Type of behavior	Material type	Elastic	-
Normal stiffness	EA	1.20E+07	kN/m
Flexural rigidity	EI	1.20E+05	kNm^2/m
Weight	w	8.3	kN/m/m
Poisson's ratio	v	0.15	-

Geogrids are slender structures with a normal stiffness but with no bending stiffness. Their main objective is to sustain tensile forces. They cannot resist compression forces. They are used to model soil reinforcements (Figure 50).

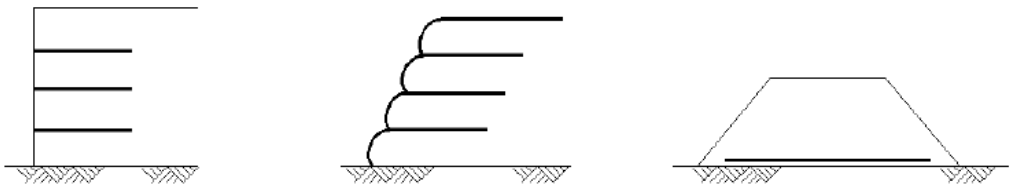

Figure 50. Application in which geogrids are used (PLAXIS 2D Reference Manual, 2002)

Geogrids were modeled using "geogrid" elements in PLAXIS. The only material property of a geogrid is an elastic normal stiffness, which is taken from PLAXIS manual.

Table 11. Geogrid material parameter

Parameter	Name	Value	Unit
Normal stiffness	EA	1.50E+05	kN/m

The modeling configuration of MSEW at Howard, Wisconsin used for analysis is presented in Figure 51. This model includes geometry, soil layers, wall facing, geogrids and the boundary conditions of the site. Boundary conditions are generated as vertical geometry lines for which the x-coordinate is equal to the lowest or highest x-coordinate in the model obtain a horizontal fixity ($u_x = 0$), horizontal geometry lines for which the y-coordinate is equal to the lowest y-coordinate in the model obtain a full fixity ($u_x = u_y = 0$).

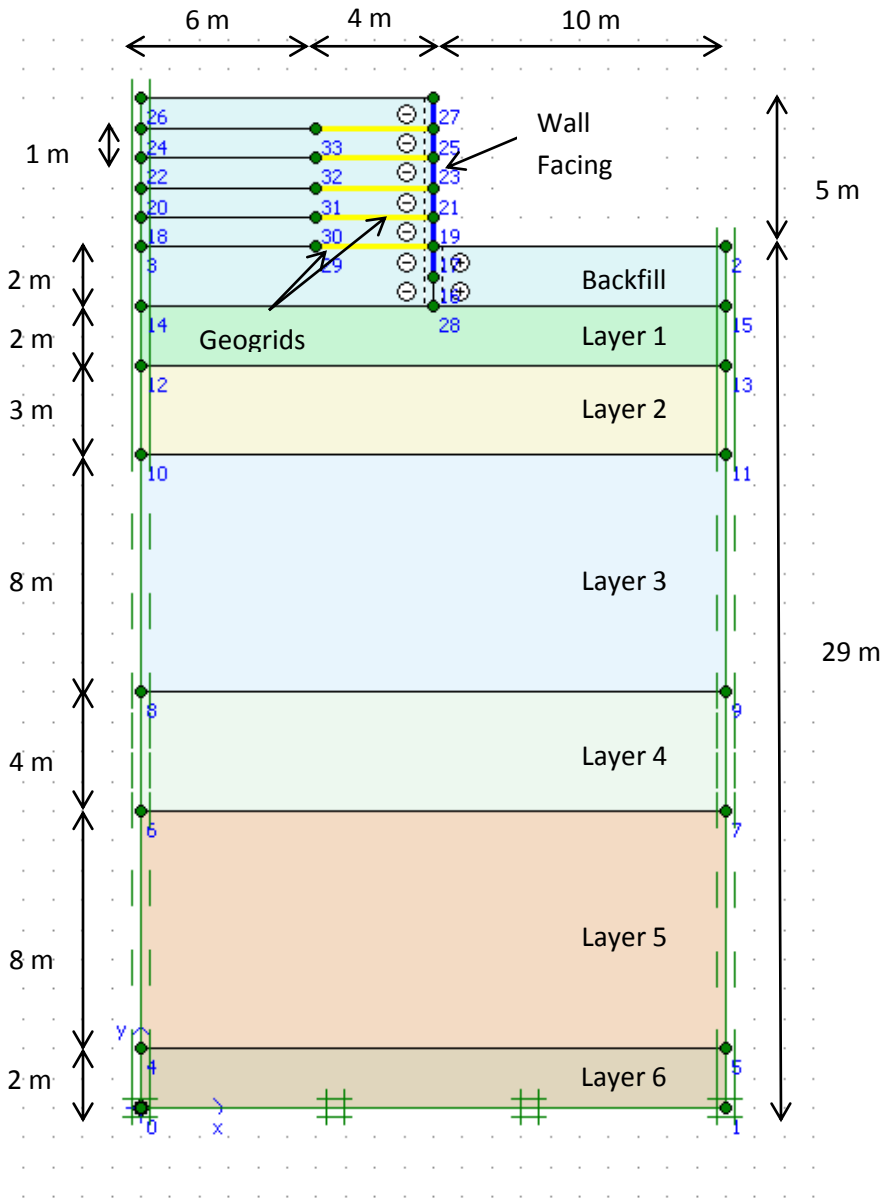

Figure 51. MSEW Model with structural elements

5.1.3 Numerical Modeling Calculations for a Parametric Study on MSEW at Howard, Wisconsin

Initial stresses which are controlled by the weight of the material and stress history of the formation. Because, the lacustrian sediments at the site are young, the soil is normally consolidated, the in situ state of stresses were generated under K_0 conditions after generating the MSEW model on PLAXIS. This stress state is characterized by an initial vertical effective stress, σ'_{v0}. The initial horizontal effective stress, σ'_{h0} is calculated by multiplying initial vertical effective stress with the coefficient of lateral earth pressure, K_0=1-sinϕ. The resultant generated initial effective stress distribution is shown in Figure 52.

The ground water was located at the layer 1 and layer 2 interfaces and the hydrostatic water pressure was generated. The resultant generated pore pressure distribution is shown in Figure 52.

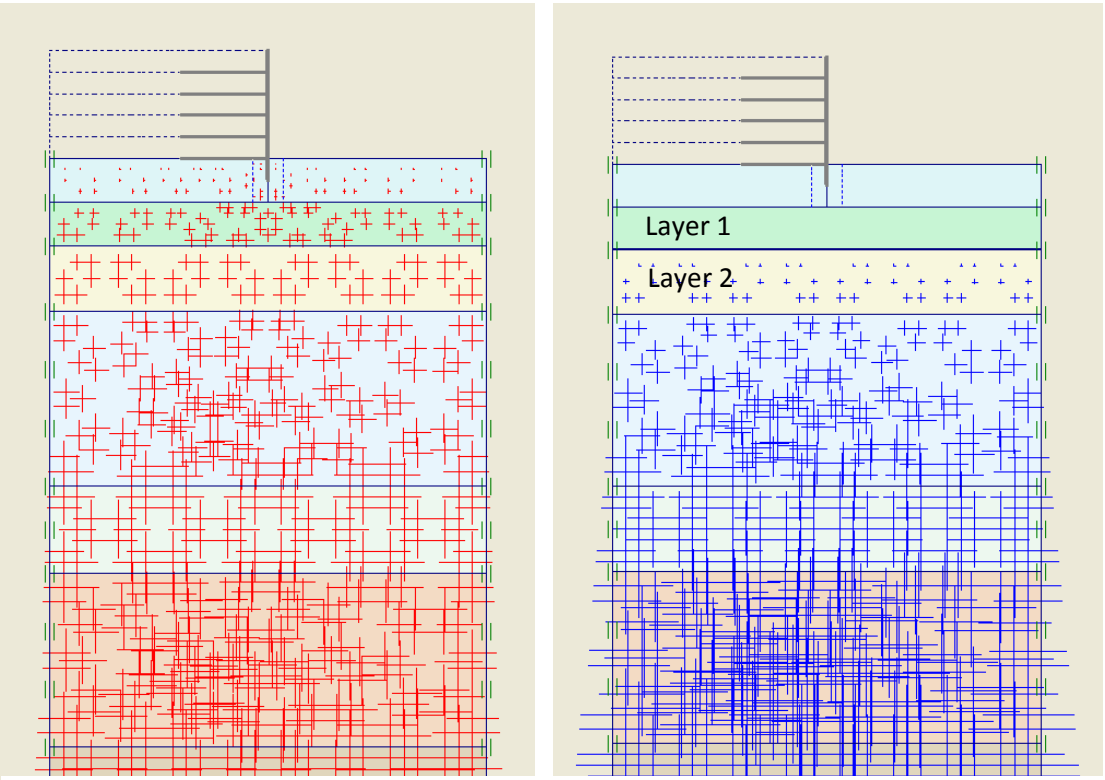

Figure 52. Initial stresses and pore pressure distribution (the size of the crosses indicate the magnitude of the stresses)

Staged construction (Figure 36) is applied since the construction of tall embankments on soft soils with low shear strength and high compressibility cannot be built at once due to the low shear strength of subgrade. “Consolidation” analysis was selected as a calculation type in PLAXIS. During the “consolidation” analysis, changes in void ratio of the low hydraulic conductivity soils are directly proportional to excess pore water pressure dissipation and thus are related to the rate of settlement.

To define the calculation phases in PLAXIS, the following steps were done:

1. *First Phase:* After selecting the “Consolidation” analysis, “Staged construction” was selected in “Parameters” tab sheet and time interval of 10 was entered. 10 days is the minimum allowable time interval for construction of a soil layer for this soil model in PLAXIS. Also, first part of the embankment in the geometry configuration was activated to present construction part (Figure 53).
2. *Second phase:* This phase is also a consolidation analysis and staged construction. This time no changes are made to the geometry as only time interval of 200 days was entered to allow the excess pore pressures to dissipate.
3. First and second steps were repeated until the last construction stage was introduced to the PLAXIS (Figure 56).

It is also important to consider the stability of the embankment and the foundation soil during the construction. There are two main failure hypothesizes, which are MSEW failure and foundation soil failure. Driving forces promote downslope movement of material and resisting forces deter movement. If driving forces are greater than resisting forces, MSEW failure will occur as seen in Figure 54.

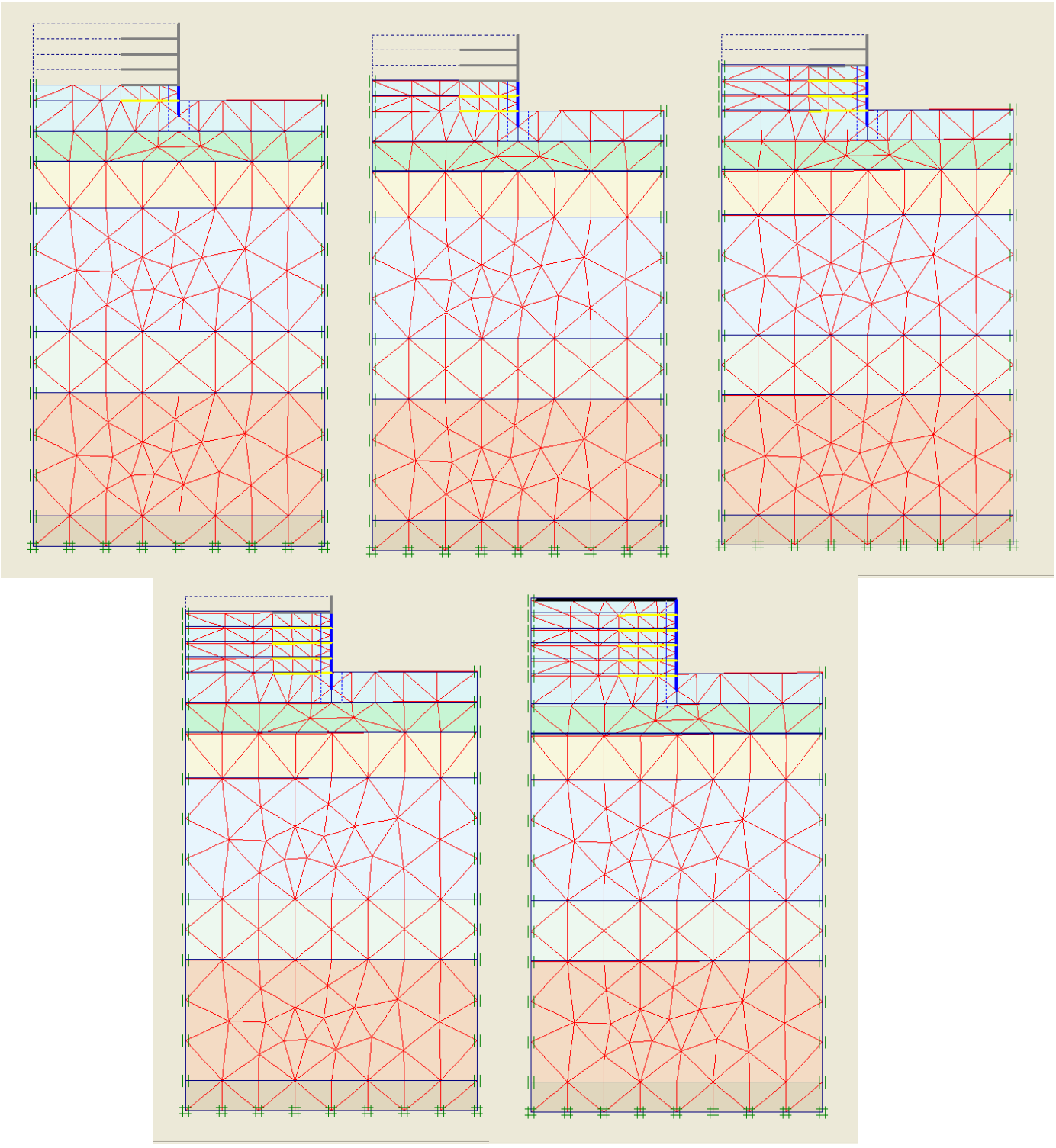

Figure 53. Staged Construction of MSEW

$$FS = \frac{Resisting\ Forces}{Driving\ Forces} \quad [5.5]$$

Besides MSEW failure, foundation soil could fail if available undrained shear strength is less than required shear strength, as shown in Figure 55.

$$FS = \frac{S_{u\ available}}{S_{u\ required}} \quad [5.6]$$

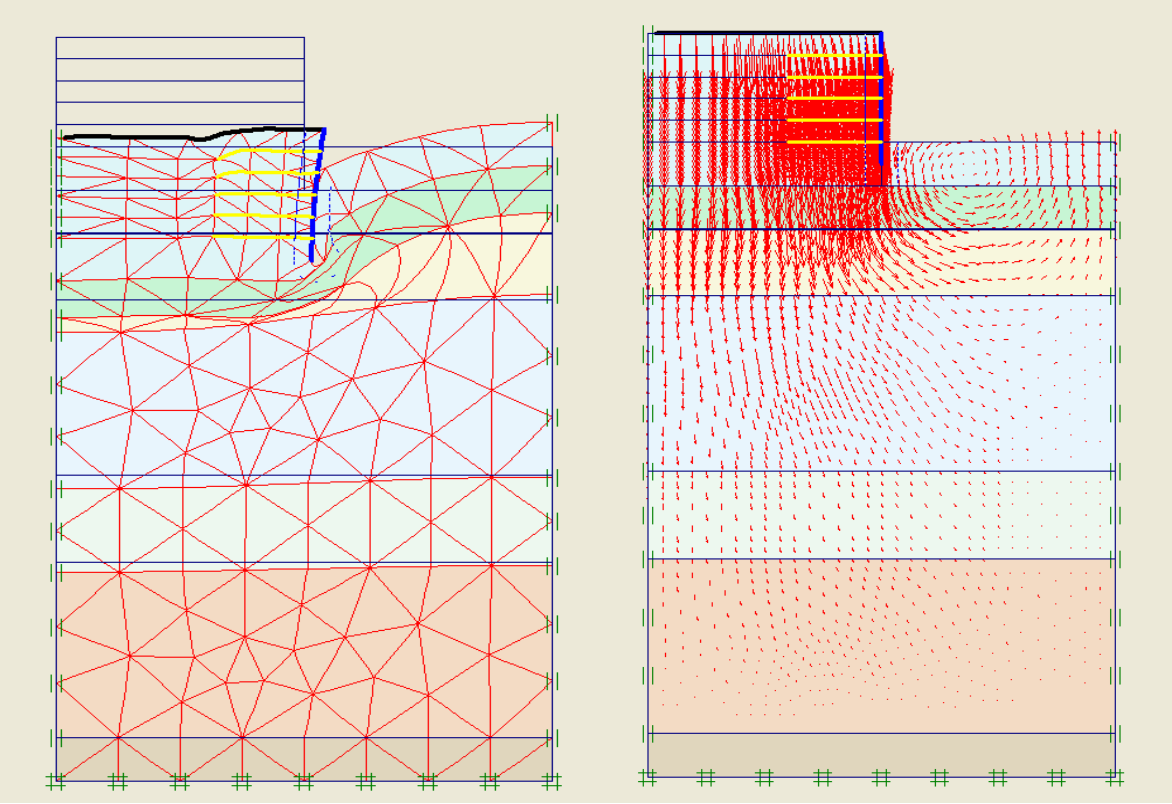

Figure 54. Deformed Shape and Total Displacement representing the MSEW Failure Mechanism (Scale 1:20)

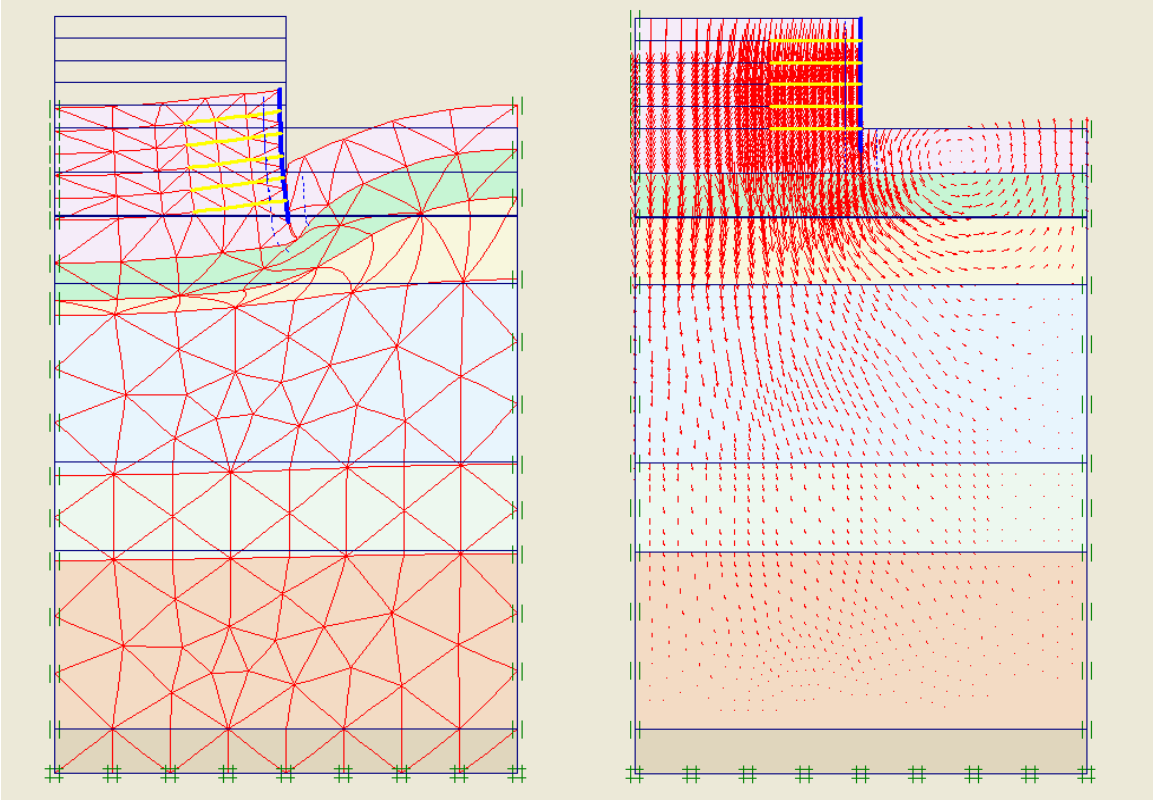

Figure 55. Deformed Shape and Total Displacement representing the Foundation Soil Failure Mechanism (Scale 1:20)

The safety factor in PLAXIS is determined as the ratio of the true strength to the required minimum strength to maintain equilibrium. PLAXIS refers to this calculation as the "Phi-c-reduction" method (PLAXIS 2D Tutorial Manual, 2002). In this method the undrained shear strength and the tangent of the friction angle are reduced in the same proportion until failure is reached.

$$Safety\ factor = \frac{S_{u_maximum\ available}}{S_{u_needed\ for\ equilibrium}} \quad [5.7]$$

$$Safety\ factor = \frac{C - \sigma_n tan\varphi}{Cr - \sigma_n tan\varphi r} \quad [5.8]$$

$$\frac{C}{Cr} = \frac{tan\varphi}{tan\varphi r} = \sum Msf \quad [5.9]$$

where c and φ are the input strength parameters and σ_n is the actual normal stress component. The parameters Cr and φr are reduced strength parameters that are just large enough to maintain equilibrium and ΣMsf is the total multiplier which controls the reduction of the strength parameters. These PLAXIS calculated factors of safety are use in the interpretation of the numerical parametric studies in this document.

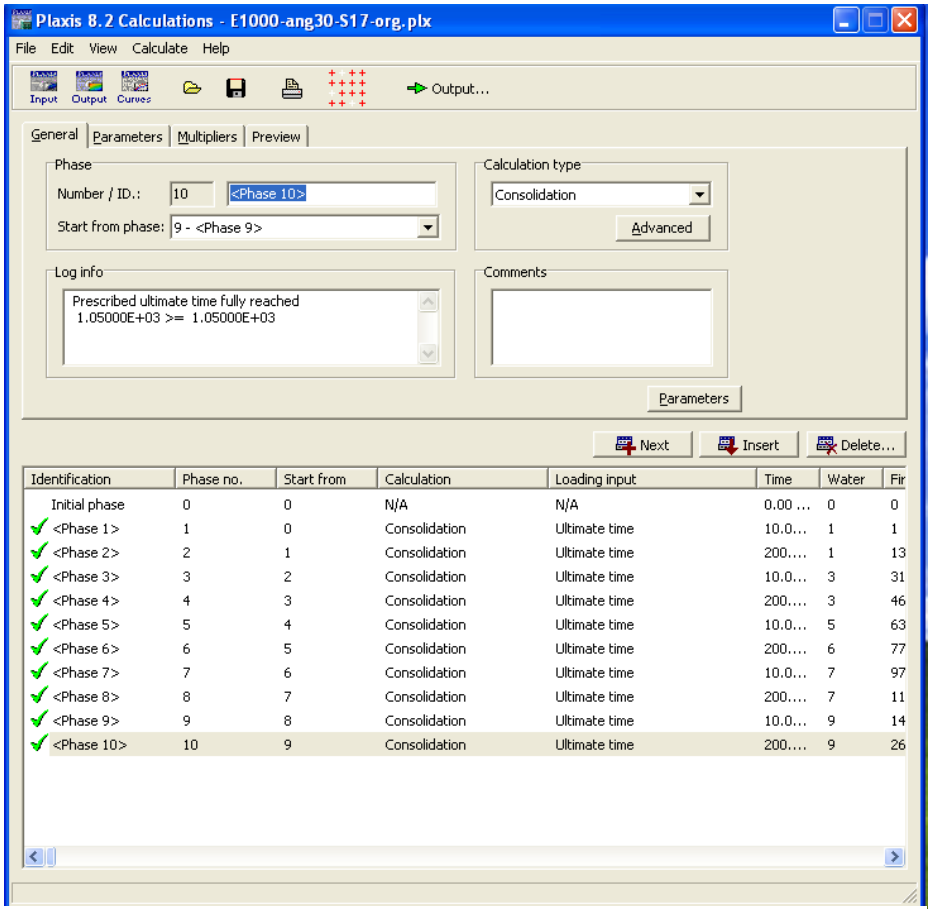

Figure 56. Calculation steps in PLAXIS

5.1.4 Numerical Modeling Results for a Parametric Study on the MSEW at Howard, Wisconsin

Various numerical parametric studies were performed to understand the potential failure mechanism of a MSEW founded on soft soils by conducting dimensional analysis as discussed in literature review part.

5.1.4.1 Effect of boundary conditions on displacements:

Before conducting the parametric studies in PLAXIS, the effect of boundary conditions was evaluated. To assess the effect, the horizontal length of the numerical model was increased and displacements were monitored.

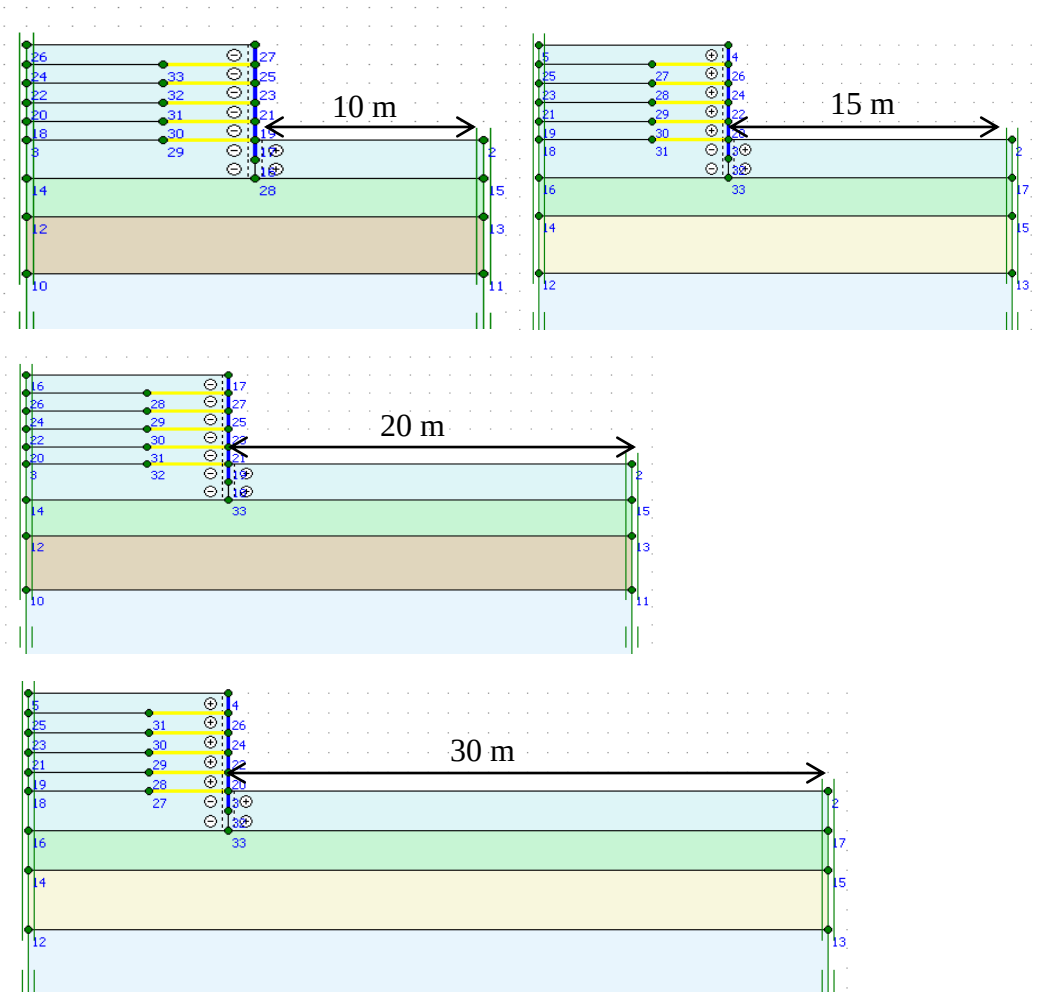

Figure 57. Effect of boundaries in MSEW System Response

Figure 57 shows cross sections of the MSEW-foundation system with different model widths. The objective of this study is to create a model which is not affected by boundary conditions. Soil, wall facing and geogrid properties were kept constant and soil behind the MSEW extended to 10 m, 15 m, 20 m and 30 m to understand the effect on boundary conditions on displacements.

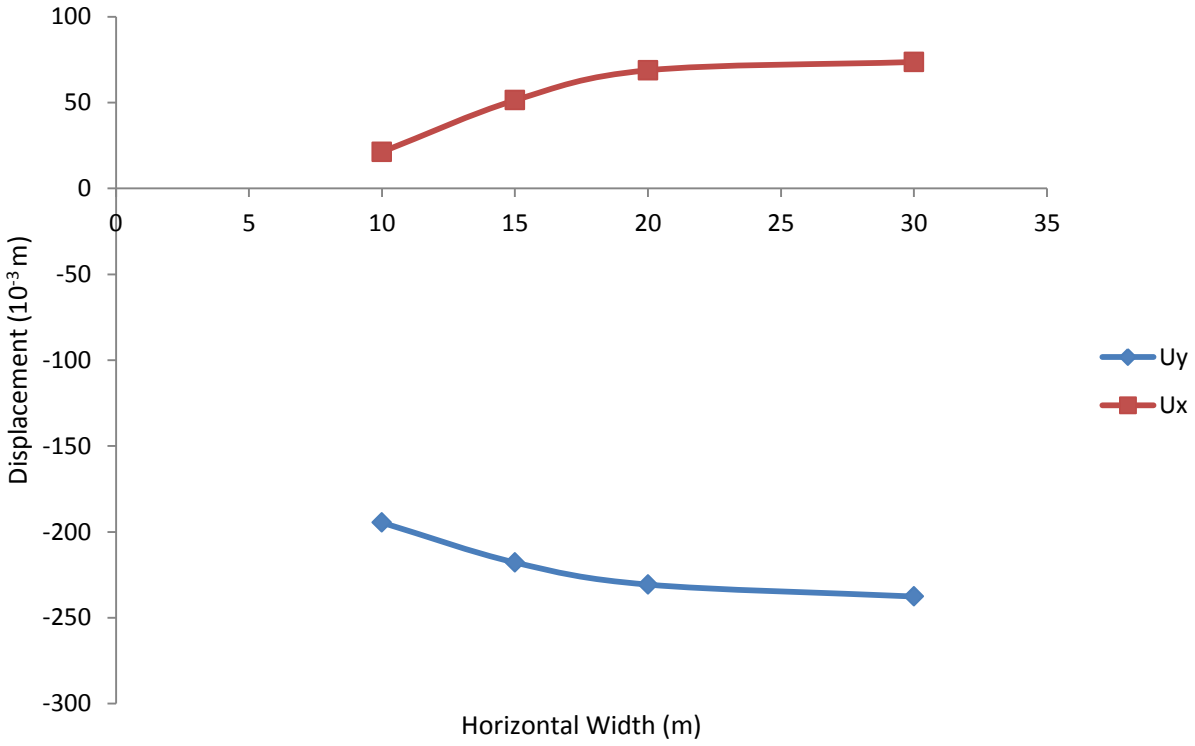

Figure 58. Effect of Boundary Fixities on Vertical (U_y) and Horizontal (U_x) Displacements at the top of the wall

Results shown in Figure 58 indicate that the boundary does not contribute to displacement for model widths beyond 20 m. Therefore, 20 m soil widths will be used for numerical model on PLAXIS. Another reason to limit the geometry of this study is to reduce the computation time of the analyses.

5.1.4.2 Effect of backfill friction angle and dimensionless ratio H/L on factor of safety:

Figure 59 shows a cross section of the MSEW-foundation soil model including an embankment height of 5 m and a reinforcement length of 4 m. After using the analysis method of "Phi-c-reduction" in PLAXIS, the global safety factor is found for different construction stages with different backfill friction angles. This study shows the effect of $\varphi_{Backfill}$ and the ratio of wall height (H) to the reinforcement length (L) on safety of the MSE Wall. Embankment height is varied at 1 m, 2 m, 3 m, 4 m and 5 m and the backfill friction angle is varied at 30°, 35° and 40°. Embankment height and the backfill friction angle are the controlling parameters, while the reinforcement length is kept constant as 4 m. Friction angle (along with effective stresses) controls the shear strength of soil and the numerical testing shows that the increase in backfill friction angle leads to an increase in the Factor of Safety. As the H/L ratio increases, the factor of safety of the MSE wall decreases since an increase in embankment height causes an increase in driving forces. Dimensionless analysis allows interpolation of different friction angles and H/L ratios. Results of this study are shown in Figure 60.

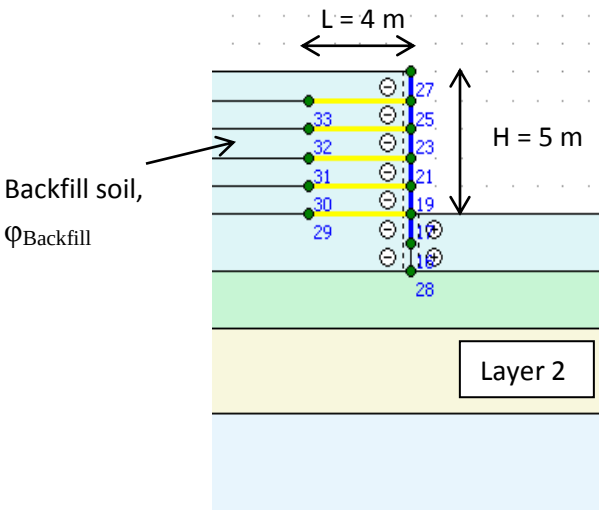

Figure 59. Cross section of MSEW

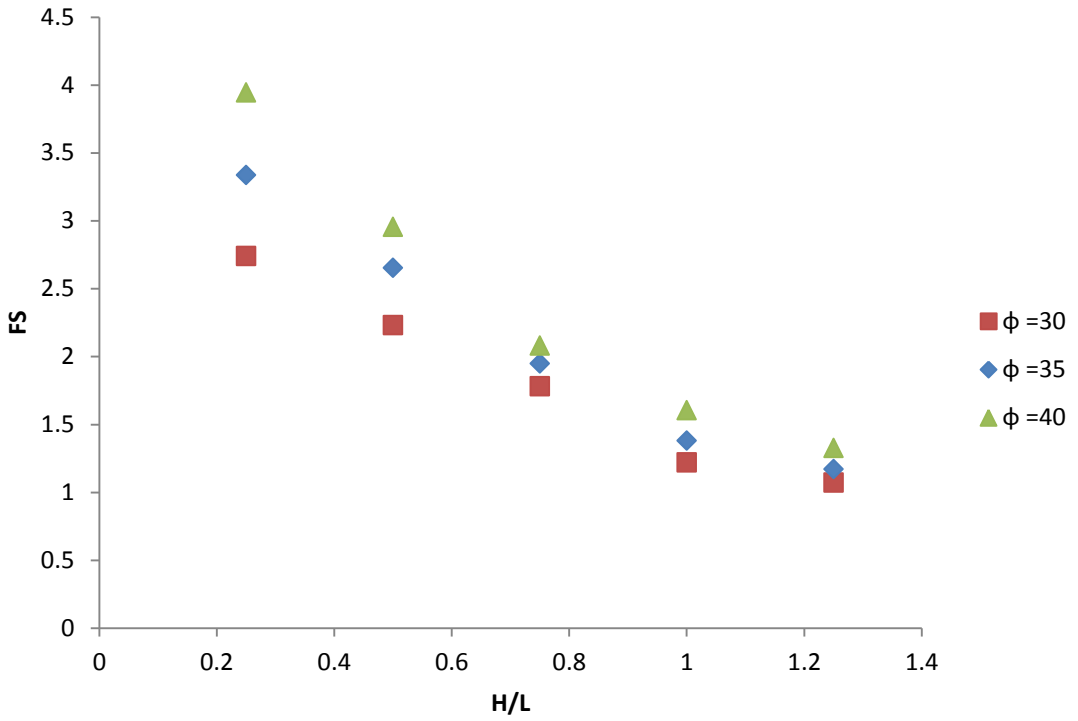

Figure 60. Effect of friction angle of the backfill and dimensionless ratio H/L on Factor of Safety

5.1.4.3 Effect of mechanical properties of soft soil layer on factor of safety:

- *Effect of dimensionless ratio S_u/E_u of Layer 2 on Factor of Safety*

Layer 2 is the critical soft soil layer since it has the lowest Young's modulus and low undrained shear strength. Hence, the effect of layer 2 on factor of safety is studied. In the first part of this parametric study, Young's modulus of layer 2 is kept constant at 1000 kPa and the undrained shear strength of layer 2 is varied as 14 kPa, 17 kPa and 24 kPa to investigate the effect of dimensionless ratio S_u/E_u of the layer 2 on factor of safety. Undrained shear strength is directly related with the safety of the foundation soil and numerical modeling results show that as the S_u/E_u ratio increases, the factor of safety increases. H/L ratio is selected as 1.25, which is

the most critical case for embankment safety as indicated in Figure 42. Result of this study is shown in Figure 61.

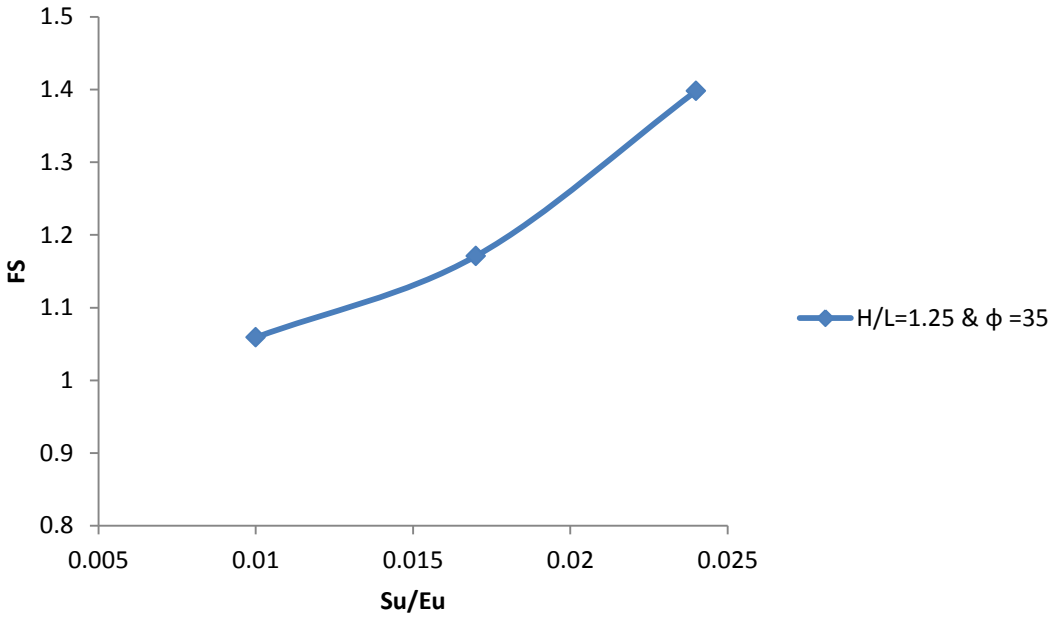

Figure 61. Effect of dimensionless ratio Su/Eu of Layer 2 on Factor of Safety

This study is also repeated with a different backfill friction angle to see the contribution of backfill friction angle on factor of safety for this analysis. For those conditions, the higher backfill friction angle has higher contribution to the embankment safety (Figure 62).

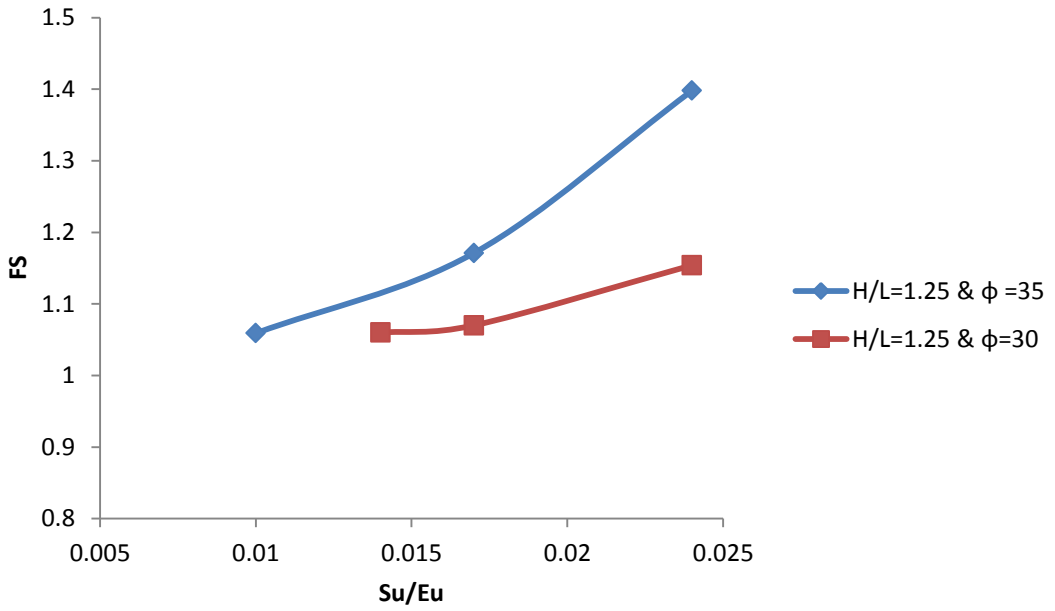

Figure 62. Effect of backfill friction angle to the factor of safety

In the second part of this parametric test, the undrained shear strength of layer 2 is kept constant at 17 kPa while Young's modulus increased from 1,000 kPa to 25,000 kPa to investigate the effect of dimensionless ratio S_u/E_u of the layer 2 on factor of safety. Deformation properties of elastic materials are described most often by Young's Modulus and Poisson's ratio and even though these parameters are defined for elastic materials under uniaxial loading, they are also used with inelastic materials such as soils (Kulhawy and Mayne, 1990). Young's modulus is the ratio of stress to strain and is a deformation-related parameter; therefore, it is concluded that Young's modulus does not have any contribution to factor of safety since factor of safety is only related with the strength of the soil layer. Results of this study are shown in Figure 63.

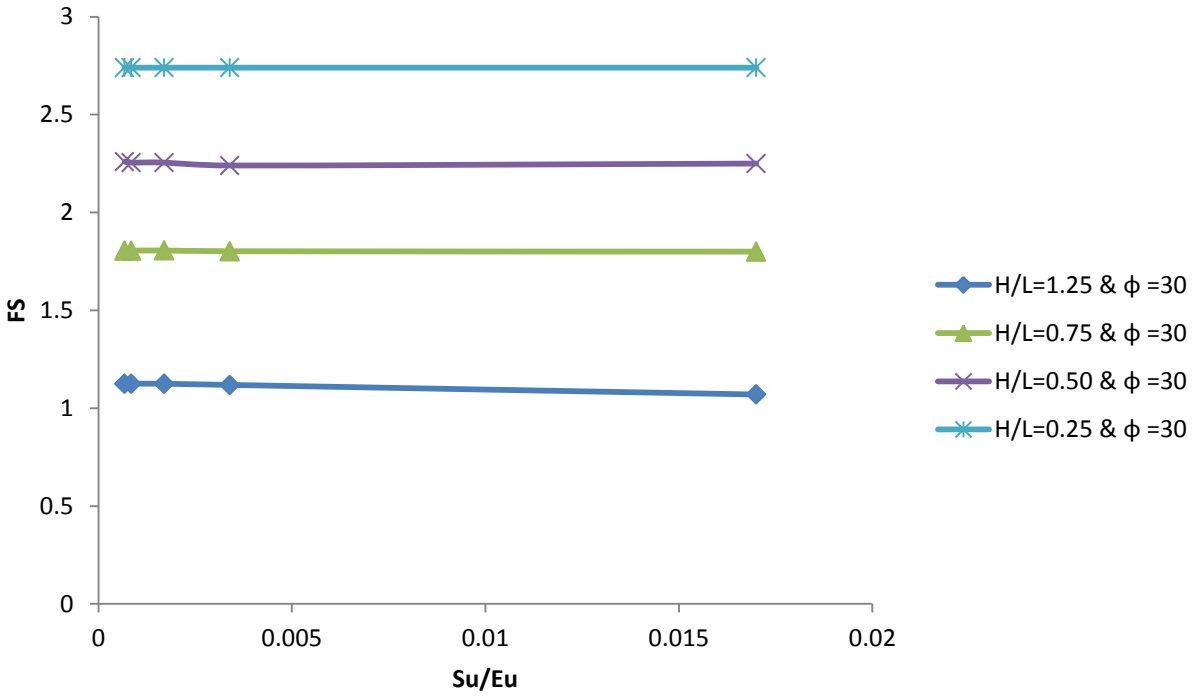

Figure 63. Effect of dimensionless ratio Su/Eu of Layer 2 on Factor of Safety

As the Buckingham's "Pi" theorem does not provide information on which one of these parameters control the behavior of the physical system, most of the dimensional parameters are evaluated using a numerical model developed in PLAXIS. Dimensionless ratio S_u/E_u is not a good parameter since material properties of undrained shear strength and Young's modulus are totally different. For instance S_u is safety related parameter; however E_u is stiffness-related parameter. Therefore, it is concluded from Figures 44 and 46 that increase in dimensionless ratio S_u/E_u gives different results in terms of factor of safety and cannot be used as a controlling dimensionless parameter.

- *Effect of dimensionless ratio $(\gamma H)/S_u$ of Layer 2 on Factor of Safety*

Since dimensionless ratio S_u/E_u is not a meaningful parameter, $(\gamma H)/S_u$ is selected for the next dimensionless parameter. This study shows the effect of backfill unit weight and change in wall height on safety of the MSE Wall. The embankment height is varied from 1 m to 5 m in steps of 1 m while the backfill unit weight was changed from 17.85 kN/m^3, to 18.85 kN/m^3, to 19.85 kN/m^3. Undrained shear strength of the layer 2 kept constant as 17 kPa. This ratio presents the interplay between load and strength and it is expected to see the effect of $(\gamma H)/S_u$ on factor of safety. Therefore, the increase in driving forces whether an increase in embankment height or backfill unit weight causes a decrease in factor o safety as shown in Figure 64.

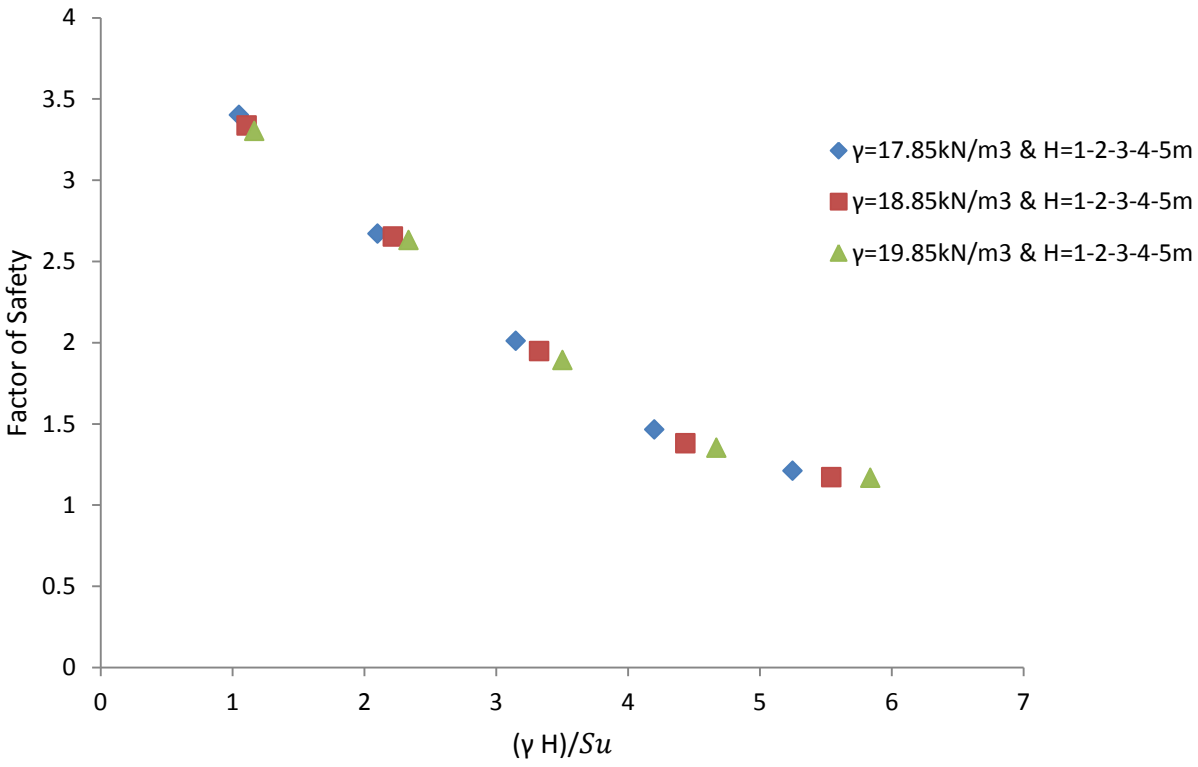

Figure 64. Effect of dimensionless ratio (γH)/S_u on Factor of Safety

- *Effect of Poisson's ratio of Layer 2 on Factor of Safety*

Poisson's ratio is defined as the negative ratio of transverse to axial strain; therefore, a change in Poisson's ratio affects displacements. Poisson's ratio does not have any contribution to factor of safety since factor of safety is only related with the strength of the soil layer as shown in Figure 65.

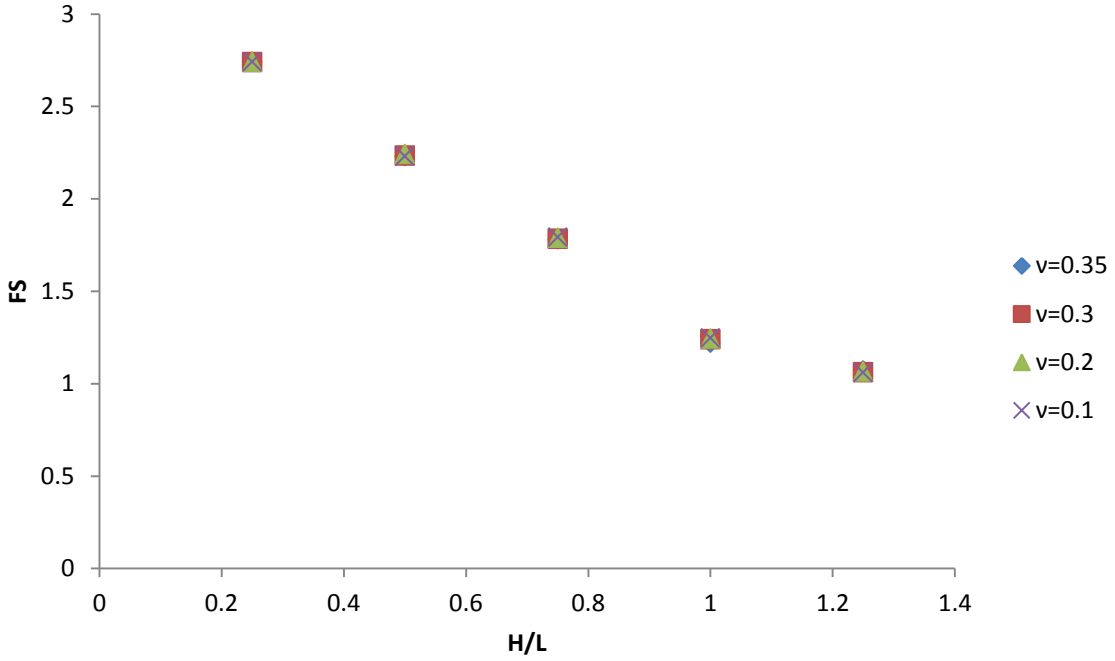

Figure 65. Effect of Poisson's ratio of Layer 2 on Factor of Safety

- *Effect of Poisson's ratio of Layer 2 on Displacements*

The effect of Poisson's ratio on displacements at the top of the wall facing (point L) is shown in Figure 66. If a material is compressed in one direction, expansion occurs in a direction perpendicular to the direction of compression. Due to embankment loading, soil beneath the embankment compresses vertically and expanding laterally. Therefore, in this case, Poisson's

ratio is the negative ratio of lateral to vertical strain. Higher horizontal settlements and lower vertical settlements result from higher Poisson's ratio values.

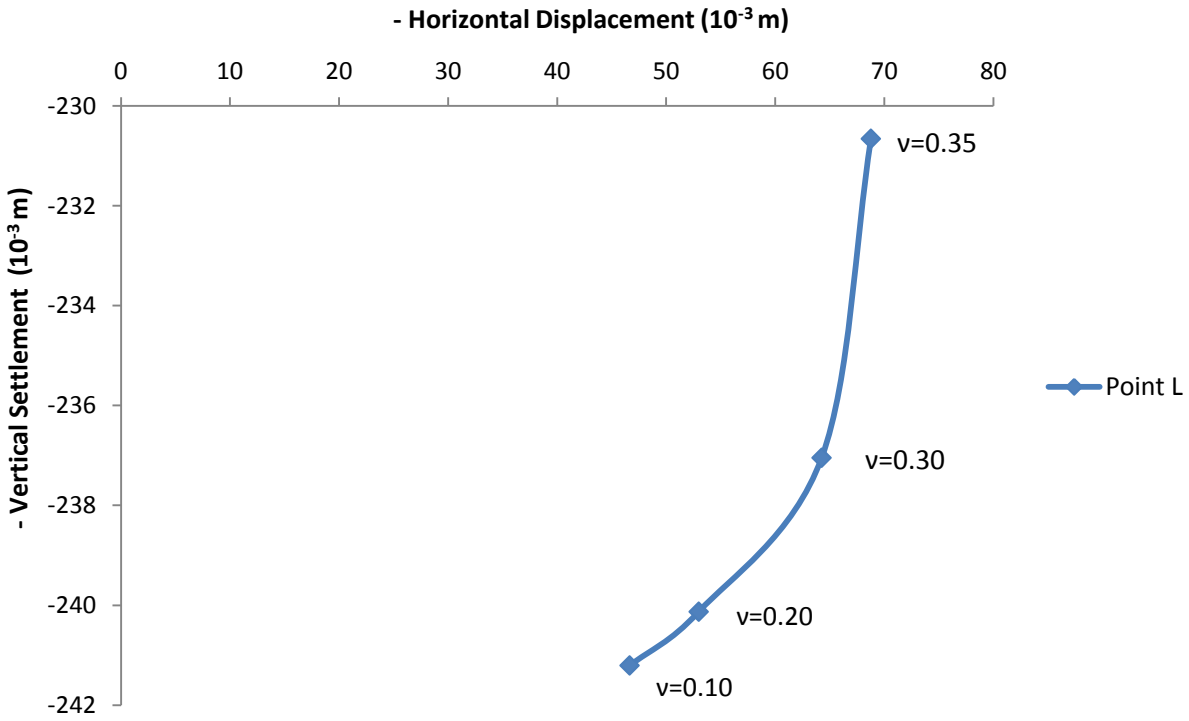

Figure 66. Effect of Poisson's ratio on displacements

- *Effect of dimensionless ratio S_u/E_u of Layer 2 on Displacements*

The effect of the dimensionless ratio S_u/E_u of the layer 2 on vertical displacements on top of the wall facing is investigated while keeping the undrained shear strength of layer 2 constant as 17 kPa and increasing the Young's modulus from 1,000 kPa to 25,000 kPa. The Mohr-Columb model is elastic perfectly plastic model and a decrease in Young's modulus leads to an increase in axial deformation while keeping the strength constant as seen in Figure 67. This

is also validated in the numerical analysis, which presented in Figure 68. As Young's modulus increases, the dimensionless ratio S_u/E_u decreases and vertical settlement decreases.

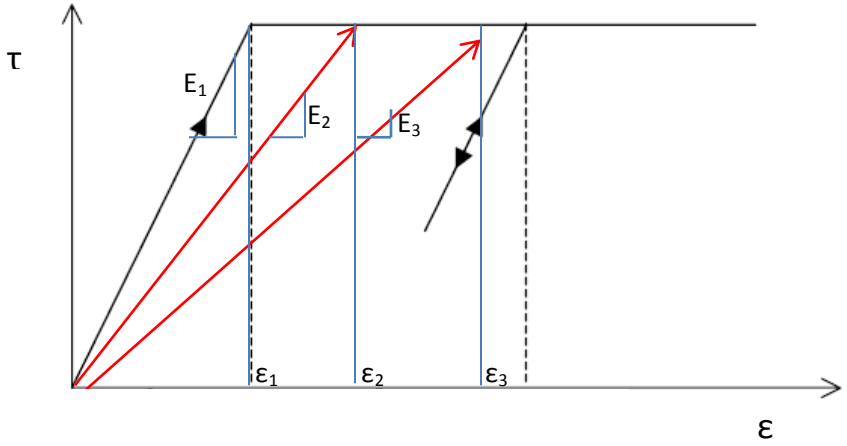

Figure 67. The elastic perfectly plastic Mohr-Coulomb Model

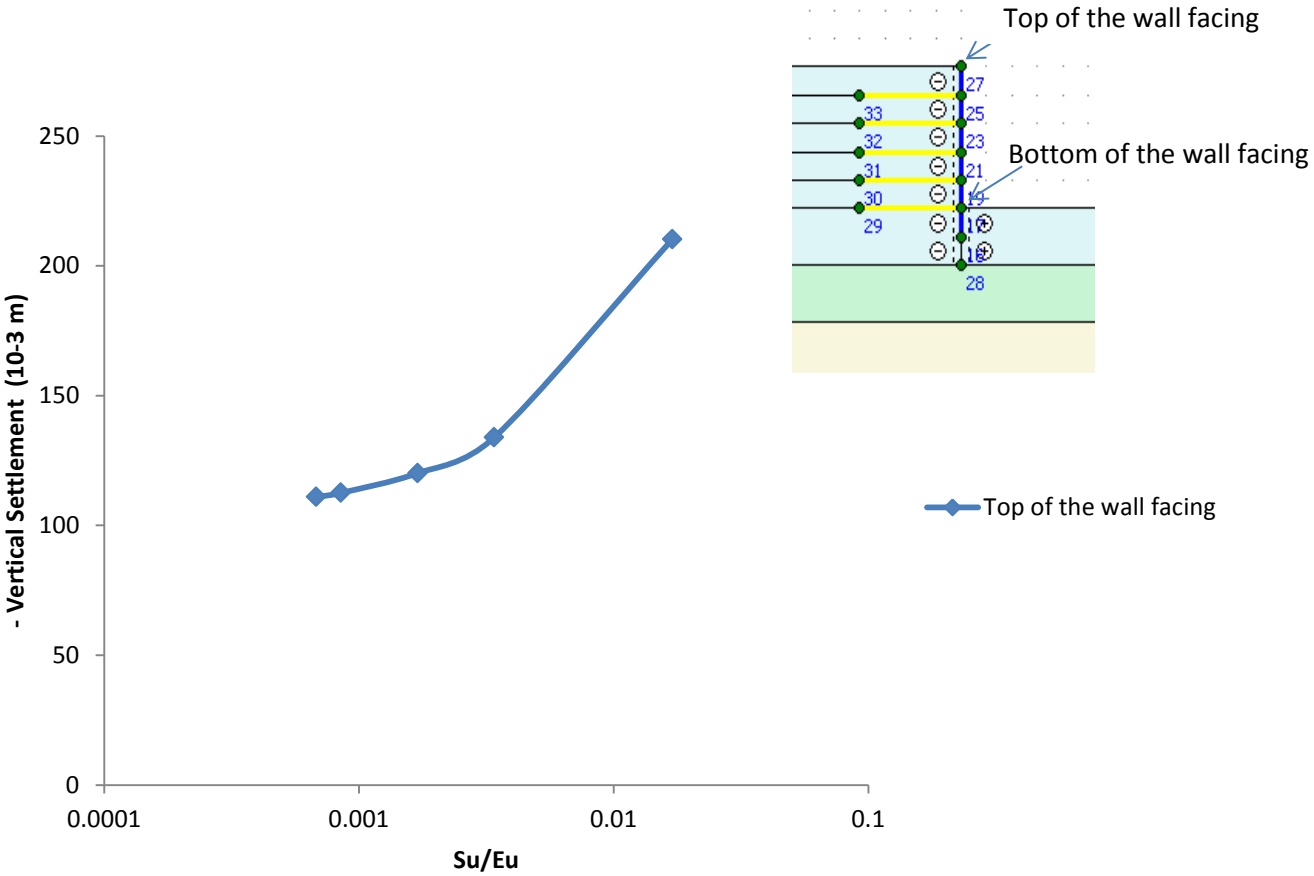

Figure 68. Effect of dimensionless ratio S_u/E_u on vertical settlements

In the second part of this study, the effect of dimensionless ratio S_u/E_u of the Layer 2 on dimensionless ratio vertical settlement to lateral displacement is investigated. While keeping the undrained shear strength of Layer 2 constant at 17 kPa and Young's modulus increased from 1,000 kPa to 25,000 kPa. In this scenario, the dimensionless ratio vertical settlement to lateral displacement is not affected by the change in Young's modulus. Results are shown in Figure 69.

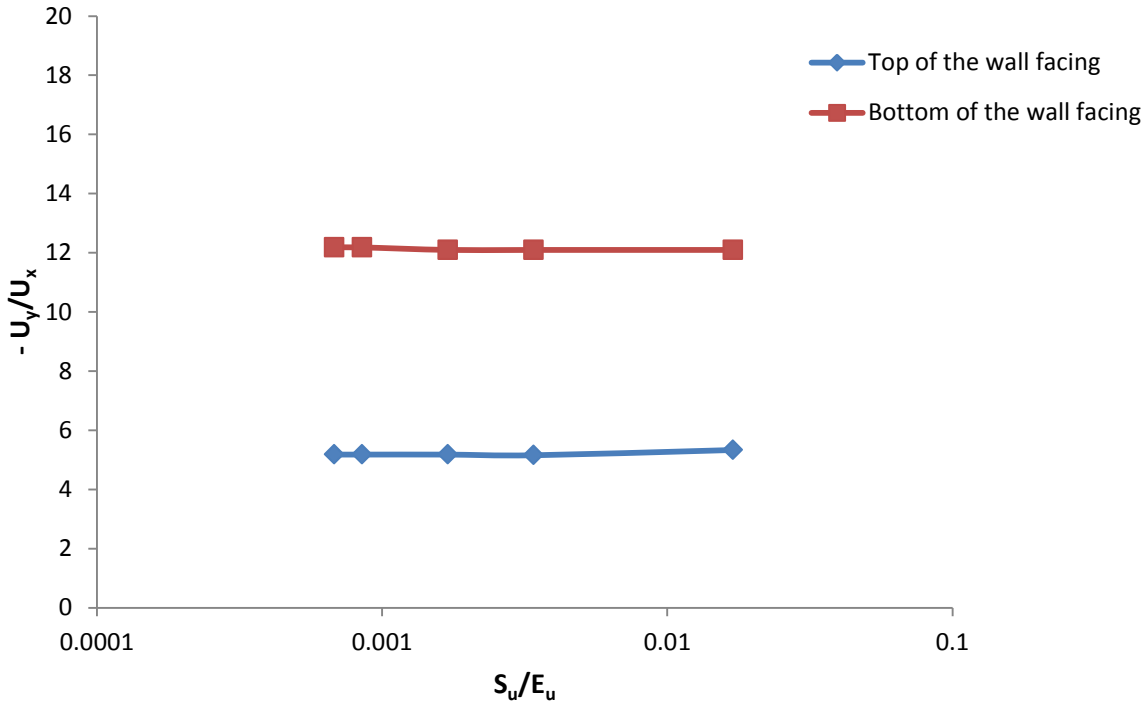

Figure 69. Effect of Dimensionless ratio S_u/E_u on dimensionless ratio $-U_y/U_x$

- *Effect of dimensionless ratio $(\gamma H)/E_u$ of Layer 2 on Displacements*

The effect of dimensionless ratio $(\gamma H)/E_u$ of the layer 2 on vertical displacements on top of the wall facing is investigated for the maximum embankment height (5 m) with a unit weight of 18.85 kN/m^3, while Young's modulus changes from 1,000 kPa, to 25,000 kPa. The changes in Young's modulus directly affect the vertical settlements as shown in Figure 70.

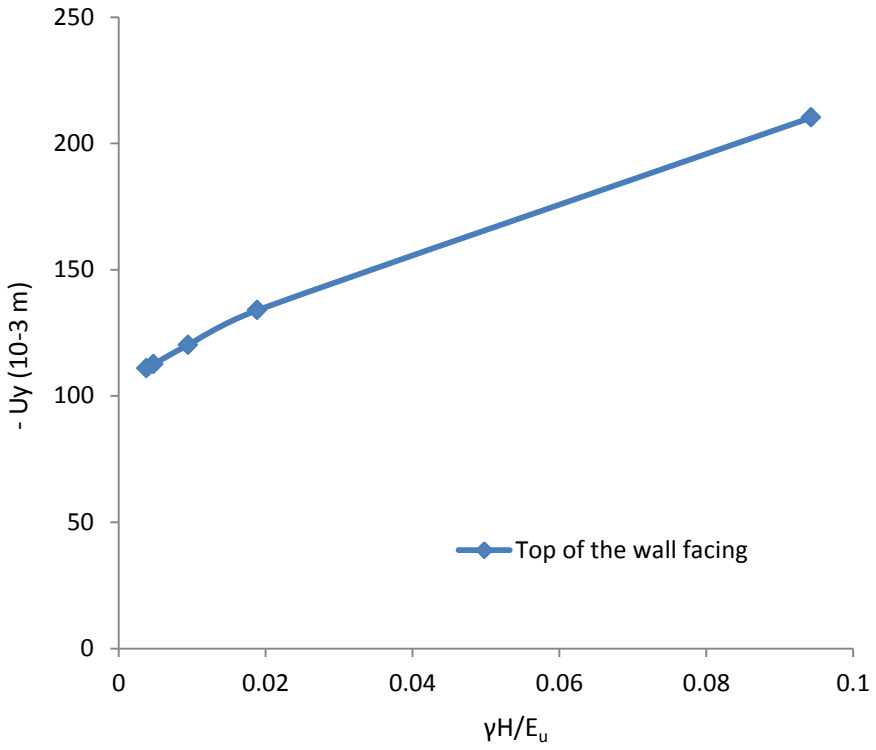

Figure 70. Effect of dimensionless ratio $(\gamma H)/E_u$ of layer 2 on vertical settlements

5.1.4.4 Contribution of Lateral Displacements on Vertical Settlements

Stress history strongly affects the undrained shear strength of clays. There is a difference in behavior between normally consolidated (NC) and overconsolidated (OC) clays due to stress history. Ladd et al. (1977) showed that the ratio of undrained shear strength to effective vertical stress of overconsolidated clays to normally consolidated clays is approximately equal to the OCR to the 0.8 power;

$$\left(\frac{S_u}{\sigma'_v}\right)_{OC} = \left(\frac{S_u}{\sigma'_v}\right)_{NC} * (OCR)^{0.8} \quad [5.10]$$

This relationship is used to calculate undrained shear strength of overconsolidated clays used in the PLAXIS model. Calculated values are shown in Table 12.

Table 12.Undrain shear strength and Young's Modulus values for OC Clays

LAYER 2							
OCR	**1**	**2**	**3**	**4**	**6**	**8**	**12**
Su (kPa)	50	87.1	120.4	151.6	209.6	263.9	365.0
Eu (kPa)	1000	1741.1	2408.2	3031.4	4193.0	5278.0	7300.4
Eu/Su	20						
Su (kPa)	75	130.6	180.6	227.4	314.5	395.9	547.5
Eu (kPa)	1500	2611.7	3612.3	4547.1	6289.4	7917.0	10950.6
Eu/Su	20						
Su (kPa)	100	174.1	240.8	303.1	362.4	419.3	527.8
Eu (kPa)	2000	3482.2	4816.4	6062.9	7247.8	8385.9	10556.1
Eu/Su	20						

Horizontal displacements for normally consolidated and highly overconsolidated clays are presented in Figure 54 and 55. It is observed that horizontal settlements are greater for normally consolidated clays and lateral expansion also exists at the ground surface. However, highly overconsolidated clay behaves like fully constrained in the lateral directions on ground surface having a zero horizontal settlement value.

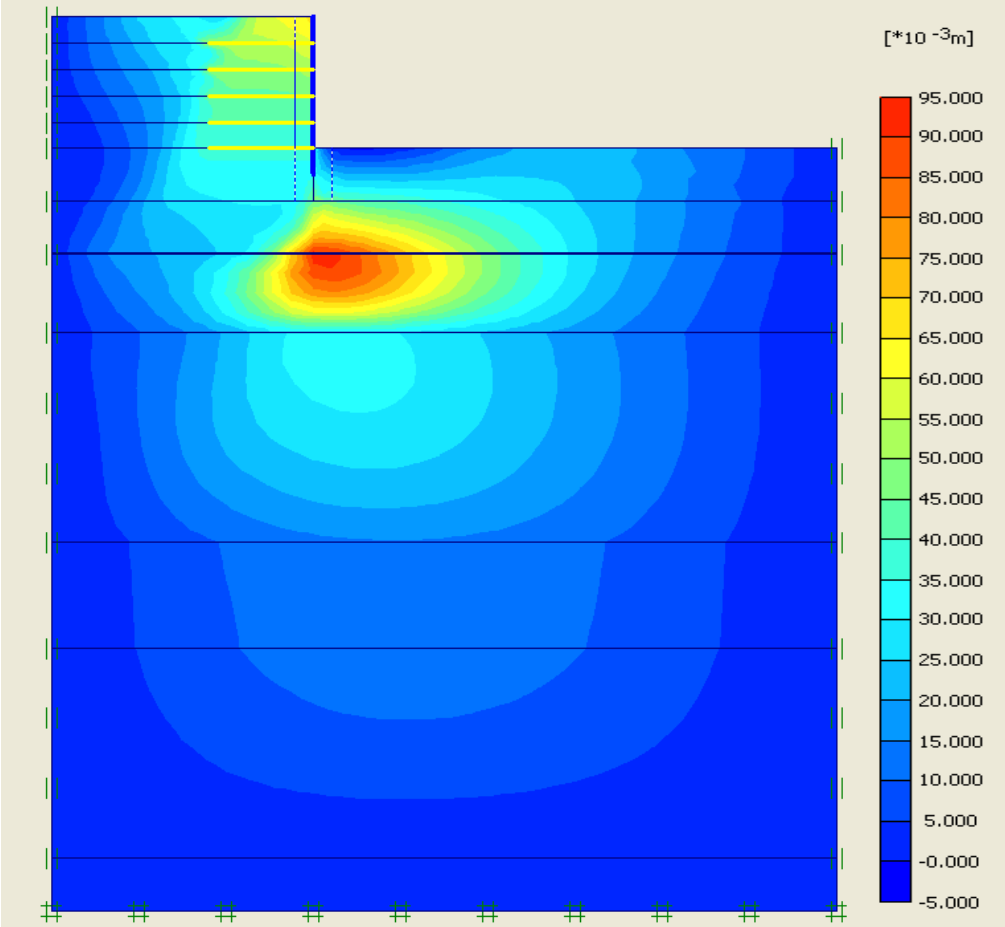

Figure 71. Horizontal Displacements for NCC (Extreme U_x = 92.54* 10^{-3} m)

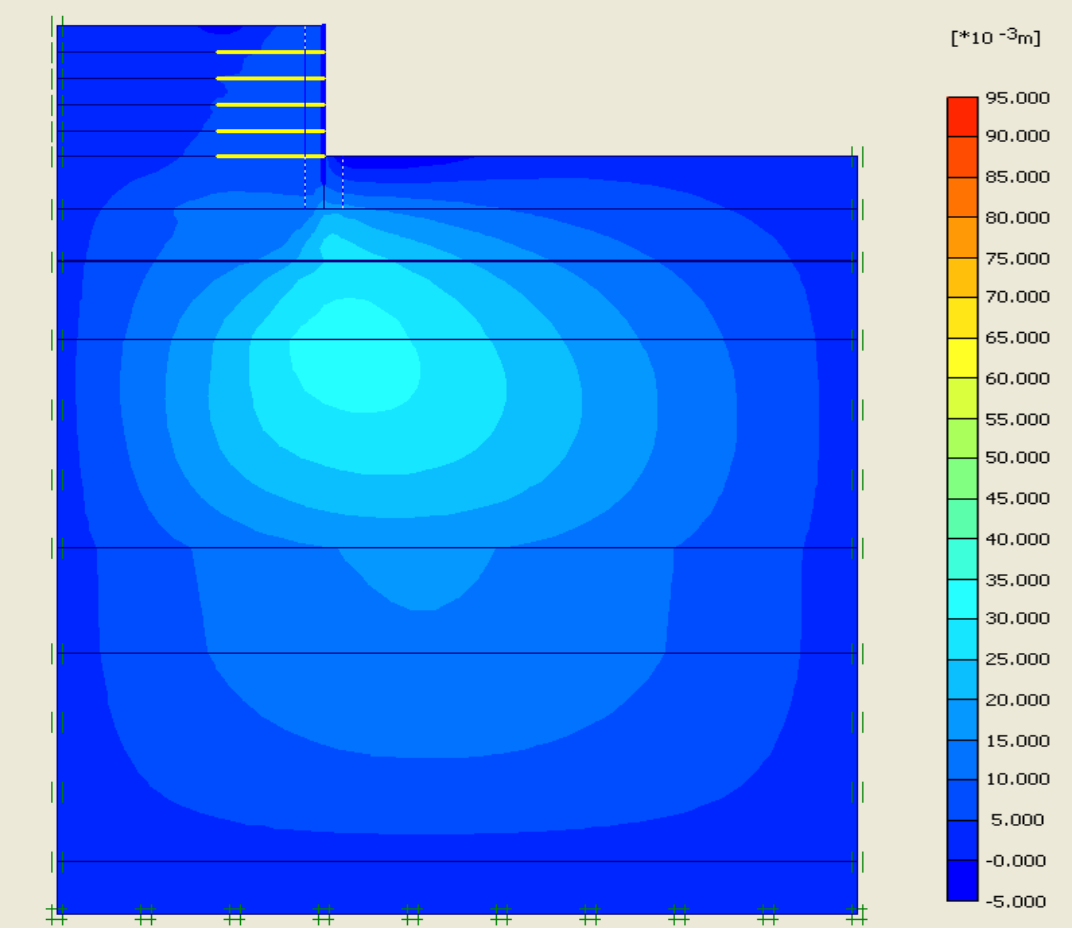

Figure 72. Horizontal Displacements for OCR = 12 (Extreme $U_x = 30.58* 10^{-3}$ m)

Vertical displacements for normally consolidated and highly overconsolidated clays are presented in Figures 56 and 57. These results show that vertical settlements are greater for normally consolidated clays due to the lateral contribution to vertical settlements. However, highly overconsolidated clays only undergo, as expected, volume deformations compressing vertically which causes less vertical settlements than normally consolidated clays.

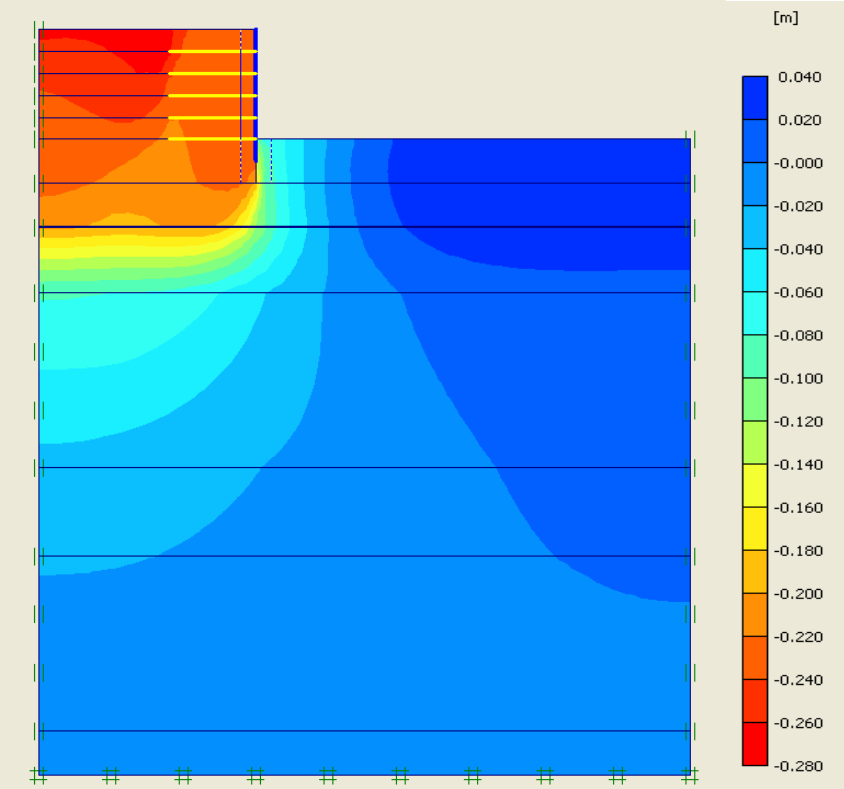

Figure 73. Vertical Displacements for NCC (Extreme U_y = -272.71* 10^{-3} m)

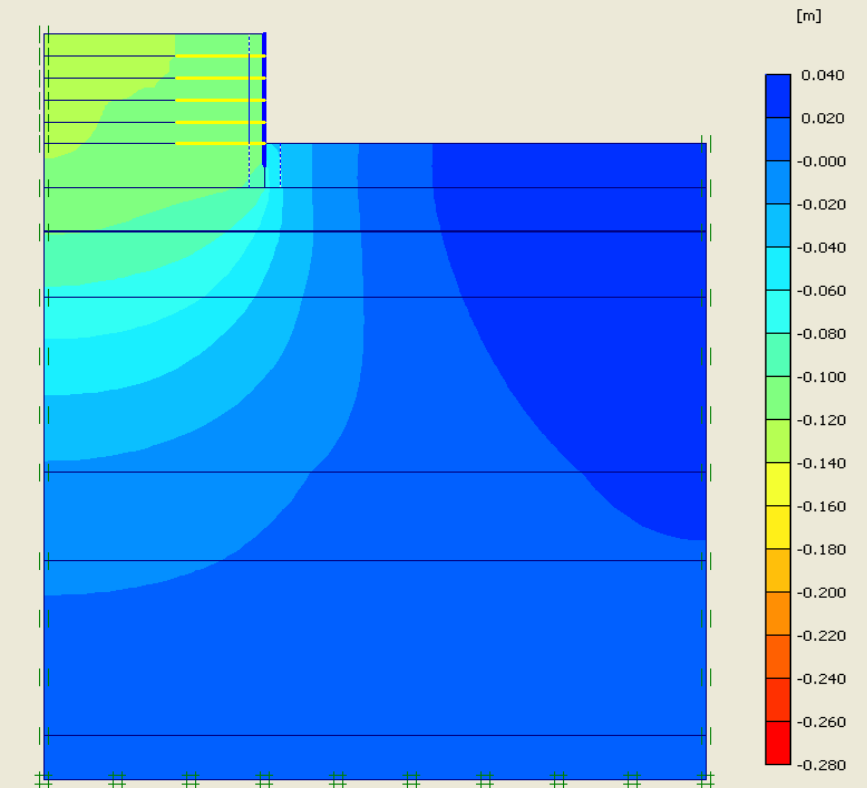

Figure 74. Vertical Displacements for OCR=12 (Extreme U_y = -133.17* 10^{-3} m)

Vertical compression and lateral expansion are the two main contributions to settlements. The contribution of lateral displacement to vertical settlement is maximum for a normally consolidated clay. As the overconsolidation ratio increases, the contribution of lateral displacements to vertical settlements decreases. Results of this study are shown in Figure 58. As OCR increases, lateral displacement goes to zero, at this time 1D consolidation is the only reason for vertical settlement. Also lower undrained shear strength and Young's modulus leads to a higher vertical settlement for NC clays. An increase in OCR leads to greater decrease in horizontal displacements than vertical settlements as shown in Figure 76.

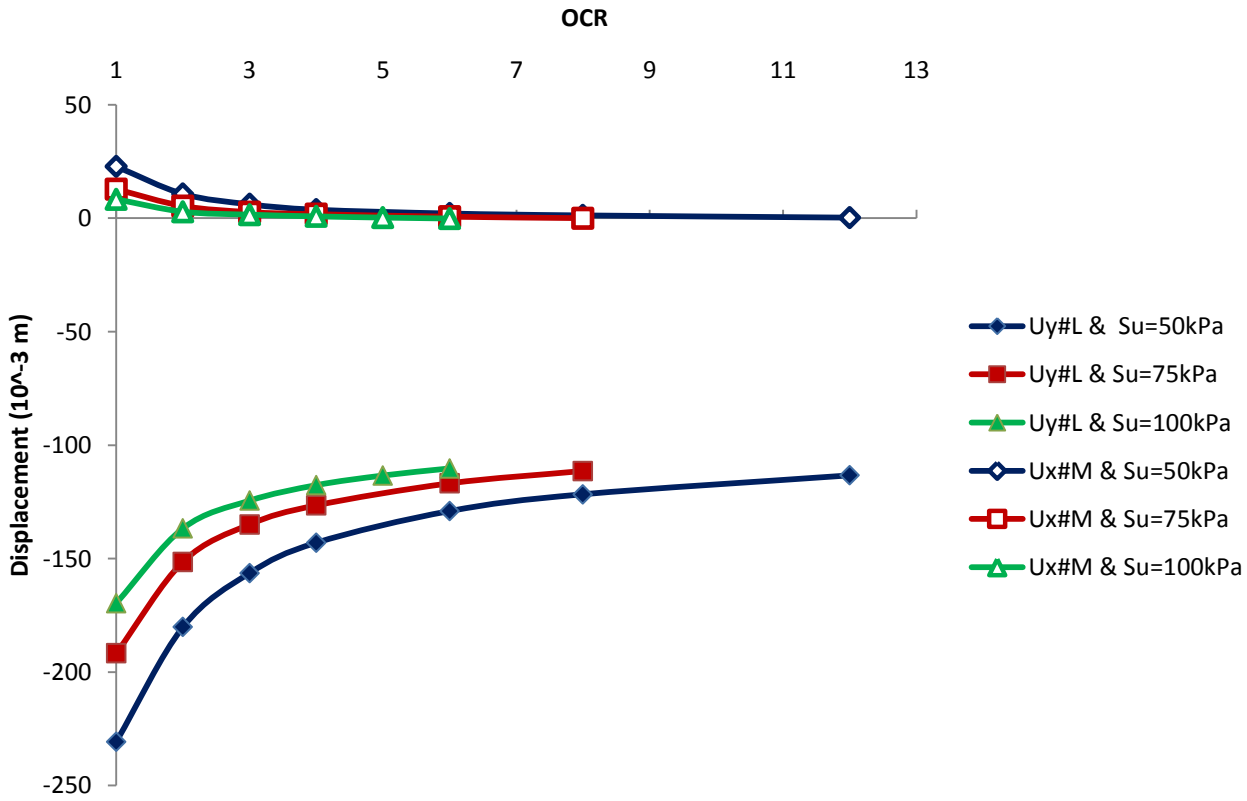

Figure 75. Contribution of Lateral Displacements to Vertical Settlements

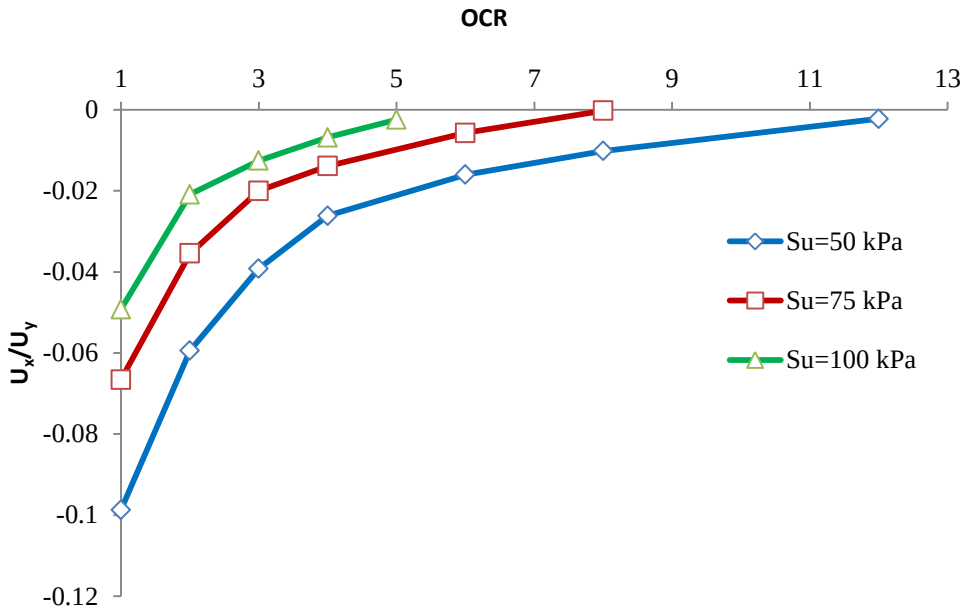

Figure 76. Ratio of Lateral Displacements to Vertical Settlements versus OCR

5.2 Parametric Studies with PLAXIS 3D

The effect of Young's modulus on both vertical and horizontal settlement was analyzed within this parametric study. All of the material properties of soil and embankment remained constant except the Young's modulus. Identical material properties were selected for both the soil and the embankment except for the friction angle. Related soil properties are provided in Table 5 and the embankment-soil geometry is provided in Figure 77.

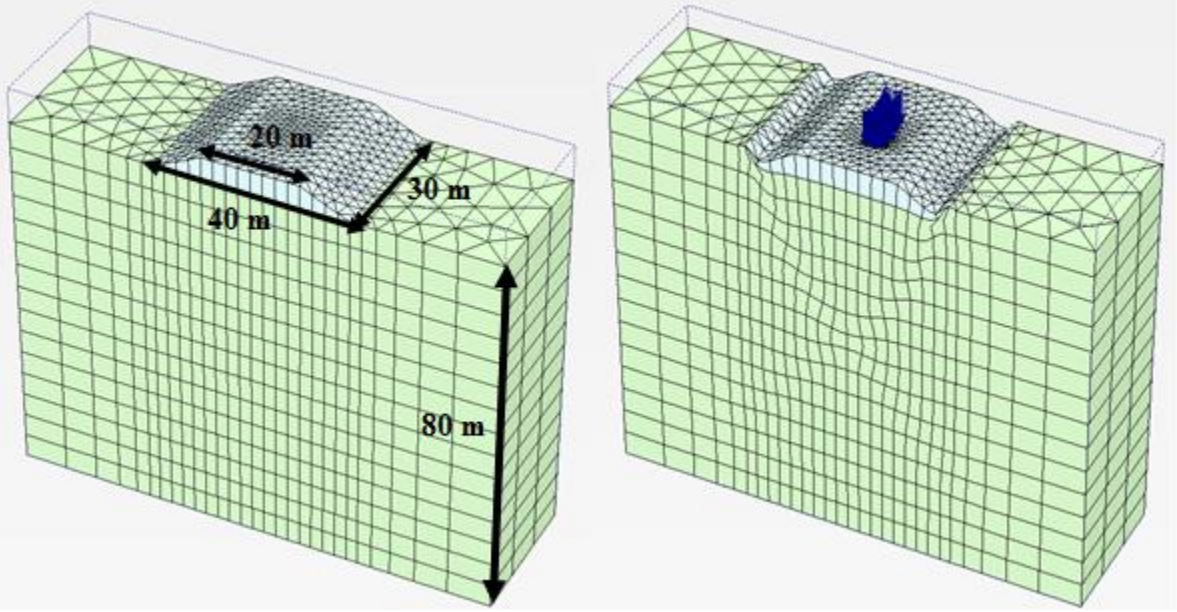

Figure 77. Soil Embankment Geometry and Deformed Shape after Consolidation (Scale 1:50)

To properly model the system, the minimum soil depth must be double of the embankment width to accommodate the depth of influence. Since the width of the embankment is 40 m, required soil depth is taken as 80 m. A pressure of 25 kPa was applied to the center of the embankment within 10 m^2 region.

Table 13. Soil and Embankment Properties

Properties	**Embankment**	**Soil**
Layers (m)	5.0 - 0.0	0.0 - (-80.0)
Young modulus E (kPa)	2000 – 10,000 -20,000 – 30,000 – 40,000	2000
Poisson's ratio ν	0.3	0.3
Friction angle ϕ (degrees)	30	20
Unit weight (kN/m^3)	17	17

The ultimate time was arranged to 365 days for consolidation to represent long term behavior and let the excess pore water pressure to escape from soil body. Selected soil depths are appropriate because there is no deformation at the bottom of the soil layer (Figure 77). Figure 78 shows the relation between embankment stiffness and the vertical displacements. As the embankment becomes stiffer with increasing Young's modulus, less vertical settlement occurs. Vertical settlements are different for the low Young's modulus value at the top, middle and bottom of the embankments. But settlements at different layers of the embankment reach to a constant value with the increase in Young's Modulus.

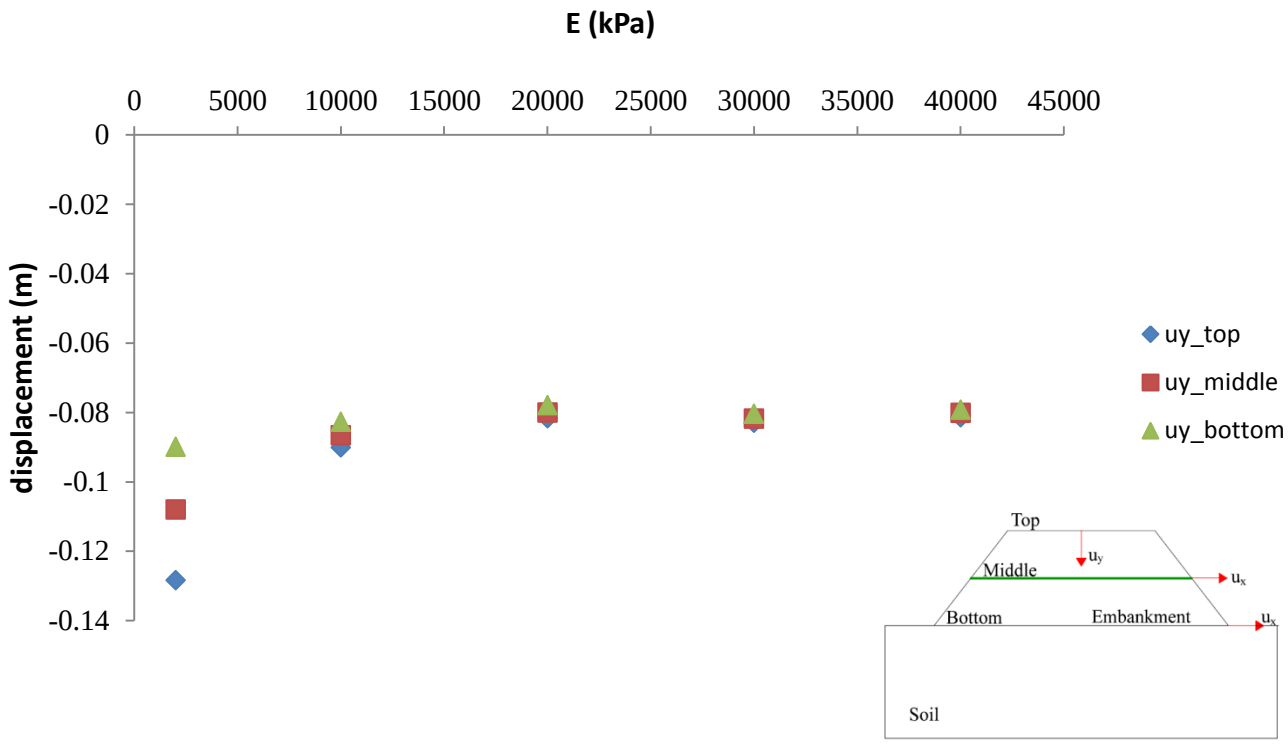

Figure 78. Relation between the changes in Young's Modulus and vertical settlements in the embankment

The total horizontal displacement plot for consolidation phase is provided in Figure 79. The highest horizontal settlement occurs at the edge of the embankment, which verifies that tall embankments are not fully constrained in the lateral directions of an embankment. The total horizontal displacement plot is a symmetric figure therefore same amount of displacement occurs at the both right and left edge of an embankment with different directions with almost zero displacement at the bottom of the model.

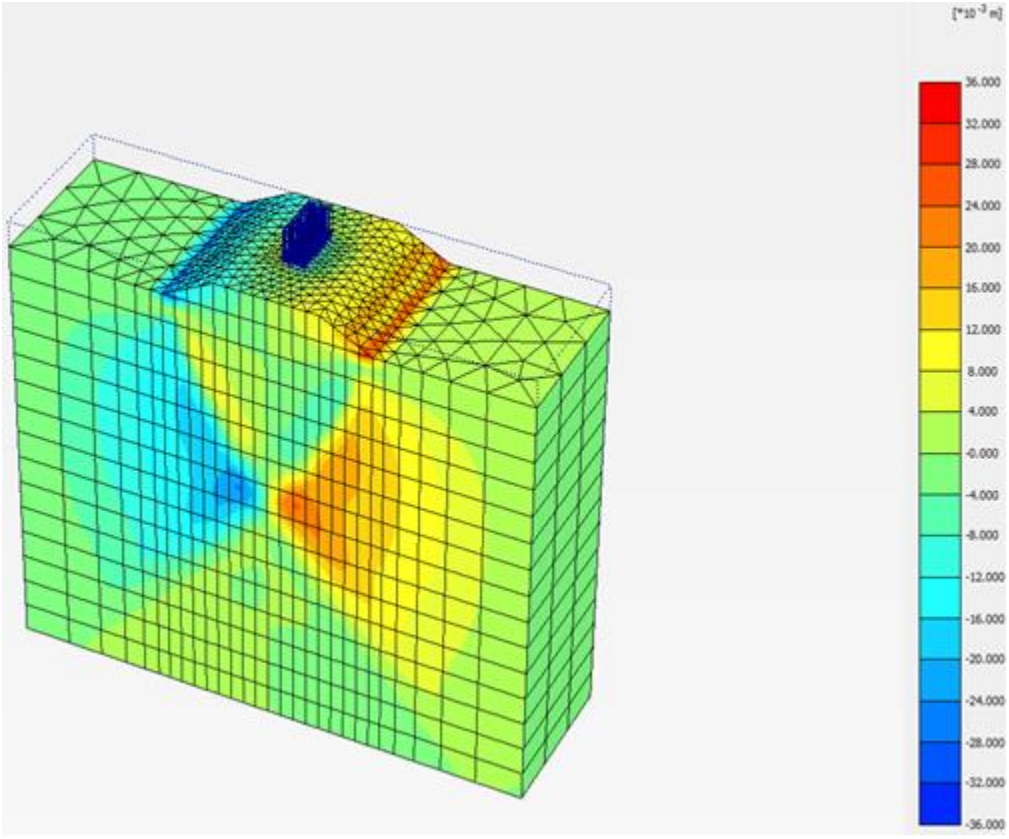

Figure 79. Total horizontal displacement plot

Lateral displacement contribution to vertical settlement is provided in Figure 80. The contribution of lateral displacement to vertical settlement increases with decrease in Young's modulus of the embankment. This study proves that Young's modulus is a deformation-related parameter, which directly affects the settlements under embankments. Since embankments are not fully constrained in lateral directions, lateral settlements contribute to vertical settlements for soils having lower stiffness values. However, for soils with high stiffness behave like they are constrained in lateral directions and lateral settlements do not contribute to vertical settlements.

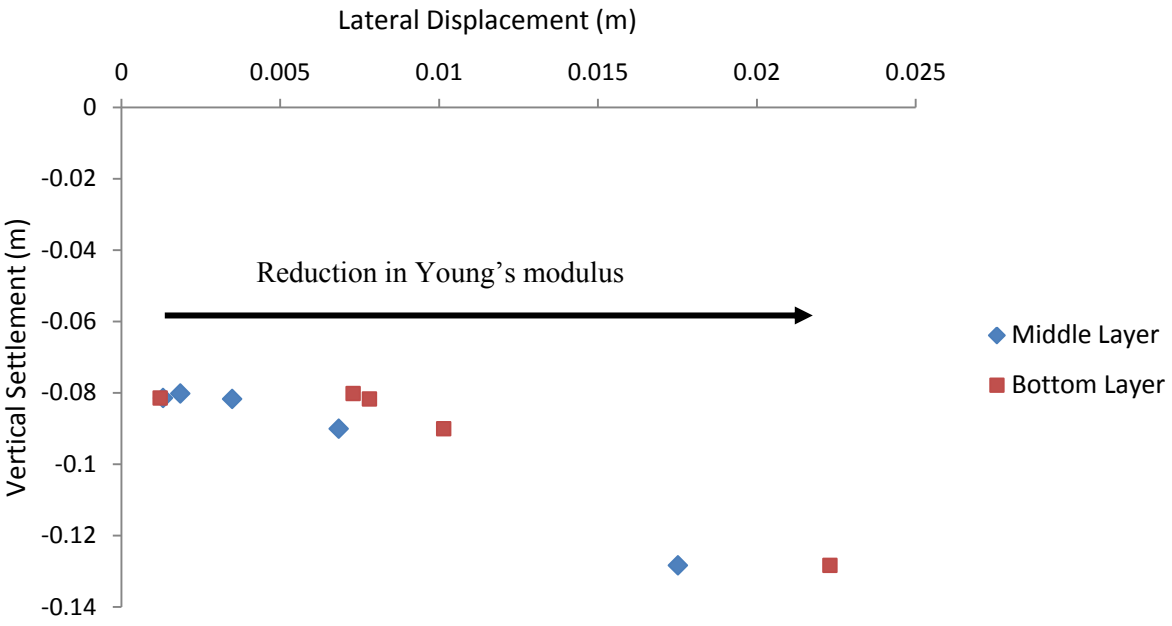

Figure 80. Lateral displacement contribution to vertical settlement

6 Conclusions

The construction of tall embankments and retaining walls on soft soils typically requires staged construction, which leads to an increase in effective stress, reduction in void ratio and settlement, and gain in shear strength. However, tall embankments are not fully constrained contributing to the potential of global failure of the foundation soil and generation of lateral movements that magnify vertical settlements of the embankments. This study systematically presented how material properties and embankment geometries influence the safety of the embankment and the relationship between lateral movements to the magnitude of vertical settlement on embankments using numerical analyses and analytical methods. The parametric studies were conducted to evaluation how combinations of embankment geometries and soft soil conditions influence failure mechanisms and the contribution of lateral deflection to vertical settlement.

The following conclusions are advanced:

- Increase in backfill friction angle leads to an increase in factor of safety. As the dimensionless ratio H/L increases factor of safety of MSE wall decreases since increase in embankment height cause an increase in driving forces.
- Increase in dimensionless ratio S_u/E_u due to an increase in undrained shear strength of the critical soil layer (layer 2) leads to an increase in factor of safety since undrained shear strength directly affect the safety of the foundation soil. Undrained Young's modulus was kept constant for this study. While an increase in dimensionless ratio S_u/E_u due to an increase in undrained Young's modulus does not affect the factor of safety since factor of safety is only related with the strength of the soil layer. Undrained shear strength was kept constant for this study. Accordingly, the dimensionless ratio

S_u/E_u is not a good dimensionless parameter since the contributions of S_u and $E_u$on safety are totally different.

- Increase in dimensionless ratio $(\gamma H)/S_u$ leads to a decrease in factor o safety because increase in driving forces whether an increase in embankment height or backfill unit weight causes a decrease in factor o safety.
- Poisson's ratio does not have any contribution to factor of safety since factor of safety is only related with the strength of the soil layer. However, change in Poisson's ratio directly affects the settlements. Higher horizontal settlements and lower vertical settlements were seen under higher Poisson's ratio values.
- Decrease in the dimensionless ratio S_u/E_u due to an increase in Young's Modulus leads to a decrease in vertical settlements. Moreover, the dimensionless ratio vertical settlement to lateral displacement is not affected by the change in Young's modulus
- The contribution of lateral displacements to vertical settlements is maximum for normally consolidated clays. As the overconsolidation ratio increases, the contribution of lateral displacements to vertical settlements decreases. For heavily overconsolidated clays, lateral displacements tend to go to zero, at this time 1D consolidation is the only reason of vertical settlements. This observation has important engineering implications, as the settlement of embankments over heavily overconsolidated soils can be calculated using simple consolidation settlement analyses (e.g., Ko-condition) while in the case of embankments founded on normally consolidated soils, strip footing analysis must still be used.
- The increase in effective stress due to staged construction leads to a sudden increase in excess pore water pressure and this value is around 30 kPa for 25 days consolidation

time interval. However, excess pore water pressure decreases to 16 kPa for 200 days consolidation time interval for each stage which shows that dissipation of excess pore water pressure is slow due to the low hydraulic conductivity of soft soils. Moreover, location of transducers affects the excess pore pressure value. Deeper transducer has the highest excess pore water pressure.

REFERENCES

Abramson L. W., Lee T. S., Sharma S., and Boyce G. M., 2002, "Slope Stability and Stabilization Methods," Second Edition, John Wiley & Sons, Inc., New York

Barbour L. S., and Krahn J., 2004, "Geotechnical News, Numerical modeling prediction and process" Geotechnical News, BiTech Publishers, Richmond, British Columbia, pp.44-52

Biot M. A., 1956, "General Solutions of the Equations of Elasticity and Consolidation for a Porous Material," Journal of Applied Mechanics, Transactions ASME, 78, pp. 91-96.

Birand A., Ergun U., and Erol O., 2002, "CE 366 Foundation Engineering 1 Lecture Notes," Middle East Technical University, Department of Civil Engineering, Ankara, Turkey.

Bjerrum L., 1972, "Embankments on soft ground. In," Proc. ASCE Spec. Conf. Performance Earth Supported Structures, Purdue University, 2: 1–54.

Buckingham E., 1916, "Model Experiments and the Forms of Empirical Equations", American Society of Mechanical Engineering, 37: 263-296

Budhu M., 2011, "Soil Mechanics and Foundations," 3rd Edition, John Wiley & Sons, Inc., New York.

Budge A. S., Bay J. A., Anderson L. R., 2006, "Calibrating Vertical Deformations in a Finite Element Model of a MSE Wall" Geo-Congress.

Burland J. B., 1987, "Nash Lecture: The Teaching of Soil Mechanics – a Personal View," Proceedings, 9th ECSMFE, Dublin, 3: 1427-1447.

Burland J. B., 1996, "Closing session Discussions, Proceedings of the First International Conference on Unsaturated Soils Conference," Paris, Vol. 3, p.1562, Proceedings published by A.A. Balkema; Editors, Alonso E. E., and Delage P.

Burland J. B., Jamiolkowski M. B., and Viggiani C., 2009, "Leaning Tower of Pisa: Behavior after Stabilization Operations", Internal Journal of Geoengineering Case Histories, 1(3):156.

Brinkgreve R. B. J., and Bakker H. L., 1991, "Non-linear Finite Element Analysis of Safety Factors," Proceedings of the Seventh International Computer Methods and Advances in Geomechanics.

Brinkgreve R. B. J., AL-Khoury R., Bakker K. J., Bonnier P. G., Brand P. J. W., and Broere W., 2002, "PLAXIS 2D- Version 8 General Information," Delft University of Technology & PLAXIS b.v., The Netherlands.

Brinkgreve R. B. J., 2004, "Time-dependent behavior of soft soils during embankment construction – A Numerical Study," Numerical Models in Geomechanic, 631-637.

Brinkgreve R. B. J., AL-Khoury R., Bakker K. J., Bonnier P. G., Brand P. J. W., and Broere W., 2007, "PLAXIS 3D Foundation General Information," Delft University of Technology & PLAXIS b.v., The Netherlands.

Cai M., and Horii H., 1992, "A Constitutive Model of Highly Jointed Rock Masses," Mechanics of Materials, 13: 217-246.

Chin Y. T., and Sew S. G., 2000, "Design and Construction Control of Embankment Over Soft Cohesive Soils," SOGISC- Seminar on Ground Improvement-Soft Clay.

Christian J. T., and Carrier W. D., 1978, "Jambu, Bjerrum and Kjaernsli's Chart Reinterpreted: Reply", Canadian Geotechnical Journal, 15: 619-620,

Clayton L., Attig J. W., Mickelson D.M., Johnson M.D., and Syverson K.M., 2006, "Glaciation of Wisconsin", Educational Series 36, Third edition,

Clough R. W., and Woodward R., 1967, "Analysis of Embankment Stresses and Deformations," Journal of Soil Mechanics and Foundation Division, ASCE, 93: 529–549.

Coduto D. P., 1999, "Geotechnical Engineering Principles and Practices," Prentice Hall, Upper Saddle River, NJ.

Craig R. F., 2004, “Craig’s Soil Mechanics,” Seventh Edition, Spon Press London and New York.

Dunnicliff J., 1993, “Geotechnical Instrumentation for Monitoring Field Performance” John Wiley & Sons, Inc.

FHWA Publication, 2001, “Mechanically Stabilized Earth Walls and Reinforced Soil Slopes Design & Construction Guidelines”, Publication Number: FHWA-NHI-00-043, http://isddc.dot.gov/OLPFiles/FHWA/010567.pdf.

Fox P. J., 2003, “Consolidation and Settlement Analysis- Chapter 19” Purdue University

Grant R., Christian J. T., and Vanmarcke E. H., 1974, “Differential Settlement of Buildings”, Journal of the Geotechnical Engineering Division, 100(GT9): 973-991

Holtz D. H., Kovacs W. D., and Sheahan T. C., 2011, “An Introduction to Geotechnical Engineering,” Second Edition, Pearson.

Hossain S., Oelchenko V., and Mahmood T., 2009, “Case History of Geosynthetic Reinforced Segmental Retaining Wall Failure,” Electronic Journal of Geotechnical Engineering, EJGE, Vol.14, Bund.

Kachanov L. M., 1974, “Fundamentals of the theory of plasticity,” MIR publishers, Moscow.

Kelln C., Sharma J., and Hughes D., 2007, “A Finite Element Solution Scheme for an Elastic-Viscoplastic Soil Model”, Computers and Geotechnics, 35: 524-536.

Kulhawy F. H., and Mayne P. W., 1990, “Manual on Estimating Soil Properties for Foundation Design”, Cornell University-Geotechnical Engineering Group, Hollister Hall, Ithaca, New York.

Ladd C. C., Foote R., Ishihara K., Schlosser F., and Poulos H. G., (1977), “Stress-Deformation and Strength Characteristics”, State of the Art Report, Proceedings of the Ninth International Conference on Soil Mechanics and Foundation Engineering, Tokyo, 2: 421-494.

Mitchell J. K. and Soga K., 2005, “Fundamentals of Soil Behavior”, Third Edition, John Wiley & Sons, Inc.

Mesri G., and Castro A., 1987, “Cα/Cc Concept and Ko during Secondary Compression,” Journal of Geotechnical Engineering, ASCE. 113(3): 230–247.

Need E. A., 1985, “Pleistocene Geology of Brown County, Wisconsin”, Wisconsin Geological & Natural History Survey.

Neher H. P., Wehnert M., and Bonnier P. G., 2001, “An Evaluation of Soft Soil Models Based on Trial Embankments,” Computer Methods and Advances in Geomechanics, 07, pp. 373-378, Tucson, New Mexico.

Nevada Department of Transportation, 2005, NDOT, “Geotechnical Policies and Procedures Manual” http://www.nevadadot.com/uploadedFiles/Geo_PPM.pdf.

O’Riordan N. J. and Seaman, J. W. (1993) “Highway Embankments over Soft Compressible Alluvial Deposits: Guidelines for Design and Construction,” Contractor Report 341, Transport Research Laboratory, Department of Transport, U.K.

Ozcoban S., Berilgen M. M., Kilic H., Edil T. B., and Ozaydin K., 2007, “Staged Construction and Settlement of a Dam Founded on Soft Clay” Journal of Geotechnical and Geoenvironmental Engineering, ASCE.

Salgado, R., 2008, “The Engineering of Foundations,” McGraw-Hill.

Sae-Tia W., Kouda M., and Kusakabe O., 1999, “Deformation and Stability of Unreinforced and Reinforced Embankment on Soft Clay,” Geotechnical Engineering Journal, 30(2): 113-127

Schanz T., Vermeer P. A., and Bonnier P. G., 1999, “The Hardening Soil Model: Formulation and Verification,” Beyond 2000 in Computational Geotechnics, Balkema, Rotterdam.

Sivakugan N. and Das, B. M., 2010, “Geotechnical Engineering, A Practical Problem Solving Approach” by J. Ross Publishing, Inc.

Sowers G. B., and Sowers G. F., 1970, "Introductory Soil Mechanics and Foundations", Third Edition, Macmillan Publishing Co., Inc. New York, Collier Macmillan Publishers London.

Stark T. D., and Choi H., 2007, "Slope Inclinometers for Landslides" Landslides DOI 10.1007/s10346-008-0126-3.

Terzaghi K.,1943, "Theoretical Soil Mechanics", John Wiley and Sons, Inc.

Poulos H. G., Booker J. R., and Ring G. J., 1972, "Simplified Calculation of Embankment Deformations," Soils and Foundations, 12(4): 1-17

Robinson K. E., and Campanella R. G., 1986, "Guidelines for Use and Interpretation of the Electric Cone Penetration Test, 3rd Ed.," Hogentogler & Co., Gaithersburg, MD, 196 p.

Vermeer P. A., and Neher H. P., 1999, "A Soft Soil Model that Accounts for Creep," Beyond 2000 in Computational Geotechnics, Balkema, Rotterdam.

Washington State Department of Transportation, 2010, WSDOT, "Geotechnical Design Manual-Embankments," M46-03.01 January.

Weech C. N., and Lister D. R., 2009 "Highway embankment construction over soft soils in the lower mainland of British Columbia," Proceedings, 29th Annual Conference of the Transportation Association of Canada.

Winterkorn H. F., and Fang, H. Y., 1975 "Foundation Engineering Handbook," Van Nostrand Reinhold, New York.

APPENDICES

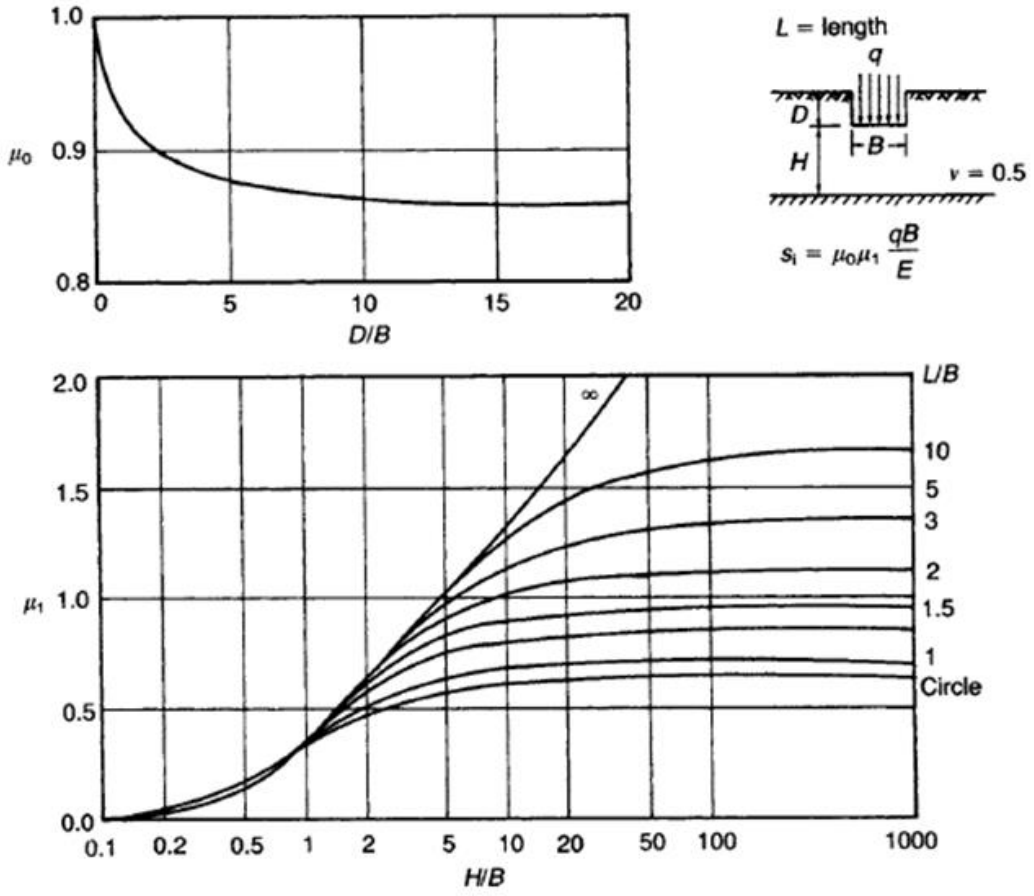

Figure A. 1. Coefficients for immediate settlement

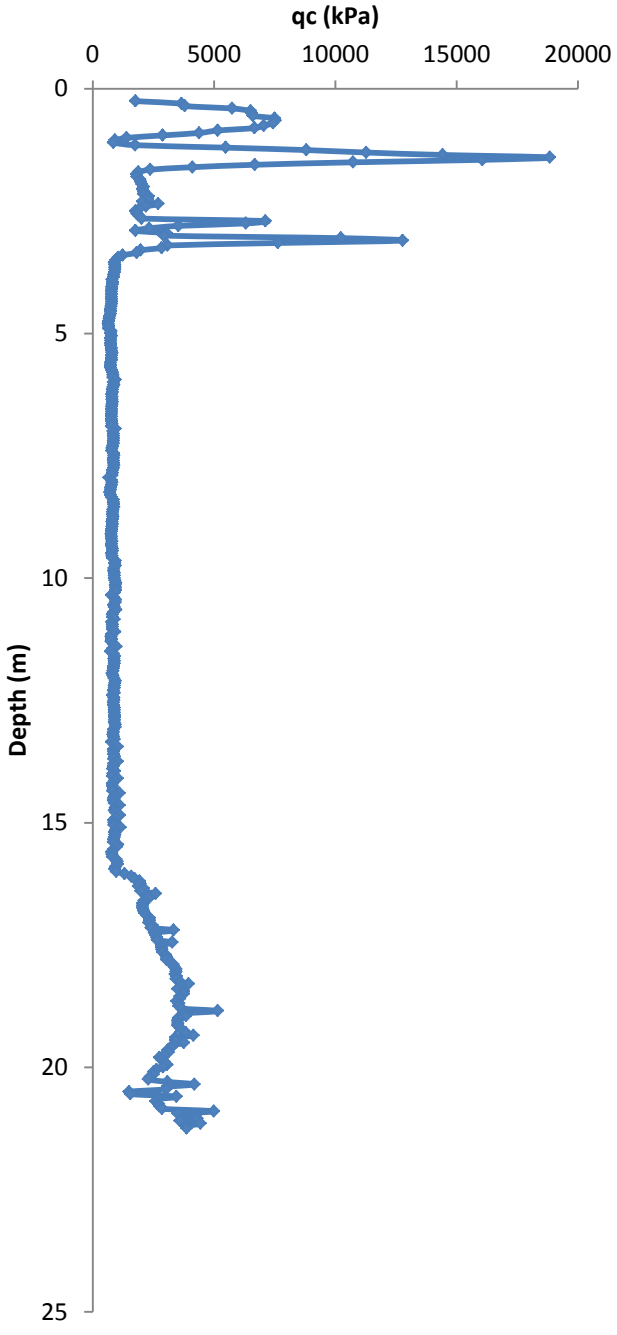

Figure A. 2. Cone resistance data (CPT-02)

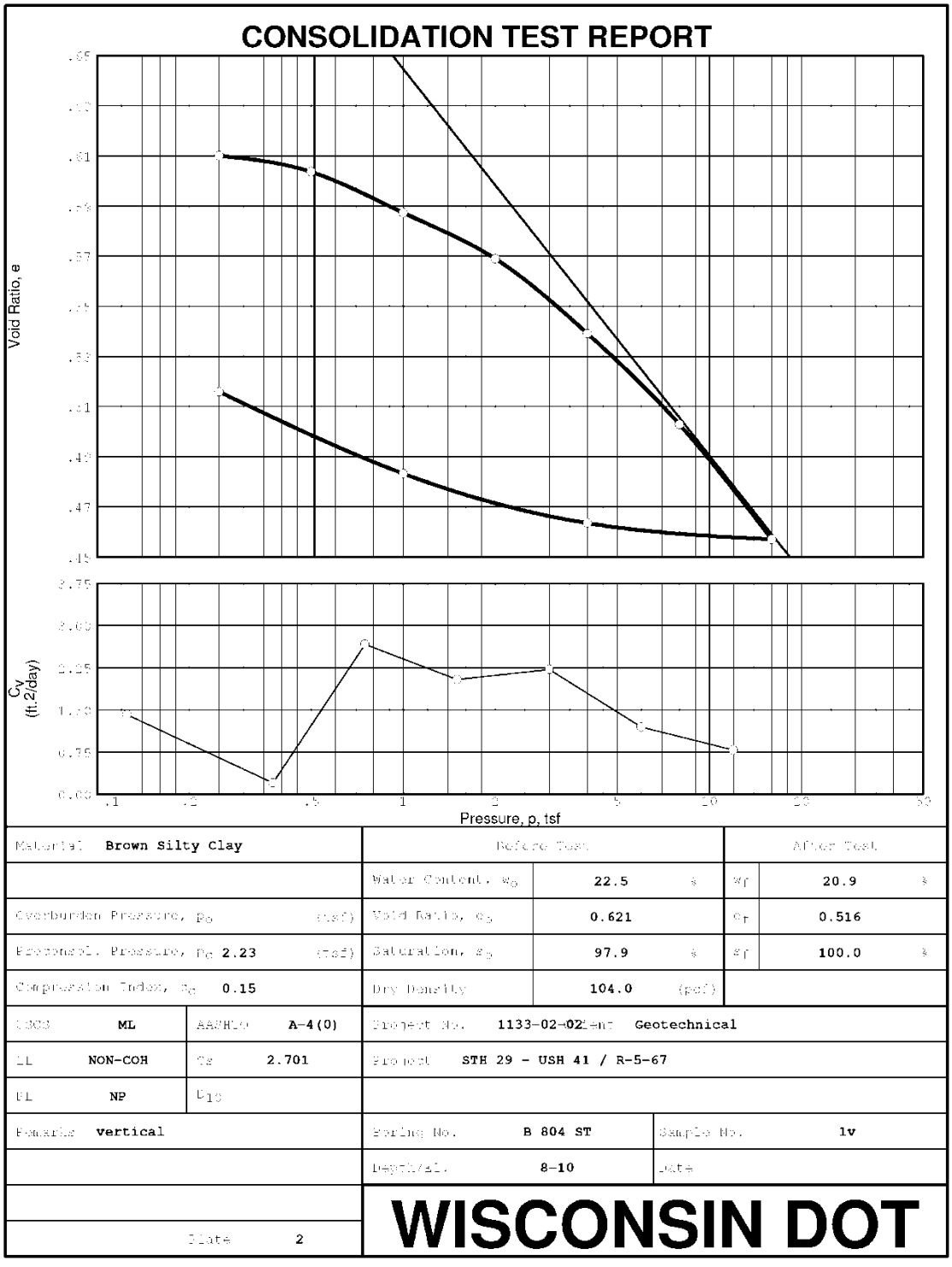

Figure A. 3. Consolidation Test Report at a depth 8-10 ft

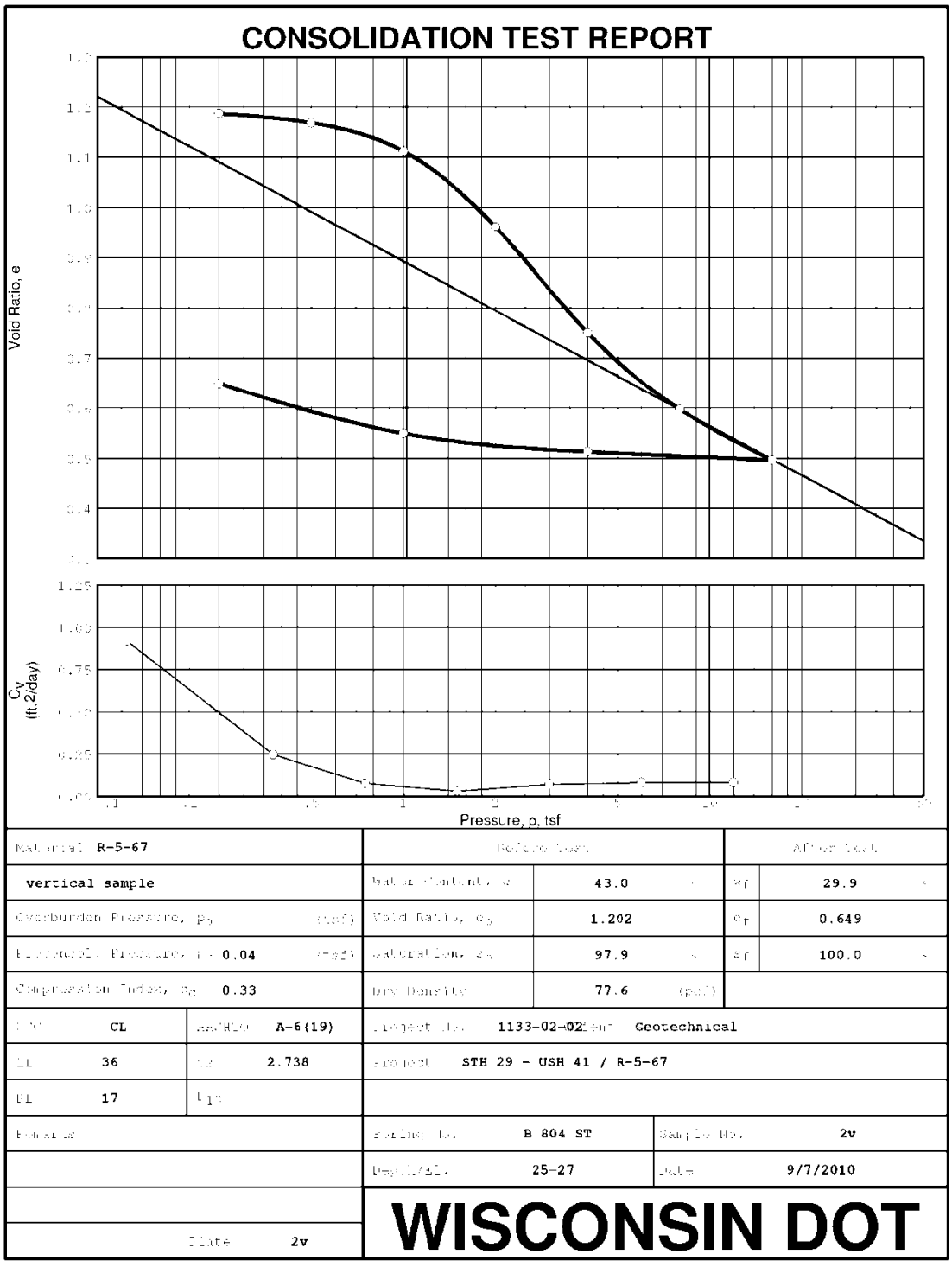

Figure A. 4. Consolidation Test Report at a depth 25-27 ft

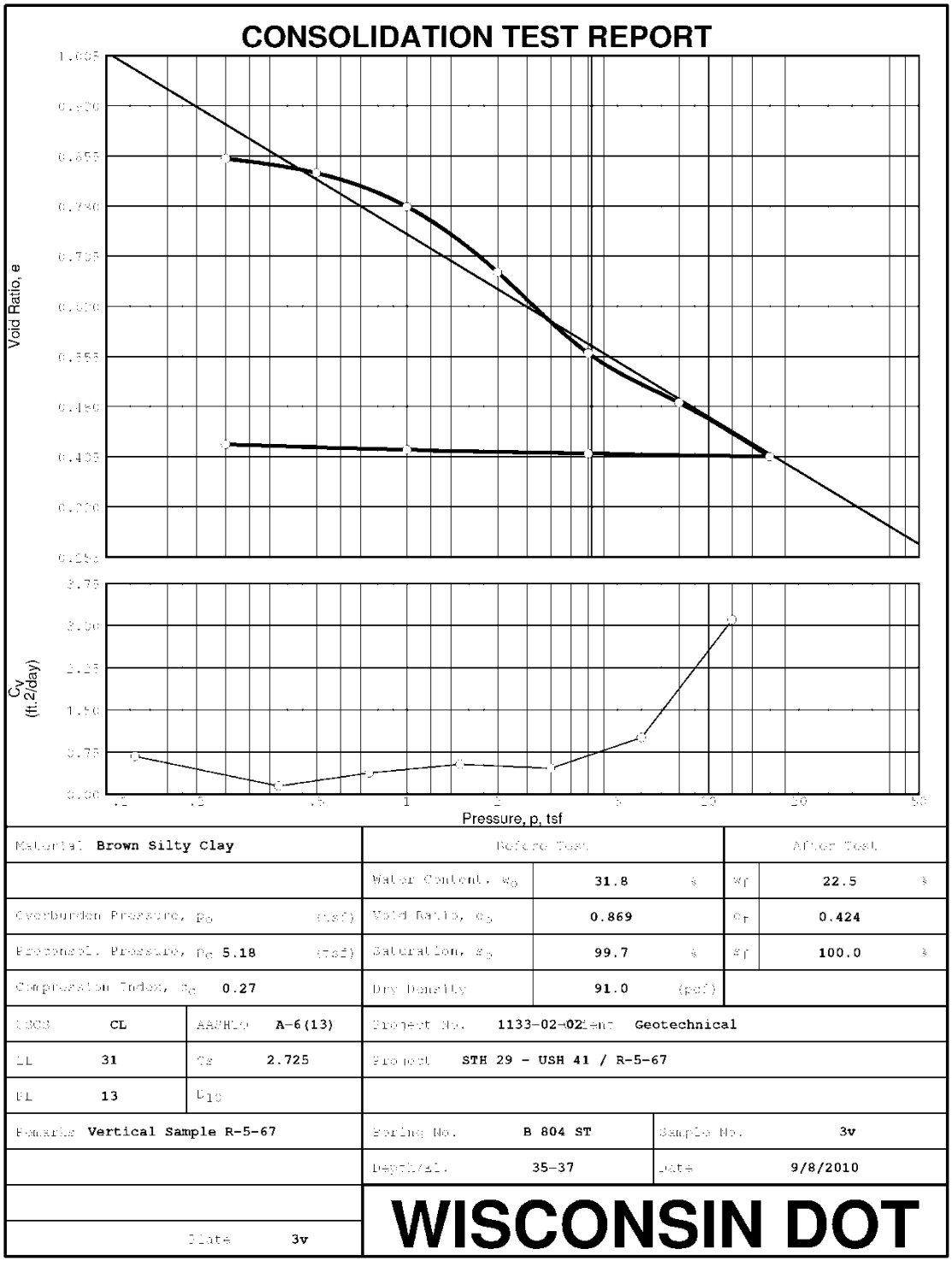

Figure A. 5. Consolidation Test Report at a depth 35-37 ft

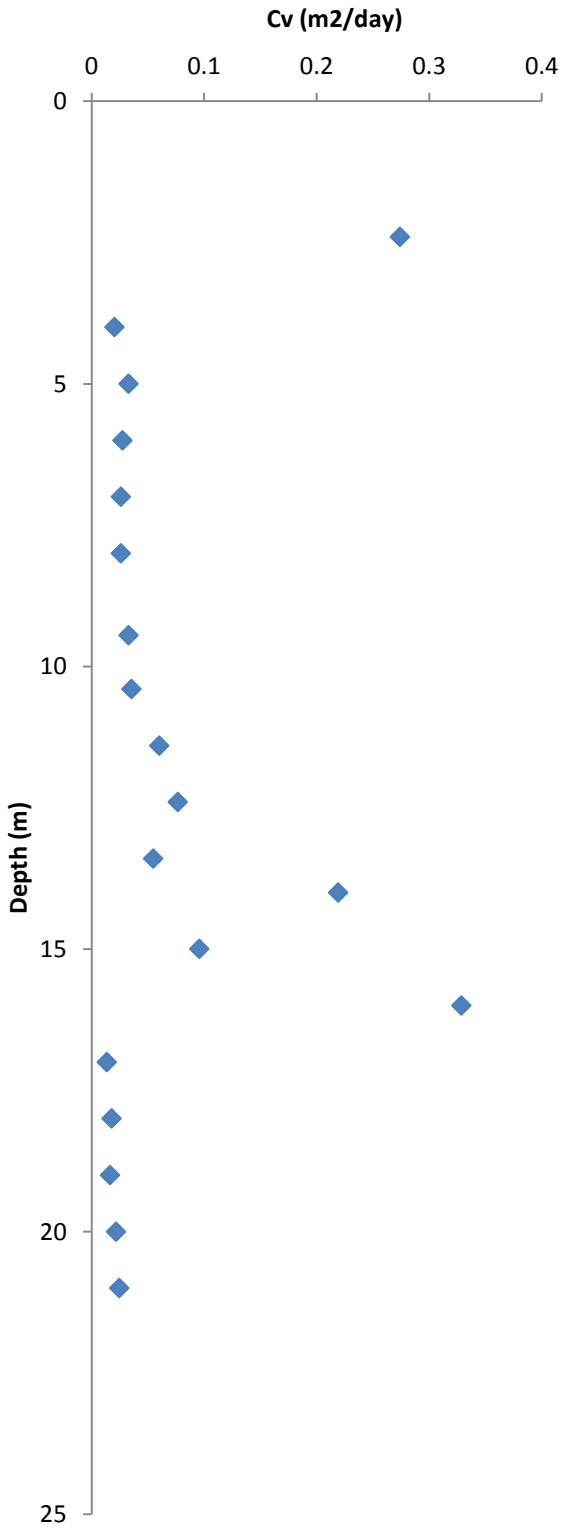

Figure A. 6. Coefficient of consolidation data